Consortium

for

Small-Scale Modelling

Newsletter

April 2008 *No. 7*

Deutscher Wetterdienst

MeteoSwiss

Ufficio Generale Spacio Aero e Meteorologia

ΕΘΝΙΚΗ ΜΕΤΕΩΡΟΛΟΓΙΚΗ ΥΠΗΡΕΣΙΑ

Instytucie Meteorogii i Gospodarki Wodnej

Administratia Nationala de Meteorologie

Agenzia Regionale per la Protezione Ambientale dell Piemonte

Agenzia Regionale per la Protezione Ambientale dell Emilia-Romagna: Servizio Idro Meteo

Centro Italiano Ricerche Aerospaziali

Amt für GeoInformationswesen der Bundeswehr

www.cosmo-model.org

Editors: Ulrich Schättler (DWD); Andrea Montani (ARPA-SIM); Massimo Milelli (ARPA Piemonte)
Printed at Deutscher Wetterdienst, P.O. Box 100465, 63004 Offenbach am Main

Table of Contents

1 Introduction

The contributions to this Newsletter are mainly summaries from the presentations given by COSMO staff during the 8th General Meeting in Bucharest (from 18.-21. September 2006). In this meeting, several units were organized as parallel sessions for the Working Groups and the Priority Projects. While it was difficult on the one hand, to choose, which session to attend, this procedure on the other hand gave most contributing scientists the opportunity to present and discuss their work in detail. During the plenary sessions we had an invited presentation by Terry Davies from the UKMO. He reported about *MOGREPS*, the *Met Office Global and Regional Ensemble Prediction System* and the plans of the Office for high resolution data assimilation.

After the Bucharest Meeting, an important change happened for the name of the model. Because all COSMO partners were very creative in finding names for their special applications of the *Lokal Modell*, the model was merely known as *aLMo*, *LAMI*, *LME* or *LMK*, resp. To make it more known as a common product of COSMO, the Consortium for Small-Scale Modelling, we decided to refer to it as the *COSMO-Model*. Applications of the COSMO-Model will be denoted by two additional letters or digits: COSMO-XX. This new convention is not yet obeyed to closely in the contributions of this Newsletter, but we hope that the new name will be accepted more and more by all COSMO scientists in the near future.

Figure 1: Participants of the 8th COSMO General Meeting in Bucharest

Nearly two years have passed since the publication of the last COSMO Newsletter in July 2006. The intention to have the publication shortly after the COSMO General Meetings in September surely has failed for this issue, but it better should be late than never. We are already in the progress of editing the publications from the last General Meeting in Athens and we hope to have the next Newsletter published a bit earlier.

Ulrich Schättler `Ulrich.Schaettler@dwd.de`
Andrea Montani `amontani@arpa.emr.it`
Massimo Milelli `Massimo.Milelli@arpa.piemonte.it`

Strategy for COSMO

M. Rotach[1], M. Ferri[2], R. Klejnowski[3], H.-J. Koppert[4], T. Paccagnella[5], I. Papageorgiou[6]

[1] *MeteoSwiss, Zürich, Switzerland*
[2] *Ufficio Generale Spazio Aereo e Meteorologia, Roma, Italy*
[3] *nstitute of Meteorology and Water Management, Warsaw, Poland*
[4] *Deutscher Wetterdienst, Offenbach, Germany*
[5] *ARPA-SIM, Bologna, Italy*
[6] *Hellenic National Meteorological Service, Athens, Greece*

1 Introduction

COSMO is one of several Consortia in Europe dealing with the development, evaluation and improvement of a limited area model for numerical weather prediction. Triggered by several external factors – such as recent enhanced collaboration between two other consortia in Europe (HIRLAM and ALADIN), or the foreseeable end of the current EUMETNET Programme on Short-Range Numerical Prediction – the Steering Committee (STC) has worked out a long-term strategy for the COSMO countries. This contribution aims at outlining the background of this strategy and its essential elements.

2 Background

In Europe the number-one global (medium range) weather forecast centre is undoubtedly the ECMWF. Its declared strategy is a reduction in their deterministic models horizontal resolution to 10 km by 2015, and a resolution of 20 km for their EPS system. With this there are no plans to enter the "non-hydrostatic world" within the next decade, but the resolution will be about as close as possible.

Plans are strong in all global modelling centres in Europe to improve the assimilation of more and more data, notably from satellites and other remote sensing instrumentation.

In the long run the strategy for (global) meteorological models aims at including non-meteorological aspects of the environment such as air quality or hydrology. Hence meteorological models will eventually become environmental prediction (or diagnostic) systems. This will, on the one hand, be natural due to including radiative information through atmospheric constituents in the assimilation cycles. On the other hand, it will enlarge the scope and applicability of (global) meteorological models.

3 Strengths and Weaknesses of the COSMO Model

The COSMO Model[1] is a non-hydrostatic meso-scale numerical model with full physical parameterisations suited for weather prediction applications (Steppeler et al. 2003). As such it is similar to many other meso-scale numerical models for atmospheric flows (e.g., RAMS, ARPS, MM5, WRF) and the models of the other European consortia (ALADIN/AROME;

[1]Note that the model has recently obtained a new generic name: COSMO. Before it has been known as *Lokal Modell (LM)*, *aLMo*, *LAMI* and other variants referring to specific applications of the model.

LACE, HIRLAM, UM). Being the primary tool for official duty at the COSMO Weather Services, however, special focus is put on operational stability as well as efficiency and portability, suitability for moist processes and suitability for particular processes of special interest to COSMO members. Lately, experiments have been performed on introducing a z-coordinate rather than the still operational "terrain influenced" sigma coordinate system (Steppeler et al. 2006). Boundary and initial conditions can be obtained from either the GME (global model of DWD) or the IFS (from ECMWF). Assimilation of observations is performed on the basis of the nudging approach. Some satellite data can be assimilated using a 1d-variational scheme.

Ever since its operational start in 1999, the COSMO Model was operated at one of the highest spatial resolutions for operational NWP worldwide. Presently most COSMO countries run it at 7 km horizontal resolution (Kaufmann et al. 2003) and projects are rather mature for reducing the resolution to some 2-3 km (2.8 km at DWD: operational since May 2007; 2.2 km at MeteoSwiss). With this COSMO will again lead the "resolution competition" in Europe (other consortia have announced plans to go down to 4-5 km in the same time frame). In terms of length of the operational record, the COSMO-Model has the longest for non-hydrostatic models, which is advantageous for verification purposes as well as possible improvements.

The COSMO Model also has a number of special features. These include the prognostic snow model, a lake model and the latent heat nudging (LHN) scheme for the assimilation of radar data (e.g., Leuenberger, 2005). Also COSMO has an up-to-date two-moment microphysics scheme at disposition (not yet operationally used). With the so-called "prognostic precipitation" (i.e., various hydrometeors such as rain, snow and graupel as prognostic variables) the COSMO Model is up-to-date in the simulation of precipitation.

Employing the COSMO Model, a local ensemble prediction system (COSMO-LEPS) has been developed within COSMO (Molteni et al. 2001, Marsigli et al. 2001). This is presently being operated as a Member's Time Critical Application at ECMWF. It has a resolution of 10 km, is integrated over 144 h and the COSMO-LEPS domain covers most of Europe. Again with its LEPS, COSMO has developed the best-resolved local ensemble prediction system and has been instrumental in devising procedures to downscaling the global EPS.

As any modelling system the COSMO Model has also weaknesses. In terms of performance the most severe weakness is certainly the precipitation forecast. Although the introduction of prognostic precipitation variables has considerably improved the performance (especially in the lee of mountains) the COSMO Model still strongly overestimates precipitation, especially in winter and over mountains. In summer magnitudes are better, but the timing is weak. Also, near-surface variables (e.g., 2m temperature or wind gusts) are often (i.e., on average) largely off. The model has problems to maintain specific synoptic situations, especially low-wind situations resulting in cold pools (e.g., in the Swiss "Mittelland") and associated fog situations.

In terms of the chosen modelling approach, the most essential limitation of the COSMO modelling system is the restriction to nudging as an assimilation tool. Even if it might be highly questionable whether variational approaches are suitable for very high resolution (on the order of 1 km), there are only limited means to test this important decision-leading implication.

Finally, *in terms of individual parameterisations* and in view of the high resolution employed and envisaged, the weakest component of the COSMO model at present is probably the manner in which the soil (including and explicitly also the soil moisture) and near-surface exchange is treated. In terms of problems related to high resolution, COSMO has those of radiation treatment and resolved vs. parameterised convection in common with all the other models.

4 Challenges for the COSMO Model

Given the strengths of the COSMO Model and the development of the global meteorological models as briefly outlined in the previous sections, the vision for a meteorological model with a scope of weather forecasting on the local scale must be as follows:

> The COSMO Model will be supported and optimally developed to operate on the short to very-short range and with very high (km-scale) resolution.

For the specific characteristics of the COSMO model this overall strategy has a number of implications:

- It is necessary to investigate which assimilation approach is appropriate and successful at the very high resolution. Given the fact that variational approaches are theoretically sound, but have problems due to linearisation requirements at high resolution, and nudging is modifying the flow properties in a not necessarily balanced manner, research should go into approaches, which attempt to overcome these limitations such as the SIR (Sequential Importance Re-sampling) Filter (van Leeuwen 2003) that can possibly be combined with the presently used nudging scheme.
- The description of surface information and exchange has to improve according to the enhanced model resolution. This is important for permanent characteristics (surface types - number and detail of classes, parameters etc.), slowly changing information (for example hydrological characteristics such as soil moisture) as well as for the detail and treatment of the surface exchange parameterisation.
- Efforts will have to be made to better exploit satellite information on the local scale, especially from EUMETSATs *Satellite Application Facilities* (e.g., the Hydro SAF, Land Surface SAF, CM SAF).
- Ongoing efforts to diagnose and improve the forecast quality will have to include verification approaches to reflect specific problems at high resolution (e.g. “double penalty”), such as in the “fuzzy verification” approach by Ebert (2006).

Hand in hand with the improved resolution of the COSMO Model, a high resolution and short range ensemble prediction system is desirable. For this, methods to perturb initial conditions and thus generate ensemble members, possibly in combination with perturbed physics at these scales need to be developed and tested.

For the time being considerations on stability and national security suggest that every COSMO country operates its own regional scale model version. This, however, should be done with the highest degree of collaboration and interaction possible. A first step into more efficient use of the COSMO human resources has been made with introducing the system of Priority Projects in 2005. It will be necessary, however, to increase especially the efforts of acquiring funding from external sources (research projects at national and international level) in order to successfully reach the above mentioned aims.

5 Strength and weaknesses of the Consortium

The efforts of the COSMO partners result in a model-system that is quality-wise on par with the models of the other European consortia (QPF-Verification of Limited Area Models performed by the UK Met Office). At the beginning of the co-operation the contribution of each partner was not rigorously defined. There was no prioritisation regarding the area of Research and Development resulting in a quite ineffective cooperation. With the definition of Priority Projects the cooperation began to be focussed on important research areas.

COSMO itself has no budget at its disposal. This hinders cooperation and hampers the exchange of experts. There is no dedicated COSMO development team that solely concentrates on the development of the COSMO Model system. COSMO experts, whose resources are partly dedicated to the priority projects, often have operational duties, which in case of "normal emergencies" regularly override their commitment to the priority projects.

Currently the Scientific Advisory Committee of COSMO (SAC) consists of the Work Package Coordinators and the Scientific Programme Manager. Although the expertise in the SAC is sound, it is a COSMO internal group and it would be beneficial to COSMO to add external expertise.

The COSMO-Consortium has no plans to admit additional members in the near future except those that already have an applicant status. Since there is a considerable external interest in the COSMO Model, the consortium members are willing to make the COSMO Model system available to others through licensing for an annual fee.

6 Summary and Strategic Goals

From the above the following strategic goals can be derived for COSMO over the next years:

- Increase of forecast quality at very high resolution (km-scale), in particular for precipitation, fog and "cold pool" situations.

- Development of a short-range ensemble prediction system (SREPS) that builds on the experience of COSMO-LEPS, extends its applicability into day one to three and has a correspondingly high spatial resolution.

- The co-operation within COSMO needs to be strengthened by going on with the Priority Projects approach on the one hand and closer exchange of results and direct collaboration on the other hand. For the latter it is necessary to have more resources, over which COSMO as a consortium can dispose.

- An important goal will be the successful collaboration among the consortia in a future European network, i.e. the possible follow-on programme to the EUMETNET SRNWP that ends by 2007. This should promote exchange of software and tools, enabled through joint procedures and generally accepted standards on formats (interoperability). Also common verification procedures, standards and exchange of approaches should be fostered. Finally, the capability of many countries' computing facilities should be exploited in order to devise joint (i.e., similar or complemental, or both) European ensemble prediction systems, possibly within the framework of TIGGE-LAM.

- Make the COSMO-Model available to third parties by offering a commercial license.

- Try to establish a budget for COSMO at its own right to support travel expenses and expert visits.

- Establish a Scientific Advisory Committee of external experts.
- As a final goal – to reach all the above and make it available to the community – COSMO (the consortium as well as the model) needs more visibility, be it through peer reviewed publications, conference contributions or representation in project consortia.

References

Ebert, B., 2006: Fuzzy verification of high resolution precipitation forecasts, *Preprints 1st MAP D-PHASE Scientific Meeting*, Vienna (A), November 6-8 2006, 85–89.

Kaufmann, P., F. Schubiger, P. Binder, 2003: Precipitation forecasting by a mesoscale numerical weather prediction (NWP) model: eight years of experience, *Hydrol. Earth Sys. Sci.*, **7(6)**, 812–832.

Leuenberger, D., 2005: High-resolution radar rainfall assimilation: exploratory studies with Latent Heat Nudging, *Dissertation* Nr. 15884, ETH Zürich.

Molteni, F., R. Buizza, C. Marsigli, A. Montani, F. Nerozzi, T. Paccagnella, 2001: A strategy for high-resolution ensemble prediction. Part I: Definition of representative members and global-model experiments. *Quart. J. Roy. Meteor. Soc.*, **127**, 2069–2094.

Marsigli, C., A. Montani, F. Nerozzi, T. Paccagnella, S. Tibaldi, F. Molteni, R. Buizza, 2001: A strategy for high-resolution ensemble prediction. Part II: Limited-area experiments in four Alpine flood events. *Quart. J. Roy. Meteor. Soc.*, **127**, 2095–2115.

Steppeler, J., G. Doms, U. Schättler, H.W. Bitzer, A. Gassmann, U. Damrath, G. Gregoric, 2003: Meso-gamma scale forecasts using the nonhydrostatic model LM. *Meteor. Atm. Phys.*, **82**, 75–96.

Steppeler, J., H.-W. Bitzer, Z. Janjic, U. Schättler,P. Prohl,U. Gjertsen, J. Parfiniewicz, L. Torrisi, E. Avgoustoglou, U. Damrath, 2006: Prediction of Clouds and Rain Using a Z-Coordinate Nonhydrostatic Model, *Monthly Weather Review*, **134 (12)**, 3625–3643.

van Leeuwen, P.-J., 2003: An ensemble smoother with error estimates, *Monthly Weather Review*, **129 (4)**, 709–728.

Walser, A., M. Arpagaus, C. Appenzeller, M. Leutbecher, 2006: The Impact of Moist Singular Vectors and Horizontal Resolution on Short-Range Limited-Area Ensemble Forecasts for Two European Winter Storms, *Monthly Weather Review*, **134**, 2877–2887.

A Tool for Testing Conservation Properties in the COSMO-Model

M. Baldauf

Deutscher Wetterdienst, Kaiserleistr. 42, D-63067 Offenbach am Main, Germany

1 Introduction

The fundamental equations of fluid mechanics, here especially those used in Meteorology can be formulated as conservation equations (or at least as balance equations) for mass, momentum and energy, as an example. Therefore an as good as possible conservation of these variables (or others, like enstrophy) should be obtained in a numerical model. Unfortunately this cannot be achieved in general but is guaranteed at most for a few variables in models which are formulated and also discretized in flux form. In all other cases it would be desirable to determine the strength of conservation violation.
To this purpose, a tool was developed to determine budgets of arbitrary scalar variables for the COSMO-Model (formerly known as LM). The budgets are calculated for an arbitrarily given cuboid volume inside of the model domain (see Figure 1).
This development was formulated as Task 3 in the COSMO-Priority Project 'Runge-Kutta'.

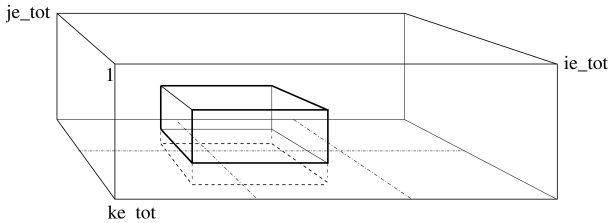

Figure 1: Integration area 'cuboid' lying in the model domain (in the transformed coordinate system). Here, a 3×2 domain decomposition is shown.

A general balance equation for a scalar ϕ (a generalized density) with an appropriate flux $\mathbf{f}_\phi$ sounds in integral form (i.e. over a steady volume V)

$$
\begin{aligned}
\frac{d}{dt}\Phi + F_\phi &= Q_\phi \\
\text{total amount:} \quad \Phi &:= \int_V \phi \, dv \\
\text{total flux:} \quad F_\phi &:= \int\int_{\partial V} \mathbf{f}_\phi \cdot d\mathbf{A} \\
\text{all sinks/sources:} \quad Q_\phi &:= \int_V q_\phi \, dv
\end{aligned}
\tag{1}
$$

In the case of ϕ being an integral conservative variable the right side of the first equation vanishes and the residuum

$$
Res := \frac{d\Phi}{dt} + F_\phi \tag{2}
$$

describes the violation of conservation.

Consequently, for the determination of these budgets, one has to be able to calculate volume integrals and surface integrals over fluxes in the model. In Section 2 the numerical implementation of such a tool is described. In Section 3 the correct implementation is tested with a strongly simplified test case. A first application is the determination of moisture balances in the Weisman-Klemp (1982)-Test in Section 4. Some remarks to implementation details and for the practical application is described in Section 5.

2 Numerical implementation

Calculation of the volume integral:

All the values of a variable in each grid element are weighted with the Jacobi-determinant D of the coordinate transformation and summed up

$$\Phi = \sum_{all\ GP \in V} \phi_{ijk} \cdot D_{ijk}\, \Delta V_{ijk} \tag{3}$$

where V denotes the volume of the cuboid, ΔV_{ijk} the volume of a grid cell in the transformed coordinate system, and D the Jacobi determinant

$$D := \left| \det\left(\frac{\partial x^i}{\partial \tilde{x}^j}\right) \right| = \frac{\partial x}{\partial \lambda} \cdot \frac{\partial y}{\partial \phi} \cdot \frac{\partial z}{\partial \zeta} \tag{4}$$

in the COSMO-model especially

$$\frac{\partial x}{\partial \lambda} = \frac{2\pi\, R_{Erd} \cos\phi}{360°}, \qquad \frac{\partial y}{\partial \phi} = \frac{2\pi\, R_{Erd}}{360°}, \qquad \frac{\partial z}{\partial \zeta} = -\sqrt{G} \tag{5}$$

$\sqrt{G}$ is the metric weight of the terrain following coordinate transformation (Doms and Schättler, 2002).

Calculation of the surface integrals.

The surface integrals are directly calculated by

$$F_\phi = \sum_{all\ GP \in \partial V} \mathbf{f}_{ijk} \cdot\ \Delta \mathbf{A}_{ijk}. \tag{6}$$

where the summation is performed over all grid points at the surface of the cuboid volume V. It is assumed, that the flux components are defined at the same positions than the velocity components in the staggered grid: f_x at the u-position, f_y at the v-position and f_z at the w-position.

At the lateral boundaries it is sufficient to multiply the area of the surface element with the appropriate perpendicular flux component. Whereas at the top and bottom boundaries one has to obey that surface elements are skewly lying in general, due to the fact that the cuboid volume is terrain following. To consider this we are looking to such a surface element at the top, whose projection onto the x-y-plane is lying in the range $[0..\Delta x, 0..\Delta y]$, and which has a slope given by $\frac{\partial z}{\partial x}$ und $\frac{\partial z}{\partial y}$. This geometrically cuts out a rhomb, whose area can be calculated with Heron's formula to

$$dA = \sqrt{1 + \left(\frac{\partial z}{\partial x}\right)^2 + \left(\frac{\partial z}{\partial y}\right)^2}\; dx\; dy. \tag{7}$$

The square root term is exactly the length of the vector $(-\frac{\partial z}{\partial x}, -\frac{\partial z}{\partial y}, 1)$ and therefore the vector of the surface element at the top boundary reads

$$d\mathbf{A} = \begin{pmatrix} -\frac{\partial z}{\partial x} \\ -\frac{\partial z}{\partial y} \\ 1 \end{pmatrix}. \tag{8}$$

At the bottom boundary it is appropriately $-d\mathbf{A}$.

3 Shift-Tests

To test the abilities of the integration tool, a simple 'shift-test' is performed: an initial distribution is given and is transported with a constant velocity through the model domain. By doing this, one obviously assumes a perfect advection algorithm reconstructing the correct solution. In the continuous case one knows of course the correct distribution of the scalar and the appropriate flux. But on a discrete grid there occur some inaccuracies in the balancing of this process which will be called in the following the 'flux calculation artefact' and the 'volume calculation artefact'.

The volume integral and the flux integral over the surface do not cancel each other in general (see Figure 2). This cancellation only takes place for a transport with a Courant number $C = v\Delta t/\Delta x = 1$ and the usage of an upwind-scheme of 1st order for the fluxes using the field values from the time step before (see Table). For a Courant number of e.g. $C = 1/2$ this balance is not longer complete, which will be called here the 'flux calculation artefact'. But even in this case, the upwind-calculation of the fluxes seems to work best (see Table) and this will be used in the following exclusively.

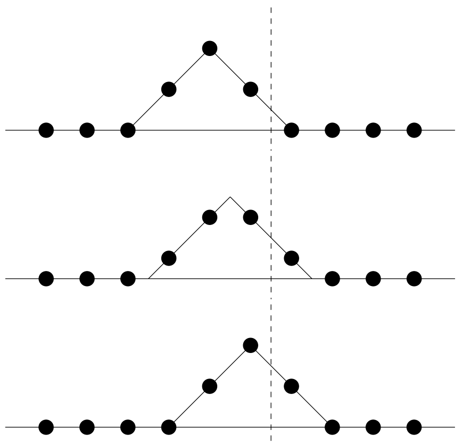

Figure 2: 'Shift-test'; explanation of the 'flux calculation artefact' at a Courant number $C = 1/2$.

n	M^n	dM/dt	F_{up}^{n-1}	F_{up}^{n}	F_{cd}^{n-1}	F_{cd}^{n}
1	4	0	0	0	0	0
2	4	0	0	1	0	0.5
3	3	-1	1	2	0.5	1.5
4	1	-2	2	1	1.5	1.5
5	0	-1	1	0	1.5	0.5
6	0	0	0	0	0.5	0
7	0	0	0	0	0	0
...						

Table 1: Shift-Test (see also the upper and lower pictures in Figure 2): transport with $v = 1 \cdot \Delta x/\Delta t$, M^n is the total mass in the integration volume at the time step t^n, F_{up} is the integral over the flux divergence with an upwind-scheme 1st order, F_{cd} with centered differences 2nd order, where the fields are used either at time step t^n or at time step t^{n-1}.

n	M^n	dM/dt	F_{up}^{n-1}	F_{up}^{n}	F_{cd}^{n-1}	F_{cd}^{n}
1	4	0	0	0	0	0
2	4	0	0	0.25	0	0.125
3	4	0	0.25	0.5	0.125	0.25
4	3.5	-0.5	0.5	0.75	0.25	0.5
5	3	-0.5	0.75	1	0.5	0.75
6	2	-1	1	0.75	0.75	0.75
...						

Table 2: Shift-Test (see Figure 2): transport with $v = 1/2 \cdot \Delta x/\Delta t$, for denotations see Table .

An other numerical problem, called the 'volume calculation artefact' arises even when the boundaries are not crossed. Assume that a distribution of the form $y = (1-x)^2$, if $y > 0$, 0 otherwise is given on a grid with $\Delta x = 1$. If this distribution is shifted with a velocity $v = 1/2\,\Delta x/\Delta t$ through the grid, then the 'total mass' fluctuates between the two values $M = 1$ and $M = 1.5$ (see Figure 3). This means even if no boundary of the integration volume is crossed by the distribution there can occur a mass change in every time step. In this case obviously a temporal mean cures this problem to a certain extent (in this example, the correct integral value is $M = 4/3 = 1.333....$) Therefore it seems to be reasonable to carry out a temporal integration over the residuum (2)

$$\Delta\Phi = \int_{t_a}^{t_e} Res\; dt. \tag{9}$$

In the following, the quotiont $\Delta\Phi/\Phi$ is called the *relative error.*

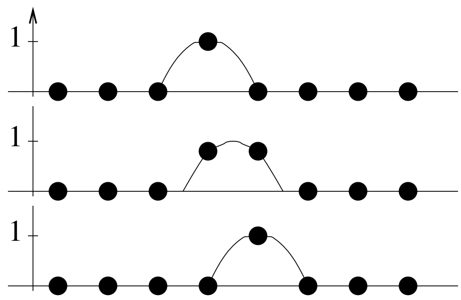

Figure 3: 'Shift-Test': 'volume calculation artefact'. The calculated masses alternate between $M = 1$ (top, bottom) and $M = 1.5$ (middle) from time step to time step.

'Shift-Test' with the integration tool: After these preliminary considerations the integration tool of the COSMO model itself will now be inspected by the 'Shift-Test'. An elliptical '3D-cone distribution ' serves as initialisation:

$$f_{cone}(x,y,z) := \begin{cases} 1-r & : \; r < 1 \\ 0 & : \; r \geq 1 \end{cases}, \qquad r := \sqrt{\left(\frac{x}{a}\right)^2 + \left(\frac{y}{b}\right)^2 + \left(\frac{z}{c}\right)^2}, \tag{10}$$

whose volume integral is

$$M := \frac{\pi}{3}\, a \cdot b \cdot c. \tag{11}$$

Shift-Test 1: The grid length is *exactly* $\Delta x = \Delta y = \Delta z = 500$ m with the transport velocity $v = 5$ m/s (in each coordinate direction $+x$, $-x$, $+y$, ...), and a time step $\Delta t = 100$ s.; this means in every time step the distribution is transported by exact one grid length. For the present no orography is used ($h = 0$).

	M	dM/dt	D	Res	delta M
...					
n= 3	0.6703411E+11	0.0000000E+00	0.0000000E+00	0.0000000E+00	0.0000000E+00
n= 4	0.6703411E+11,	0.7629395E-07	0.0000000E+00	0.7629395E-07	0.7629395E-05
...					
n=23	0.6703411E+11	0.0000000E+00	0.0000000E+00	0.0000000E+00	-0.1005852E-20
n=24	0.6703411E+11	0.0000000E+00	0.0000000E+00	0.0000000E+00	-0.1005852E-20
n=25	0.6667258E+11	-0.3615338E+07	0.3615338E+07	0.1001172E-06	0.1001172E-04
n=26	0.6536316E+11	-0.1309420E+08	0.1309420E+08	-0.2123415E-06	-0.1122244E-04
n=27	0.6271460E+11	-0.2648554E+08	0.2648554E+08	0.9313226E-07	-0.1909211E-05
n=28	0.5852479E+11	-0.4189810E+08	0.4189810E+08	0.1266599E-06	0.1075678E-04
n=29	0.5279093E+11	-0.5733864E+08	0.5733864E+08	-0.1341105E-06	-0.2654269E-05
n=30	0.4571720E+11	-0.7073733E+08	0.7073733E+08	0.1937151E-06	0.1671724E-04
n=31	0.3770282E+11	-0.8014380E+08	0.8014380E+08	-0.1043081E-06	0.6286427E-05
n=32	0.2933130E+11	-0.8371522E+08	0.8371522E+08	0.1490116E-06	0.2118759E-04
n=33	0.2131692E+11	-0.8014380E+08	0.8014380E+08	0.1490116E-07	0.2267770E-04
n=34	0.1424318E+11	-0.7073733E+08	0.7073733E+08	0.5960464E-07	0.2863817E-04
n=35	0.8509318E+10	-0.5733864E+08	0.5733864E+08	0.1490116E-07	0.3012829E-04
n=36	0.4319508E+10	-0.4189810E+08	0.4189810E+08	0.1490116E-07	0.3161840E-04
...					

Table 3: Shift-test 1; total mass M, its change in one timestep $\Delta M/\Delta t$, the surface integral of the fluxes D, residuum Res and its temporal sum ΔM.

Table 3 shows the result for a transport in -x-direction. As long as the cone lies in the interior of the cuboid, the volume integrals M are identical up to machine accuracy (up to time step $n = 24$). They are even exactly identical ($dM/dt = 0$), as long as the cone lies in the interior of one processor domain (up to $n = 3$). When processor domain boundaries are crossed by the distribution there occurs an error by the summation over all processors in the order of the machine accuracy. When crossing the boundary of the cuboid the surface integrals are almost exactly balanced with the mass change and the relative error $\Delta M/M$ is only about 10^{-14}. For a transport in $+x$, $-y$, $+y$, $-z$, $+z$-direction the results are almost identical. A domain decomposition with 3×2 processors was used, therefore the parallelisation of the integration tool seems to work properly.

Shift-test 2: As Shift-test 1, but now the (very small!) curvature of the earth surface is considered (crlat(:,:) $\neq 1$). Even in this small integration area there occurs a relative error of about 10^{-7}.

Shift-test 3: As Shift-test 1, but with the half of the velocity ($v = 2.5$ m/s in all 6 coordinate directions), i.e. in every time step the cone distribution will be transported about exactly 1/2 grid length. The errors are rather big in the meantime (Figure 4) and even at the end of the transport, when the distribution lies outside of the integration cuboid, the relative error is about $|\Delta M/M_0| \approx |-0.514 \cdot 10^7/0.670 \cdot 10^{11}| \approx 10^{-4}$. This is clearly due to the 'flux calculation artefact' where the mass changes and the sum of the fluxes over the boundaries do not cancel each other. For a transport in $+x$, $-y$, $+y$, $-z$, $+z$-direction the results are looking almost exactly the same. The reason is that we do not see any longer the roundoff errors but the truncation error which is nearly the same in all directions.

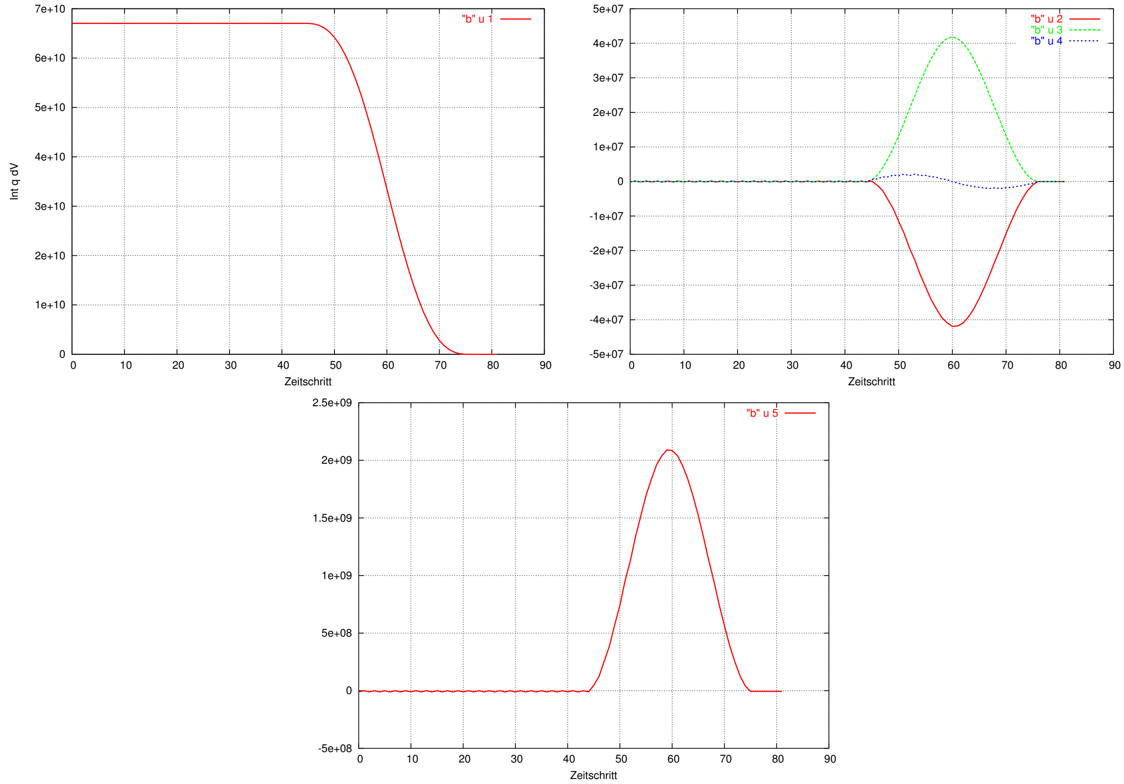

Figure 4: 'Shift-Test 3', Mass of moisture variables Φ (above, left), above, right: the balance terms $\Delta\Phi/\Delta t$ (red), F_ϕ (green), and the residuum (blue); below, left: the temporal integral of the residuum ΔM.

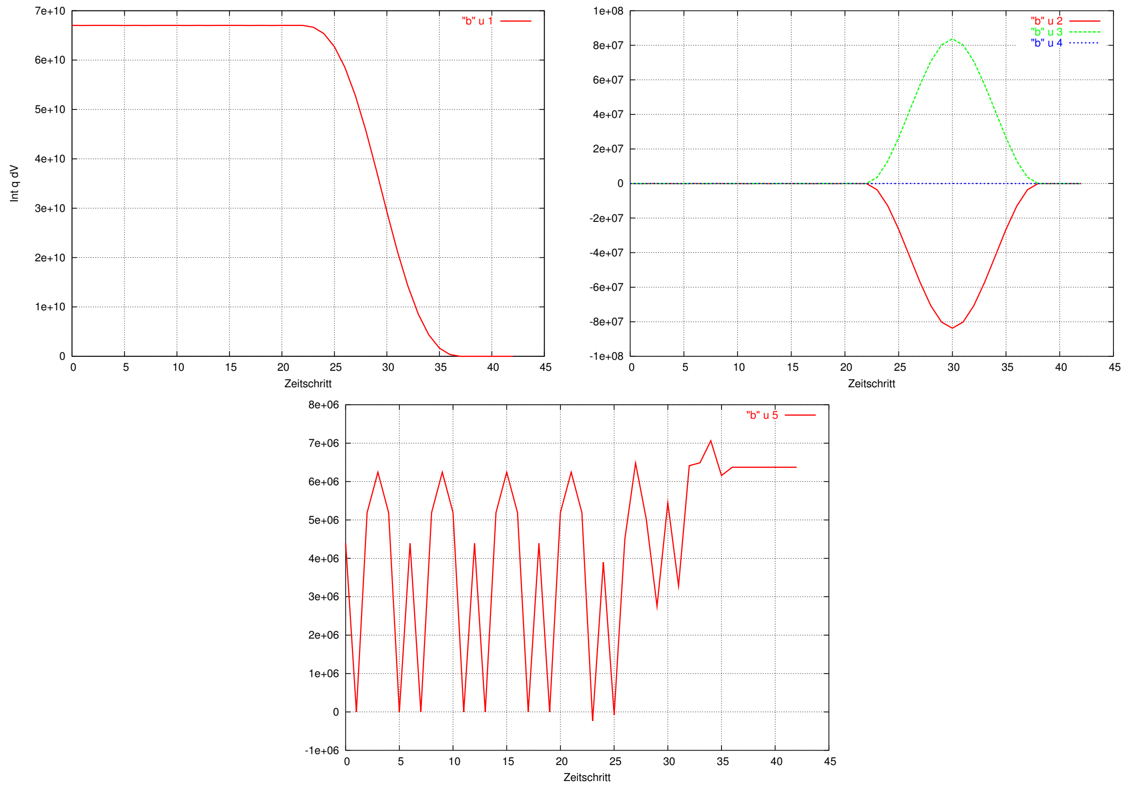

Figure 5: 'Shift-Test 4', denotations as in Figure 4.

Shift-test 4: As Shift-test 1, but with orography (sinus hill lines with $h = 500\text{m}$ and $L = 12dx = 6km$). Figure 5 shows, that the relative error is about 10^{-4}. It is in the same order of magnitude for a transport in z-direction; this indicates that the somewhat more complicated surface integral over the top and bottom boundary of the cuboid seems to work. For a transport in the other space directions there is a little bit more direction dependence of the results which comes from a stronger asymmetry (compared to shift-test 1) induced by the orography.

4 The Weisman-Klemp test case

A first application of the integration tool was carried out with the idealised Weisman-Klemp-test case (Weisman and Klemp, 1982). An ellipsoidal warm bubble serves as an initial disturbance with a maximum increase of temperature of $\max \Delta T = 2$ K, whose center lies in a height of 1400 m and which has the radii 10000 m, 10000 m, 1400 m (therefore it just touches the ground).

The horizontal grid length is $\Delta x = \Delta y = 2$ km, and the time step $\Delta t = 10$ sec. The atmosphere is in steady state at the beginning. The physics parameterisations are completely switched off, only the saturation adjustment (condensation and evaporation) is active. Therefore only water vapour q_v and cloud water q_c can occur, i.e. the density of total water is

$$\rho_x = \rho(q_v + q_c).$$

Further on there occur only advective fluxes $\mathbf{v}\rho_x$, but no turbulent or sedimentation fluxes.

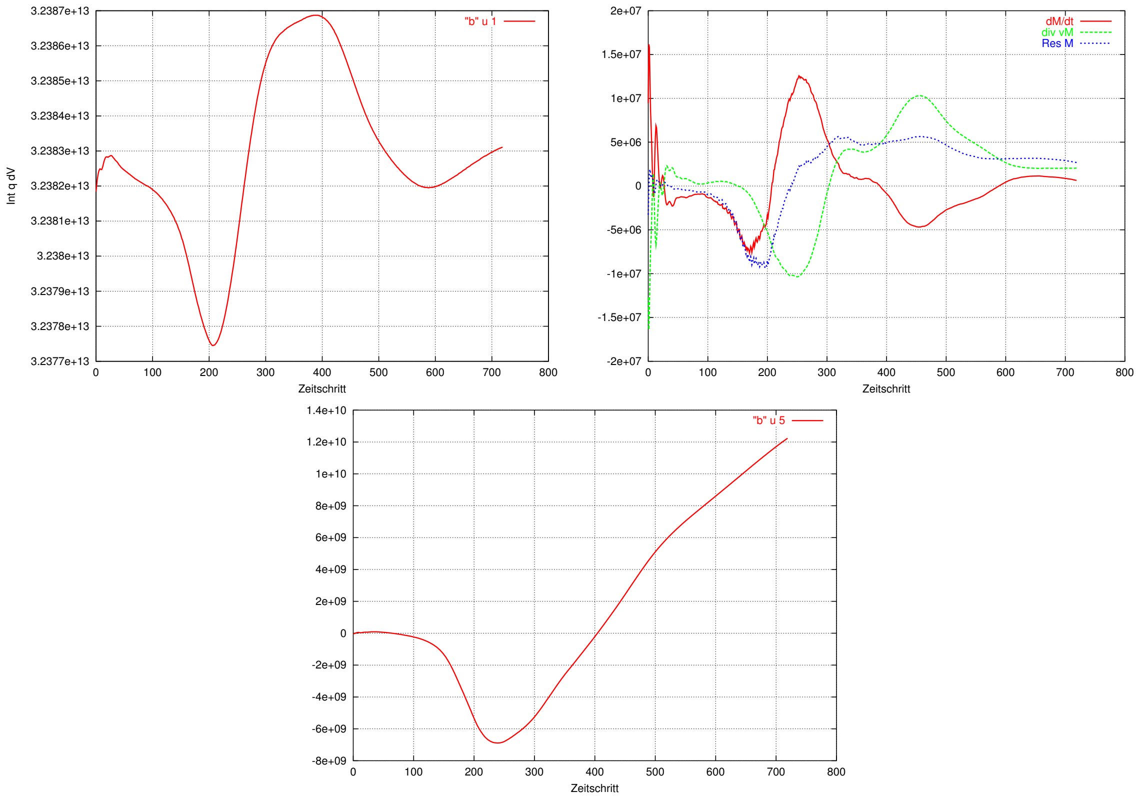

Figure 6: Exp. WK1: Weisman-Klemp-test case, density ρ, total mass M (left), temporal integral of the residuum ΔM (right).

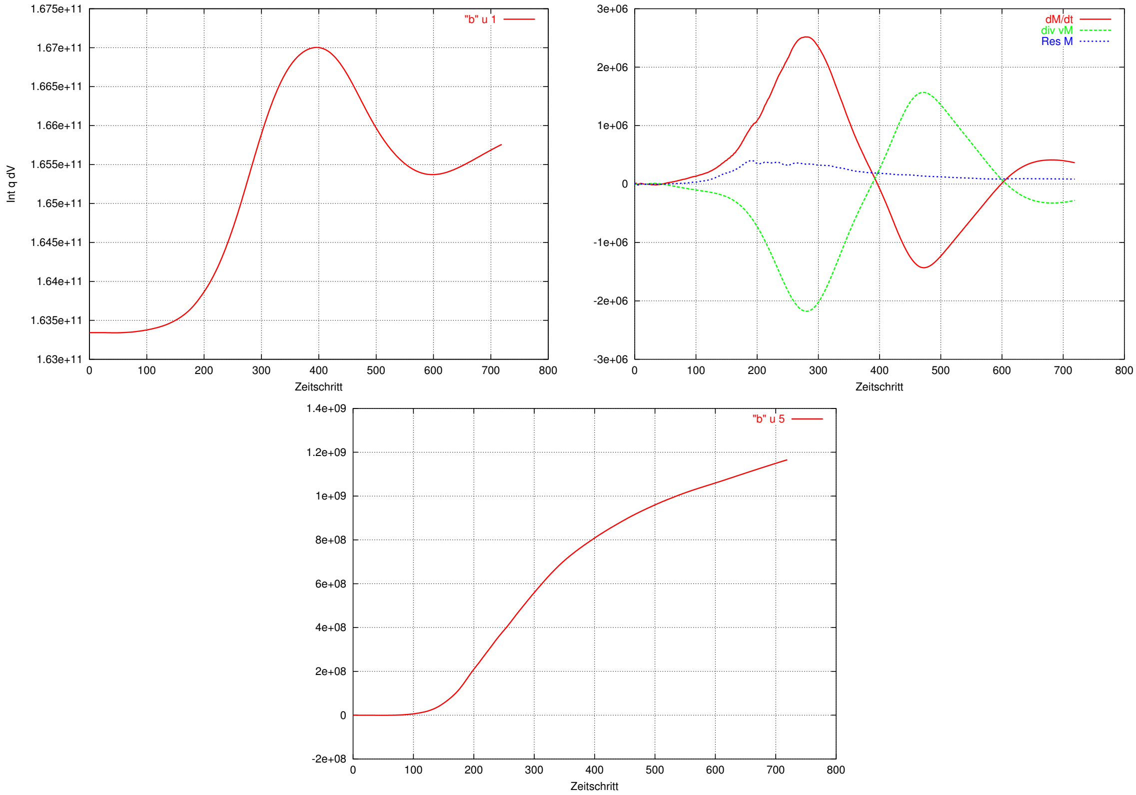

Figure 7: Exp. WK1: Weisman-Klemp-test case, density of moisture $\rho_x = \rho(q_v + q_c)$, total mass of moisture Φ (above, left), above, right: balance terms $\Delta\Phi/\Delta t$ (red), F_ϕ (green) and the residuum (bue), an the temporal integral of the residuum ΔM (below).

The moisture transport is carried out with a Semi-Lagrange-advection scheme with a tricubic interpolation (Baldauf, 2004), in which the mass conservation is guaranteed globally by a multiplicative filling (Rood, 1987). There were also carried out experiments with the Bott-advection scheme (Förstner et al., 2006) for which the following results are mainly the same.

The integration area was chosen in a manner, that no relaxation boundary zone is crossed. Of course, relaxation zones destroy any conservation property (the upper relaxation zone starts in $z = 13700$ m; the upper boundary of the cuboid lies in kmin=10, i.e. in $z = 12900$ m. The lateral Davies-relaxation zone has a width of 20 km, i.e. 10 grid points).

Figure 6 shows the total mass of the first experiment (Exp. WK1). There exist a certain mass conservation violation indicated by the the residuum (blue line in the upper right picture) and by its temporal integration (lower picture) leading to a relative error of $1.2 \cdot 10^{10} kg/3.24 \cdot 10^{13} kg \approx 0.04\%$.

In Figure 7 the balance of the moisture mass is shown. During the rising of the bubble (approximately the first 400 timesteps) moist air is sucked especially from the lower portions of the atmosphere. When the buoyancy is reduced, the bubble expands sidewards and blows out the moist air (timesteps 400-600). During this process the positive tendency of the mass change is not very well balanced by the negative tendency of the flux divergence (and vice versa); the residuum is rather big (upper left picture in Figure 7). And therefore the relative error is about $1.2 \cdot 10^9 kg/1.65 \cdot 10^{11} kg \approx 0.7\%$.

Therefore the question arises if this is a real error in the model or an artefact by the inte-

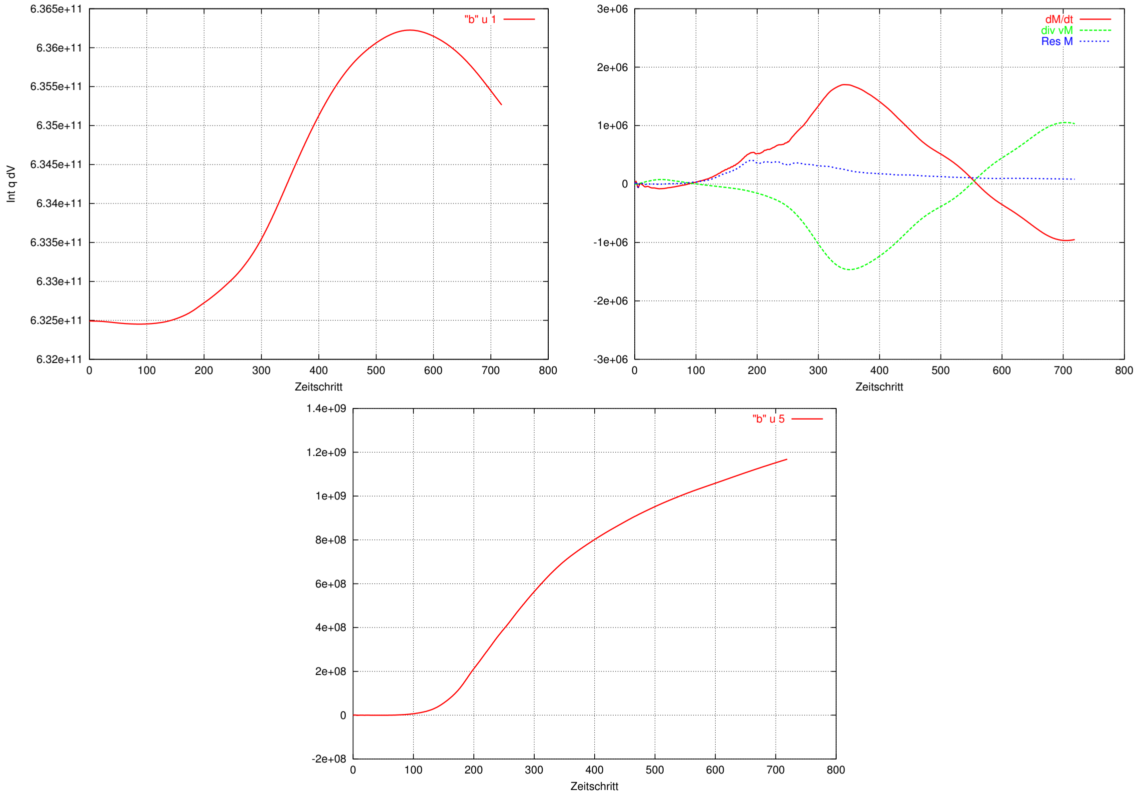

Figure 8: Exp. WK8: denotations are the same as in Figure 7.

gration tool. Because the Bott-advection scheme delivers very similar results, the problem seems not to be due to the advection scheme. The error in the total mass calculation of the above mentioned 0.04% seems to be too small to explain this moisture mass change.

To reduce artefacts by the calculation of the flux integrals the integration area was increased by a factor of 2 in x- and y-direction (experiment WK8). The upper left picture in Figure 8 shows the nearly 4 times more moisture mass compared to the case WK1. Due to the bigger integration area the signal of the rising bubble arrives later at the integration boundaries and therefore the temporal slope of the moisture mass and the balance terms seems to be stretched compared to case WK1, although the physical process of the rising bubble is exactly the same than in WK1. The only signal which is nearly the same and therefore independent of the integration box, is the residuum. This indicates, that the violation of the conservation is not induced by the inflow through the boundaries, but there seems to be a violation of conservation by the description of the physical process by the model.

To inspect this assumption, the saturation adjustment was switched off in experiment WK9. Because the buoyancy is drastically reduced due to the lack of latent heat release, a much warmer bubble was chosen; otherwise it would not rise very high. Here the temperature perturbation was increased from 2K to 10K.

In Figure 9 the residuum is (apart from the first few timesteps), clearly closer to zero than in experiment WK8. This also shows the sufficient conservation property of the Semi-Lagrange-advection in this case The only cause then for violation of conservation seems to be the saturation adjustment. Indeed, the saturation adjustment in the COSMO-model conserves the specific mass (and specific energy) but not mass (and energy) themselves.

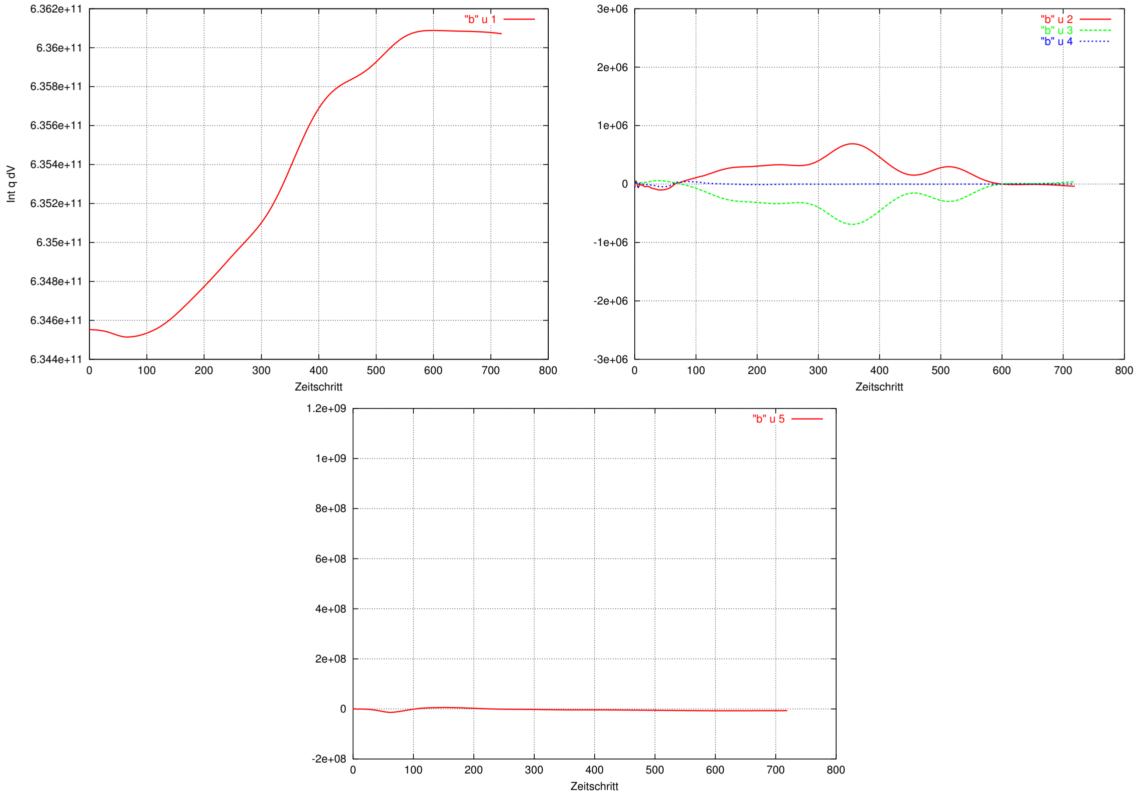

Figure 9: Exp. WK9: Weisman-Klemp-test case with a '10K bubble', without condensation, denotations are the same as in Figure 7.

5 Implementation

The integration tool is activated by the NAMELIST-switch `l_integrals`. The coordinates of the cuboid corners `imin_integ, imax_integ, jmin_integ, jmax_integ, kmin_integ, kmax_integ` are read from the NAMELIST-parameter group `DIACTL`. If they are not set, then the whole COSMO-model area is used as the integration area by default (be aware of relaxation boundary zones then) The module `src_integrals` in file `src_integrals.f90` contains the following subroutines: in `init_integral_3d` the data structure 'integ_cuboid' (of type `cuboid_multiproz_type`) is initialised. Especially the domain decomposition of the cuboid and the location of its surfaces appropriate to the domain composition of the model domain is carried out there. `integral_3d_total` calculates the volume integral over the cuboid and `surface_integral_total` calculates the 6 surface integrals over the N-, S-, O- and W-boundary and over the top and bottom boundary. Subroutine `calc_sqrtg_r_s` delivers the metric coefficient $1/\sqrt{G}$ at the location of the scalars (this is needed only in the 3-timelevel version, the 2-timelevel version calculates it automatically).

The basic subroutine for organizing the computations is `organize_integrals (yaction)`. The parameter `yaction` can take one of the three values `'init'`, `'compute'`, or `'final'`.

A first example for the calculation of total mass conservation is done by the subroutine `check_rho_conservation`. It calls as an example for calculating purely advective fluxes $\mathbf{F} = \rho \cdot \mathbf{v}$ (which only arise in the continuity equation) the subroutine `adv_fluxes_upwind`.

6 Conclusions

A tool to calculate balances in the COSMO-model was developed. Although such a tool itself has some inherent sometimes misleading properties as was discussed in Section 3, it can be used successful at least in idealised simulations and can give valuable hints for the violation of conservation properties. Here the boundaries often can be set far away from the interesting physical process and therefore the 'flux calculation artefact' can be reduced. Up to now no experiences with the application in real case simulations were made. For example, the Weisman-Klemp test showed an rather constant increase in total mass. It would be interesting to inspect this behaviour further on in real case studies.

References

Baldauf, M., 2004: The Lokal-Modell (LM) of DWD / COSMO. *Proceedings of ECMWF: Recent developments in numerical methods for atmospheric and ocean modelling*, 6.-10. September 2004, *http://www.ecmwf.int/publications/library/do/references/list/161*, 41–52.

Doms, G., U. Schättler, 2002: *A Description of the Nonhydrostatic Regional Model LM, Part I: Dynamics and Numerics*, Offenbach, Germany; Deutscher Wetterdienst.

Förstner, J., M. Baldauf, A. Seifert, 2006: Courant Number Independent Advection of the Moisture Quantities for the LMK. *COSMO-Newsletter*, No. 6, 51–64.

Rood, R., 1987: Numerical advection algorithms and their role in atmospheric transport and chemistry models. *Rev. Geophys.*, **25 (1)**, 71–100.

Weisman, M., J. Klemp, 1982: The dependence of numerically simulated convective storms on vertical wind shear and buoyancy. *Mon. Wea. Rev.*, **110**, 504–520.

Precipitation Forecast of the Z-Coordinate vs. the Terrain Following Version of LM over Greece

E. Avgoustoglou, V. Tirli and I. Papageorgiou

Hellenic National Meteorological Service, El. Venizelou 14, Hellinikon, Athens 16777, Greece

1 Introduction

The Z-coordinate version (LM_Z) of LM (Refs. Steppeler, 2002, and others) was validated in a previous work (Ref. Avgoustoglou, 2006) against the standard terrain following version (LM_TF) for cloud cover and precipitation regarding moderate frontal activity over Greece. Motivated by the resulting preponderance of LM_Z over LM_TF in reference to observations and satellite pictures as well as the need to test a newer version of the LM_Z code, we considered another case with significantly stronger precipitation events in order to check the extent that this preponderance persists.

2 Case Study

The geographical domain of Greece is characterized by an almost equipartitioned land-sea mask interchange combined with a complex orography and a large number of mountainous islands providing a challenging candidate towards the relative evaluation of LM_Z against the terrain following coordinates operational version (LM_TF). In this study, the frontal development during the three day period of the 17^{th}, 18^{th}, and 19^{th} of November 2005 is investigated. From the synoptic analysis as well as the satellite pictures (Fig. 1), it can be seen that on November the 17^{th}, low pressures in the Adriatic and the North Balkans extended Southwards were associated with the relatively high pressures over Turkey. A barometric low associated with a cold front along West Greece was moving Eastwards leading to significant precipitation events over the country as well as strong to gale winds over Eastern Greece. This activity was paled down on November 18 but it was followed by a new frontal activity associated with low barometric pressures over North Italy and North Aegean Sea that affected Greece on November the 19^{th}. In relevance to our previous work (Ref. Avgoustoglou, 2006), the precipitation observations were overall significantly higher. Consequently, any important difference in the forecasted precipitation between LM_Z and LM_TF could be of interest from the operational standpoint.

In Figs. 2, 3, 4, we show the relative forecasted low, medium and total cloud cover for LM_TF and LM_Z respectively. We used boundary conditions from the Global Model of the German Meteorological Service (DWD) with analysis of 00 UTC for every date under consideration. Even though, the total cloud cover forecasted by LM_Z looks closer to the satellite pictures of Fig. 1, the agreement between the two versions of LM looks satisfactory.

However, there are rather significant differences between the forecasted low and medium cloud cover. This feature looks consistent with Fig. 5 where the 12-hour forecasted accumulated precipitation in LM_Z is overall downgraded and less dispersed in reference to LM_TF, particularly over the sea surface. Regarding observation, the measured values of the 12-hour accumulated precipitation over the local meteorological stations were compared to the forecasted values of the nearest grid point. By summing these values, it was found that the total forecasted precipitation for LM_Z was closer to the total precipitation measured (Table 1).

In Fig. 6, we depict with “R” the positions of the meteorological stations where the observed value for the precipitation was closer to LM_TF and with “Z” when this value was closer to LM_Z. The bullet sign corresponds to stations where precipitation was neither observed nor predicted by any version of LM. Within this context, it may be seen again that the forecasted values from LM_Z are relatively closer to observation.

	November 17 57 Stations	November 18 55 Stations	November 19 55 Stations
Observed: Total	615.4	26.0	358.1
Average	10.80	0.47	6.51
LM_TF: Total	1024.5	588.5	788.8
Average	17.97	10.7	14.34
LM_Z: Total	632.5	65.6	487.8
Average	11.10	1.19	8.87

Table 1: Total and average observed and forecasted precipitation height (mm)

3 Summary and Outlook

For the test case under consideration, LM_Z forecast shows relative preponderance over LM for the 12-hour accumulated precipitation as was the case in our previous work (Ref. Avgoustoglou, 2006). It should be noted, that a later version of LM_Z code was used. Indications are rising that LM_Z might be an important tool towards the forecast of quantitative precipitation. It might be worth to run the code in parallel with the operational LM for a continuous period of time in order to address its validity on a systematic fashion.

References

Steppeler J., H.-W. Bitzer, M. Minotte, L. Bonaventura, 2002: Nonhydrostatic Atmospheric Modeling using a z-Coordinate Representation. *Mon. Wea. Rev.*, **130**, 2143-2149.

Bitzer, H.-W., J. Steppeler, 2002: A Description of the Z-Coordinate Dynamical Core of LM. *COSMO Technical Report*, No. 6, Deutscher Wetterdienst (DWD), Offenbach.

Steppeler J., H.-W. Bitzer, 2002: The Z-Coordinate Version of the LM. *COSMO Newsletter*, No. 2, 111-112.

Steppeler J., H.-W. Bitzer and U. Schättler, 2003: New Developments Concerning the Z-Coordinate Version of the LM. *COSMO Newsletter*, No. 3, 177-178.

Steppeler, J., Z. Janjic, H.-W. Bitzer, P. Prohl and U. Schättler, 2004: The Z-Coordinate LM. *COSMO Newsletter*, No. 4, 151-154.

Steppeler, J., H.-W. Bitzer, Z. Janjic, U. Schättler, P. Prohl, J. Parfiniewicz, U. Damrath and E. Avgoustoglou, 2005: A Z-Coordinate Version of the Nonhydrostatic Model LM. *COSMO Newsletter*, No. 5, 149-150.

Steppeler, J., H.-W. Bitzer, Z. Janjic, U. Schättler, P. Prohl, U. Gjertsen, J. Parfiniewicz, L. Torrisi, E. Avgoustoglou, U. Damrath, 2006: Prediction of Clouds and Rain Using a z-Coordinate Nonhydrostatic Model. *Mon. Wea. Rev.* **134**, 3625-3643.

Avgoustoglou, E., T. Tzeferi, V. Tirli, I. Papageorgiou: Application of the Z-Coordinate Version vs. Terrain Following Version of LM Nonhydrostatic Model over Greece. *COSMO Newsletter*, No. 6, 74-80.

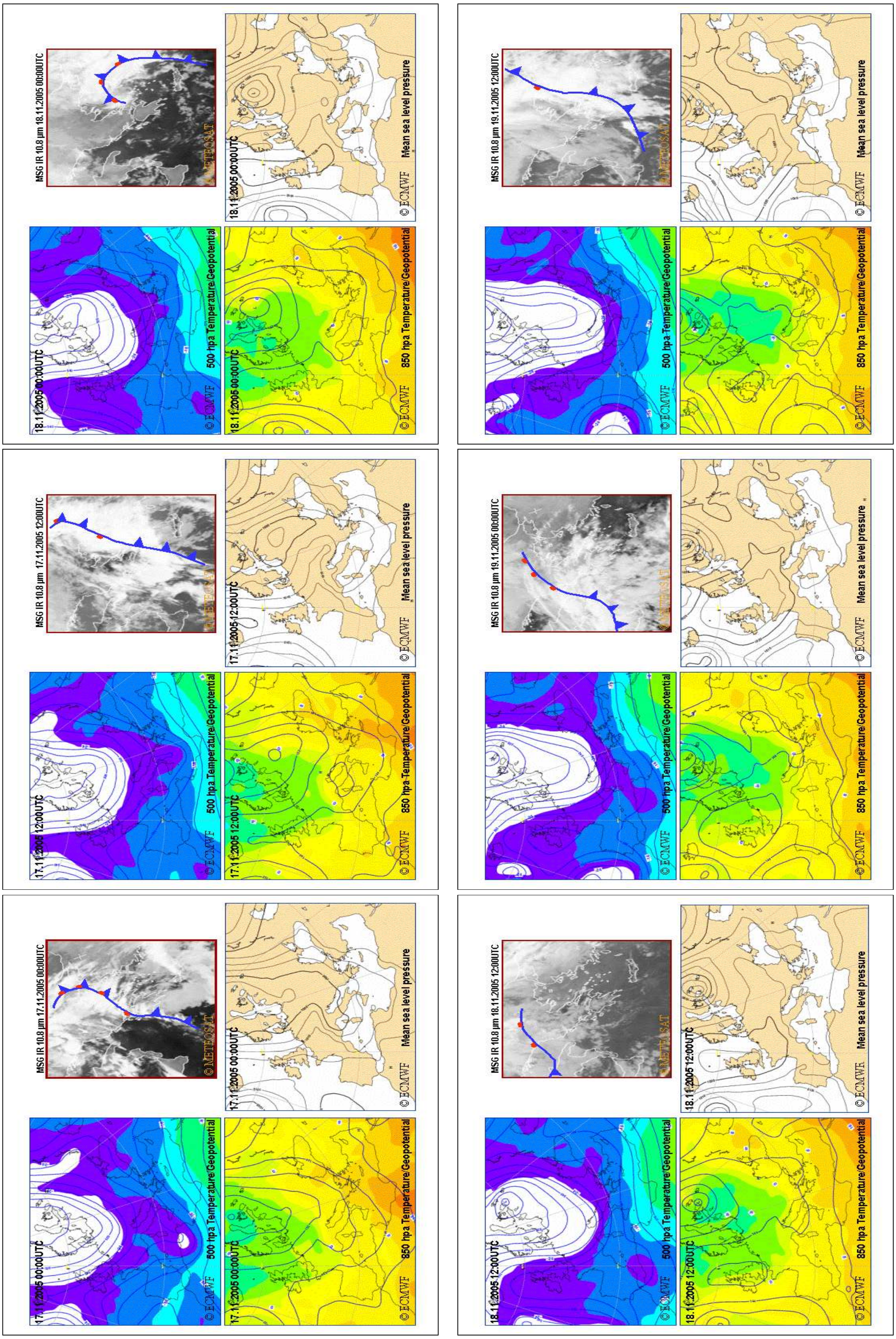

Figure 1: Satelite pictures and analysis charts for 17, 18 and 19 of November 2005.

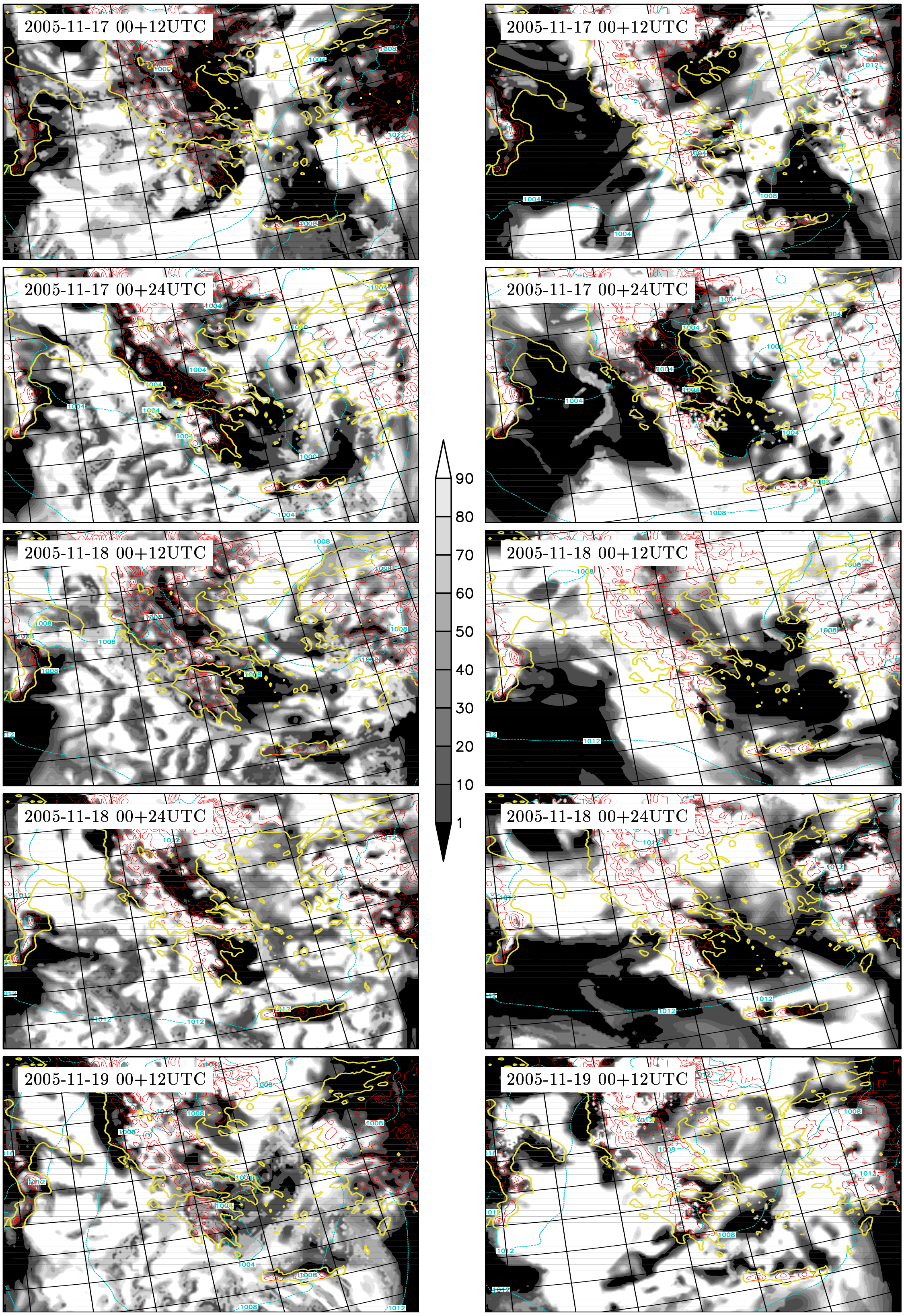

Figure 2: Low cloud cover forecast (%) and PMSL (HPa) from LM_TF (left column) and LM_Z (right column).

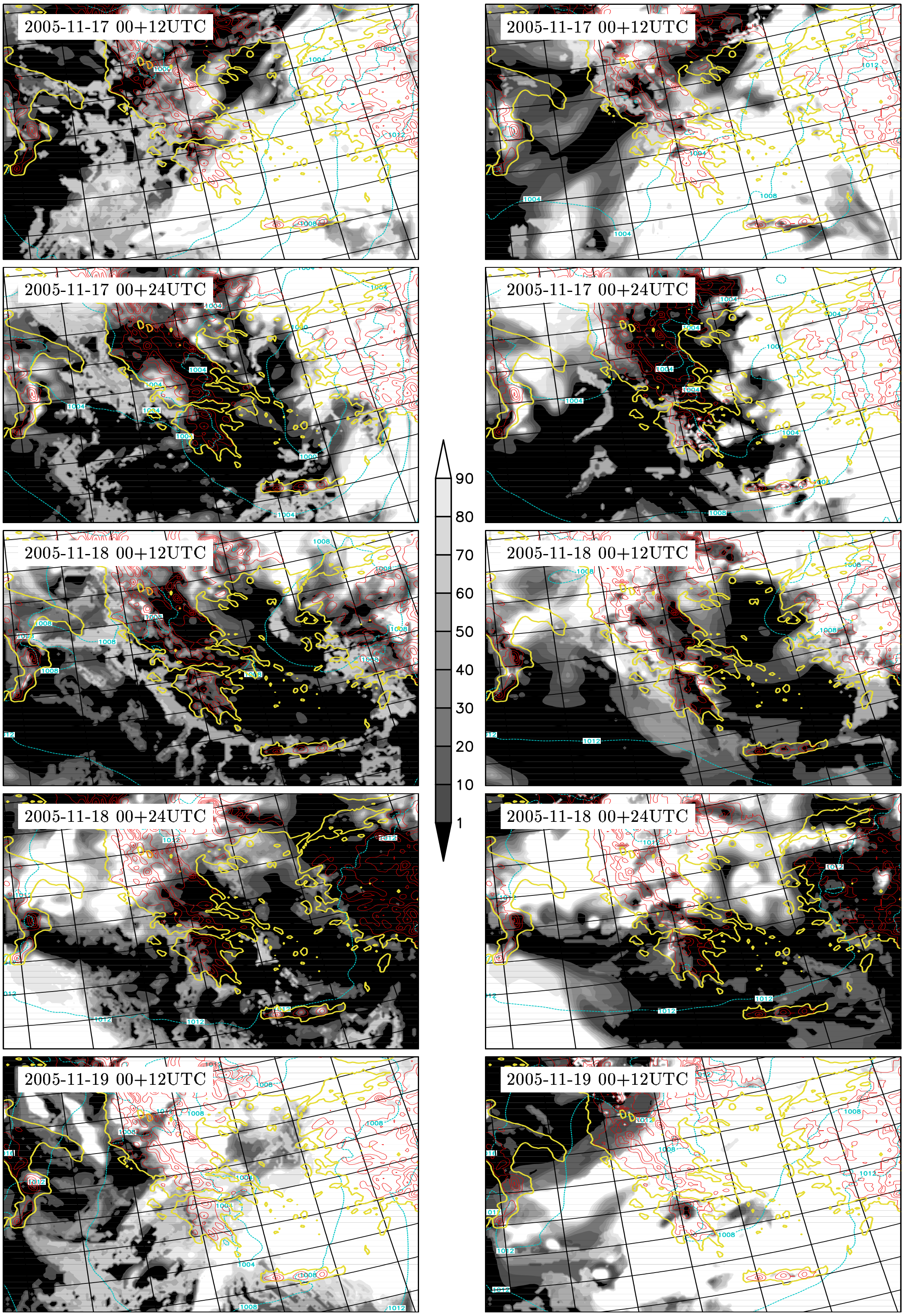

Figure 3: Medium cloud cover forecast (%) and PMSL (HPa) from LM_TF (left column) and LM_Z (right column).

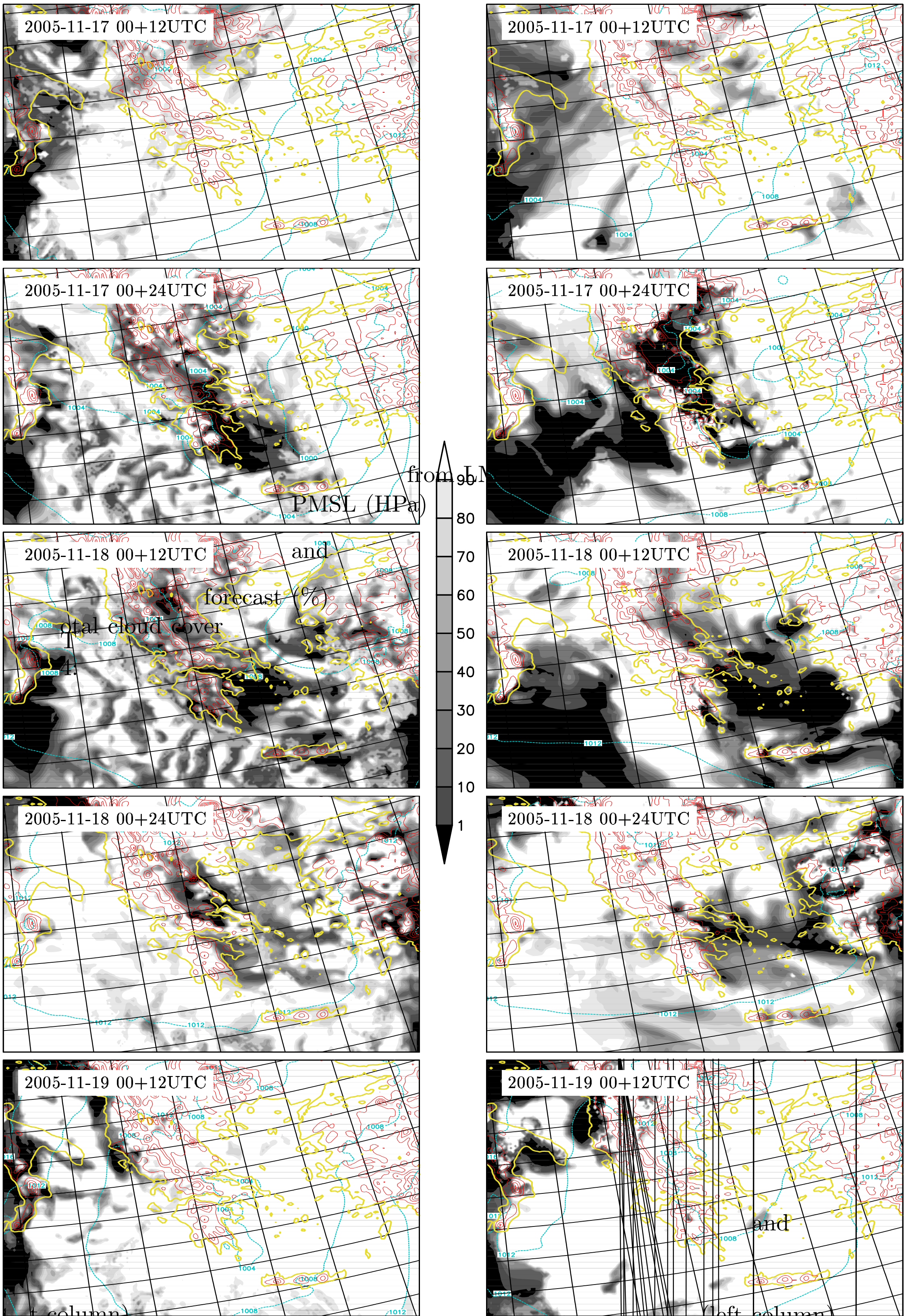

Figure 4: Total cloud cover forecast (%) and PMSL (HPa) from LM LM_Z (right column) and LM_TF (left column).

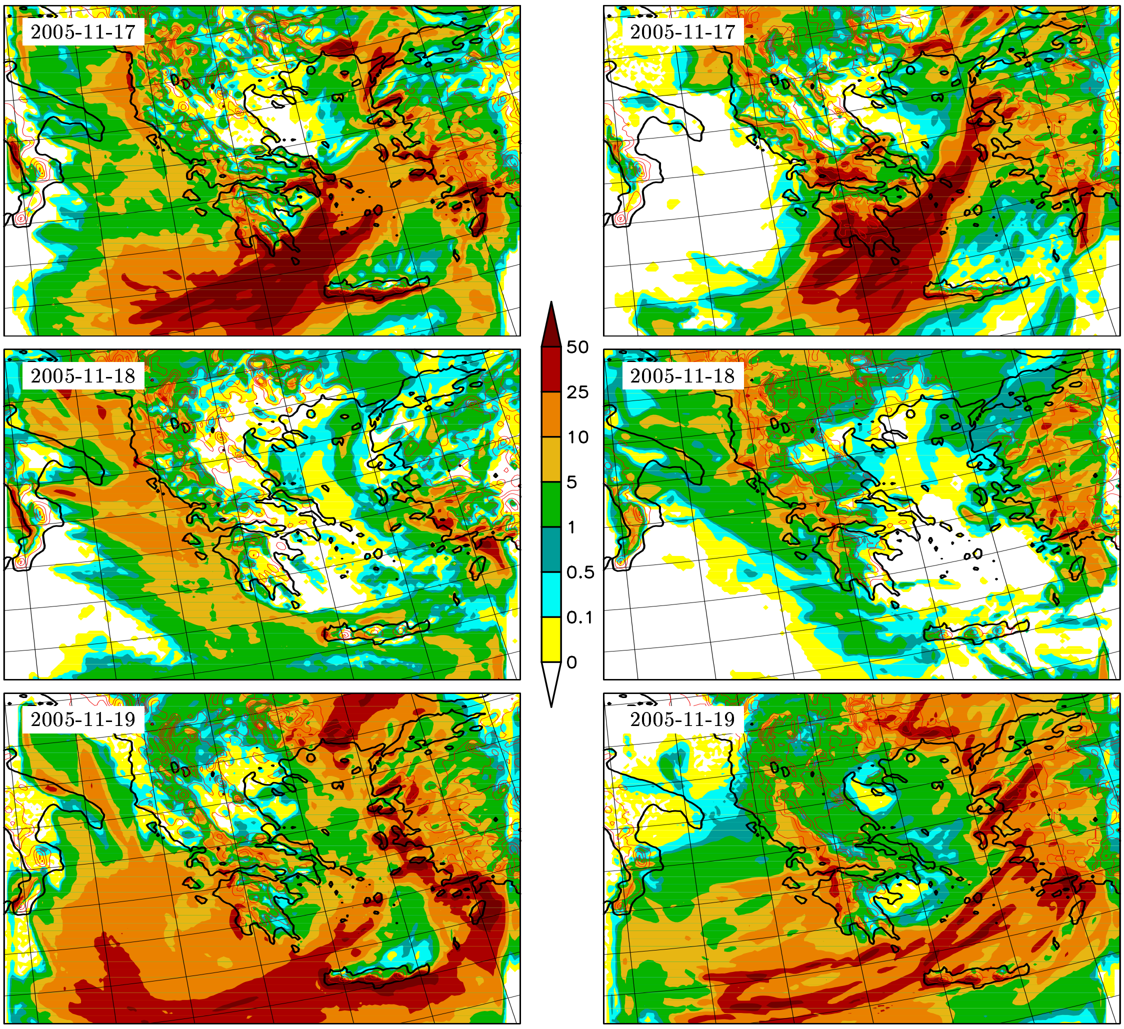

Figure 5: 12-hour accumulated precipitation (mm) from LM_TF (left column) and LM_Z (right column).

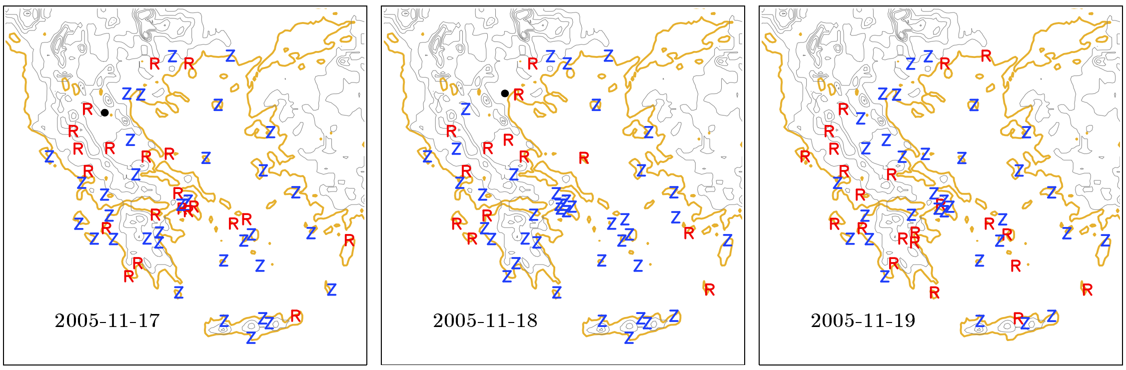

Figure 6: Represantation of the positions of the meteorological stations in reference to the relation of measured against the 12-hour accumulated precipitation; "R" and "Z" stand for stations where LM_TF and LM_Z forecast was closer to observation respectively. The "bullet" sign stands for stations where no precipitation was observed or forecasted by any version of LM.

A Revised Cloud Microphysical Parameterization for COSMO-LME

A. Seifert

Deutscher Wetterdienst, Kaiserleistr. 42, D-63067 Offenbach am Main, Germany

1 Introduction

Quantitative precipitation forecasting (QPF) is one of the major applications of limited-area numerical weather prediction (NWP) models. With a limited-area NWP model, like the 7-km COSMO-LME at DWD, the detailed orography and the explicit simulation of mesoscale dynamical structures should lead to an increased forecasting skill compared to global models with coarser horizontal resolution.

Unfortunately, the last years have shown some problems with the precipitation forecasts of COSMO-LME. For example, an overestimation of orographic precipitation, a too frequent occurence of very light precipitation (drizzle) and a general overestimation of the wintertime precipitation amounts.

One possible cause for some of these problems on the meso-β-scale are simplifications within the cloud microphysical parameterization. Therefore a revised version of the COSMO-LME microphysics scheme has been developed and brought into operations.

2 Microphysics of COSMO-LME

The grid-scale microphysics parameterization of COSMO-LME predicts the four hydrometeor species cloud droplets, raindrops, cloud ice and snowflakes using the mixing ratio of each hydrometeor type as prognostic variable and includes horizontal and vertical advection for all species. For most cloud microphysical processes the scheme follows the work of Rutledge and Hobbs (1983) and a detailed description is given in Doms and Schättler (2004). At DWD this scheme has been operational since 16 September 2003.

As an attempt to improve the mesoscale precipitation structures predicted by COSMO-LME several modification have been made recently:

- The Kessler-type autoconversion/accretion scheme has been replaced by the parameterization of Seifert and Beheng (2001) assuming a constant cloud droplet number concentration of 5×10^8 m^{-3}.
- Based on measurements of Field et al. (2005) a new parameterization of the intercept parameter $N_{0,s}$ of the exponential snow size distribution

  $$f(D) = N_{0,s} \exp(-\lambda D),$$

  is introduced, replacing the constant $N_{0,s} = 8 \times 10^5$ m^{-4} in COSMO-LME. In the revised scheme the intercept parameter is parameterized as a function of temperature T and snow mixing ration q_s by:

  $$N_{0,s} = \frac{27}{2} a(3,T) \left(\frac{q_s}{\alpha}\right)^{4-3b(3,T)}$$

  with $\alpha = 0.069$. The functions $a(3,T)$ and $b(3,T)$ are given by Table 2 of Field et al. (2005).

Especially at cold temperatures this leads to a higher intercept parameter, i.e. smaller snowflakes which fall out much slower.

- For the autoconversion of cloud ice and the aggregation of cloud ice by snow a temperature dependent sticking efficiency has been introduced similar to Lin et al. (1983):

$$e_i(T) = \max(0.2, \min(\exp(0.09(T - T_0)), 1.0))$$

with $T_0 = 273.15$ K.

- The geometry of snow has been changed to a mass-diameter relation of $m = \alpha\ D^2$ with $\alpha = 0.069$ and a terminal fall velocity of $v = 15\ D^{1/2}$ with D in m, m in kg and v in m/s.

Overall these changes lead to a slower formation of rain and snow as well as a reduced sedimentation velocity of snow. The terminal fall velocity of snow of $v = 15\ D^{1/2}$ is somewhat lower than usually assumed based on observations or labratory measurements. This 'tuning' can be justified by the fact that a 7-km model cannot yet fully resolve the updraft structures of mesoscale orography, as e.g. shown by Garvert et al. (2005) who compare simulations with 4 km and 1.3 km resolution with observations.

3 Results

Figure 1 shows two example forecasts of 11 January 07 and 22 December 06. For 11 Jan COSMO-LME overestimates the orographic precipitation in the mountainous regions of Germany. This effect is reduced with the new version of the cloud microphysics scheme (LMEp). The COSMO-LME forecast of 22 Dec 06 shows widespread light precipitation in Brandenburg and Sachsen (East Germany) which was not observed. The LMEp with the new microphysics does not show this problem. In a test period of 6 weeks the new version showed a significant improvement in the TSS and FBI of surface precipitation (not shown).

4 Summary and Conclusions

The new version of the COSMO-LME microphysical scheme has been tested in an operational setup including data assimilation over several weeks in December 2005 and December/January 2007. The results show a better representation of orographic precipitation, e.g. reducing the common overestimation over the Black Forest mountains, and a reduction of drizzle events. Both leads to an improved QPF skill during wintertime and demonstrates the importance of cloud microphysics on the mesoscale. Unfortunately, but not unexpected, the general overestimation of wintertime precipitation cannot be cured by this change of the microphysical parameterization. The revised microphysics scheme is now in operation in the 7-km COSMO-LME at DWD since 31 January 2007 9 UTC.

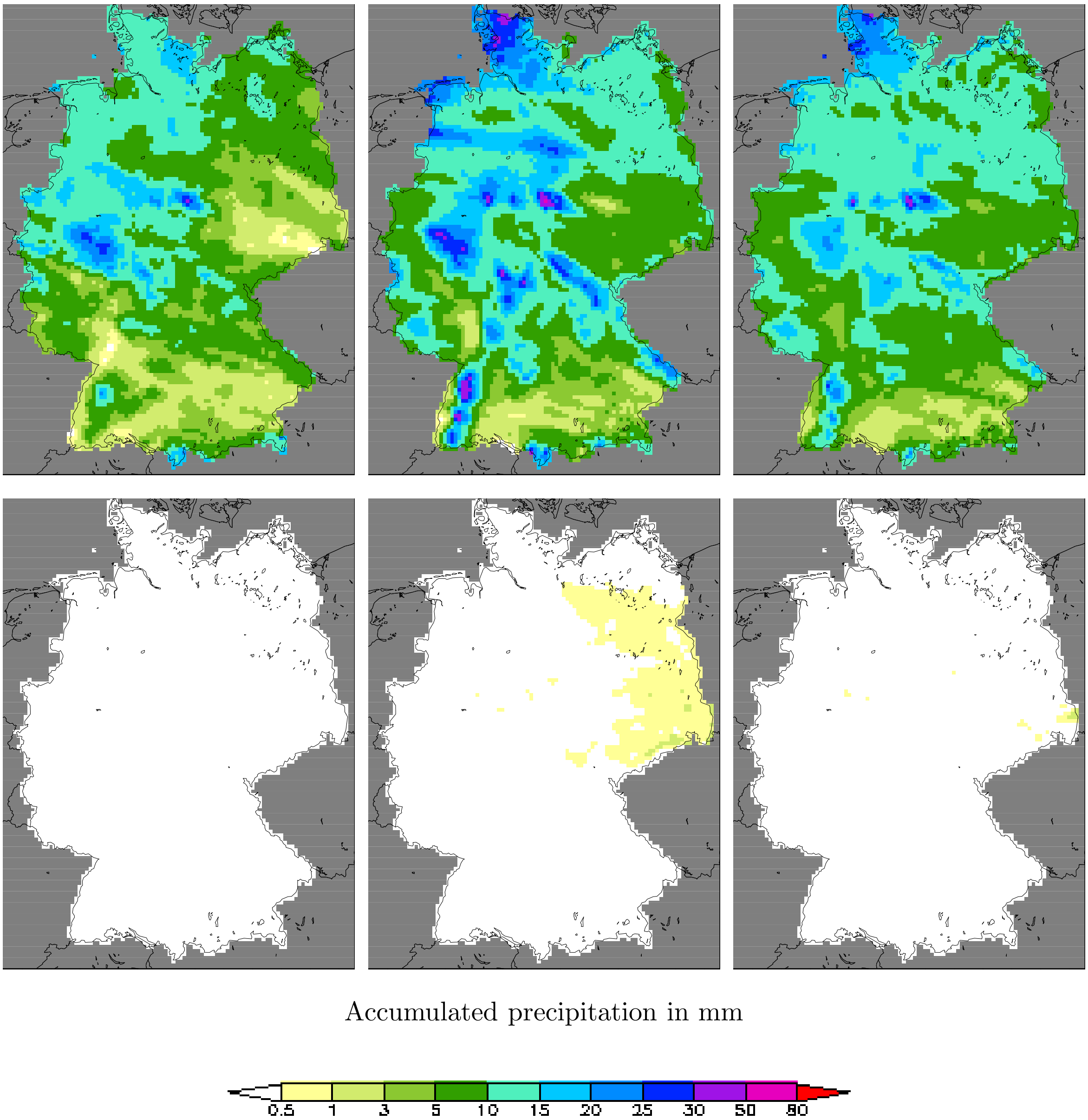

Figure 1: Accumulated precipitation 06-06 UTC from 00 UTC forecasts of 11 Jan 07 (top) and 22 Dec 06 (bottom). Shown are observations (left), LME: old microphysics (middle), LMEp: revised microphysics (right)

References

Rutledge, S.A., P.V. Hobbs, 1983: The Mesoscale and Microscale Structure and Organization of Clouds and Precipitation in Midlatitude Cyclones. VIII: A Model for the 'Seeder-Feeder' Process in Warm-Frontal Rainbands, *J. Atmos. Sci.*, **40**, 1185-1206.

Doms G., J. Förstner, E. Heise., H.-J. Herzog, M. Raschendorfer, R. Schrodin, T. Reinhardt, G. Vogel, 2005: A Description of the Nonhydrostatic Regional Model LM. Part II: Physical Parameterizations, *Deutscher Wetterdienst*, Offenbach, 139 pages. Available at: www.cosmo-model.org.

Seifert, A., K. D. Beheng, 2001: A double-moment parameterization for simulating autoconversion, accretion and selfcollection, *Atmos. Res.*, **59-60**, 265–281.

Field P.R., R.J. Hogan, P.R.A. Brown, A.J. Illingworth, T.W. Choulartona, R.J. Cotton, 2005: Parametrization of ice-particle size distributions for mid-latitude stratiform cloud, *Quart. J. Roy. Met. Soc.* **131**, 1997–2017.

Lin Y.-L., R.D. Farley, H.D. Orville, 1983: Bulk parameterization of the snow field in a cloud model, *J. Clim. Appl. Meteorol.*, **22**, 1065–1092.

Garvert M.F., B.A. Colle, C.F. Mass, 2005: The 13-14 December 2001 IMPROVE-2 Event. Part I: Synoptic and Mesoscale Evolution and Comparison with a Mesoscale Model Simulation, *J. Atmos. Sci.*, **62**, 3474–3492.

Romanian Contribution in Quantitative Precipitation Forecasts Project

Rodica Dumitrache, Victor Pescaru, Liliana Velea, Cosmin Barbu

National Meteorological Administration, Bucharest, Romania

1. Introduction

The performance of LM model on Romanian territory is evaluated by means of objective and subjective verification for the period of February-August 2005, corresponding to first preoperational model runs in NMA Bucharest. Combination of these methods will facilitate the understanding of model limits and its capacity to simulate realistically physical processes on the integration domain and will suggest directions of improvement of model performances. Some special weather situations are investigated concerning quantitative precipitation forecast, using LM Romanian operational version and LM standard version, and the results of a qualitative analysis for three studied cases are presented.

Starting from March 2005, LM model is run in a pre-operational regime in NMA, Bucharest. The assessment of model performances has been done by objective verification measures as well as by subjective evaluation methods. The aim of this paper is to make a comparison between the observed precipitations and simulated precipitation fields from both LM versions. Regarding the forecast precipitations we can conclude that there are some situations where the simulated field is very realistic, but in general both model versions overestimate. There are also few centers of high amounts with location errors. LM Romanian operational version is integrated using a 14 km horizontal resolution and 35 vertical levels. The time step is 80s. Initial and lateral boundary conditions are provided by GME run for 00 UTC, with a frequency of updating LBC of 3 hour. The two-category ice scheme is used for grid-scale precipitation and Tiedtke scheme is used for convection parameterization. There is no data assimilation. The forecast anticipation is 54 hour.

2. Parallel experiments

In order to identify the characteristics of cases with very poor performance of LM model on Romanian territory with respect to precipitation, the results of pre-operational runs of the model in the period February-September 2005 were compared with the observed fields of precipitation. The comparison was only a qualitative one and it has been restricted to the Romanian territory, where observational data from stations were available. The comparison allowed to choose some extreme cases, characterized by:

- Errors in the location of area with, mainly, heavy precipitation.
- Significant over- or underestimation of observed amounts, that is at least twice larger / smaller than observed.

The seven cases selected took place in May-June-July, a period characterized in general by very intense precipitation in Romania. For these cases, the analysis concentrates on:

- Analysis of the synoptic situation.

- Comparison with the observed field of precipitation with respect to location and amounts.
- Type of precipitation (in reality and in the model).
- Comparison of 24 hour and 48 hour anticipation for each case.

In choosing the significant cases, we did not start with the analysis of seasonal verification, since our data set used here covers only 8 months. Instead, daily qualitative analysis of model results, using also the input from forecasters, showed that May-July and September were periods characterized by heavy precipitations, thus meaningful for the aim of this report.

The situations analyzed here represent episodes when precipitations over Romania were mainly of frontal nature, but having, each time, a support in the middle troposphere due to some cold troughs moving toward Romania. The geographical position of our country determines the existence of two principal frontal approaches: on one hand, there are the systems associated with baric depressions in Mediterranean Sea, often extended toward Black Sea, and on the other hand the category of West-North-West approaches, in this case the frontal systems being associated to the trough of Icelandic Low. An intermediate situation between the two categories, often generating heavy precipitation in Romania, is represented by cases when the trough of Icelandic Low extends until the Mediterranean basin. A cold advection, well defined in the middle troposphere, accentuates the ascending and contributes to reactivate the cyclonic processes near the surface, generating, too, important quantities of precipitations.

23 June 2005

In the middle troposphere, the development, toward central and southern part of the continent, of the trough associated to the baric low over Russian Plain favored the penetration of cold air mass over the Romanian region. In the second part of the day and during night the axis of the trough was located over Romania, the closed nucleus accentuating the ascending motion in the eastern and southeastern regions. In the lower troposphere, the mass separation was manifested through a cold atmospheric front, which crossed Romania from NW to SE. The real location of the altitude nucleus during the night, more to the north than it is simulated in the model, might explain the underestimation of precipitation in the model for Eastern Carpathians. On the other hand, the values for the geopotential at 500 mb (Fig. 2) are lower than in reality, which may be the reason for the excessive quantities forecasted for the extreme east of the country.

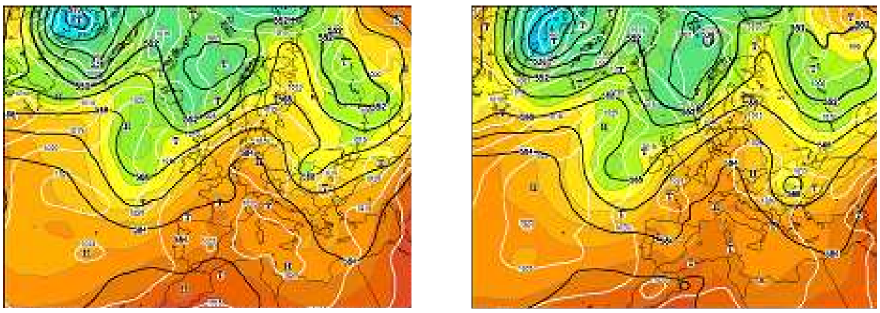

Figure 1: Synoptic situation (GME reanalysis) for 23.06.2005: 12 UTC (left) and 24 UTC (right).

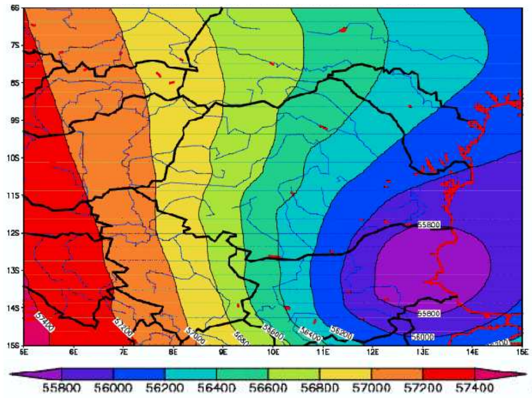

Figure 2: Geopotential field at 500mb, for 23.06.2005, 30h anticipation.

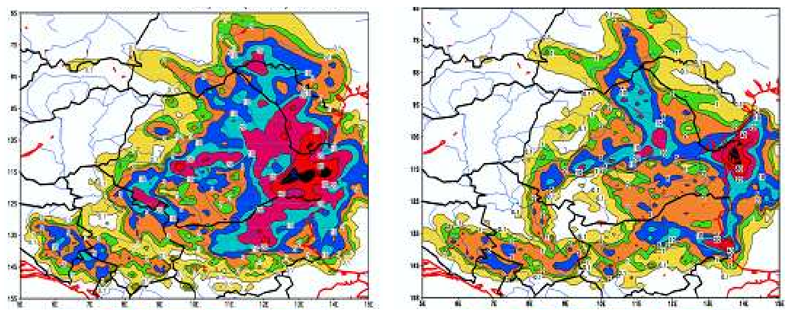

Figure 3: Operational Romanian version. 24 hour accumulated precipitation for 23.06.2005: 24 hour anticipation (left); 48 hour anticipation (right).

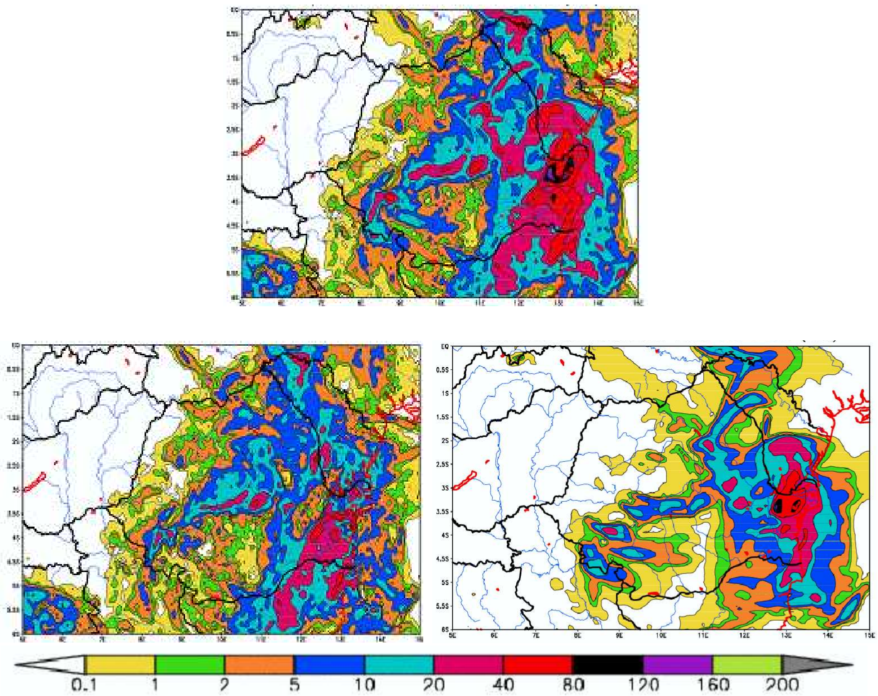

Figure 4: Standard version. 24 hour accumulated precipitation, for 23.06.2005: total precipitation (above); convective precipitation (below left); grid scale precipitation (below right).

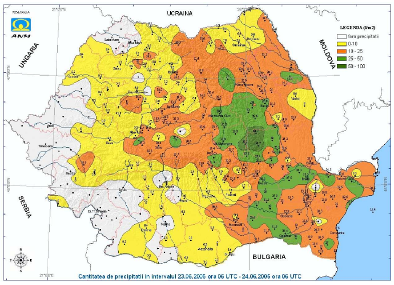

Figure 5: 24 accumulated observed precipitation for 23.06.2005.

For 24 hour anticipation, both model versions Romania operational LM (14 km) and standard version LM (7 km), show a false maxima in the SW of the country (about 40 l/m^2 in the model, no observed precipitation). The eastern part of the country is in generally overestimated, more specifically in SE (Dobrogea region) there is a strong overestimation in the models (about 80-120 l/m^2), while in the observed field, the values are around 15-20 l/m^2. In this region the convection seems to play in important role in the model, leading to about 55 l/m^2 in 24hour. In this case, the overestimation in all regions seems to be determined by convective processes. The operational version simulated field at 48 hour anticipation is very similar with respect to spatial distribution, but with smaller values, especially in the East, thus being more realistic for this area.

02 July 2005

The tropical air mass, from the previous case, still persists at the beginning of the interval 2-3 July over the south of the continent but it was slowly replaced by a mass with polar characteristics, associated to troughs in Nordic regions. One of these troughs extends significantly toward south, forming a closed nucleus over south-western part of Romania. The pressure field at surface presents a low in the eastern basin of Mediterranean Sea, in extension toward Black Sea, having an energetic support from the altitude nucleus. In these conditions, there was precipitation in the most parts of the country. The model overestimated the quantities in East, where, in reality, the altitude ridge blocking persisted (too fast trough evolution to east in the model?)

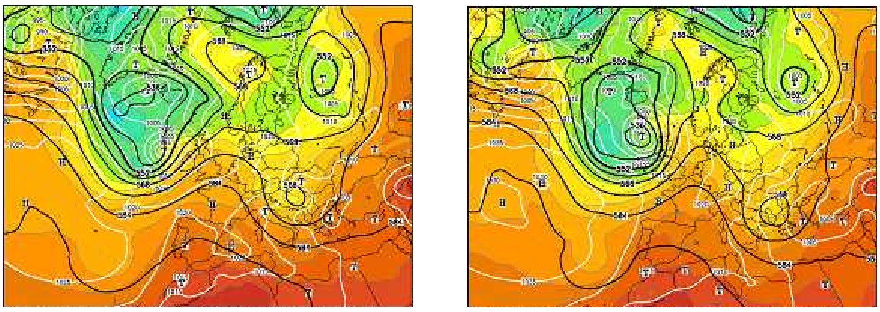

Figure 6: Synoptic situation (GME reanalysis) for 02.07.2005: 12 UTC (left) and 24 UTC (right).

In NE-E of the country where no precipitation was observed, both models overestimated the quantity of precipitation (40 l/m^2 simulated). The high precipitation amounts, simulated by the models in extreme West, intra-Carpathian region and in the south-eastern part of South Carpathians, were not observed in reality. At the same time, the area with high amounts of precipitation observed (66-110 l/m^2) is significantly underestimated by both model versions

(20 l/m^2 in the models). There is a little bit difference between LM Romanian operational version and LM standard version. In the LM standard version you can see that the position of center with the high precipitation amounts is slightly moved to the west. For the anticipation of 48 hour, the eastern part of the country is better simulated by the Romanian operational version, while there still is an overestimation on a small region in the W-NW, but in the rest of the country the amounts are underestimated, like in the previous cases.

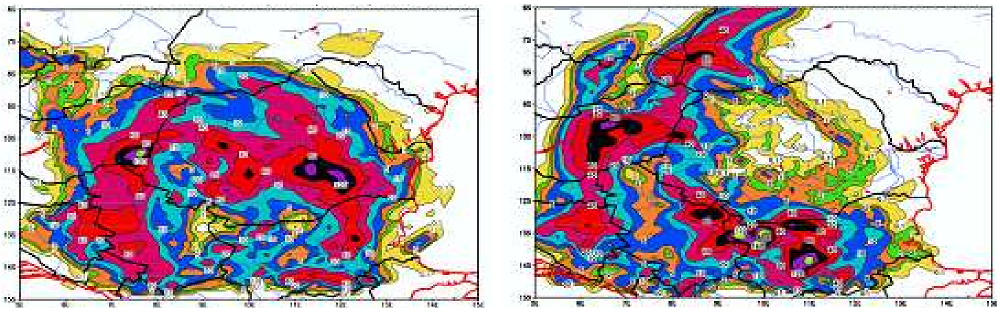

Figure 7: Operational Romanian version. 24 hour accumulated precipitation for 02.07.2005: 24 hour anticipation (left); 48 hour anticipation (right).

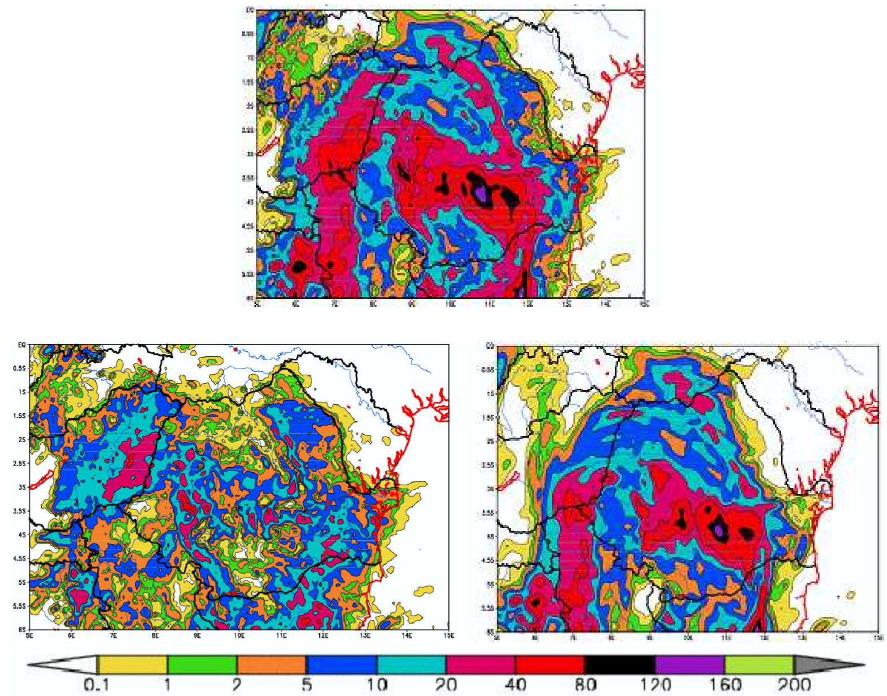

Figure 8: Standard version. 24 hour accumulated precipitation, for 02.07.2005: total precipitation (above); convective precipitation (below left); grid scale precipitation (below right).

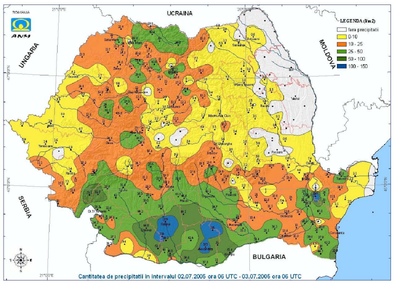

Figure 9: 24 accumulated observed precipitation for 02.07.2005.

12 July 2005

The circulation in the middle troposphere between 11-13 July was ultra-polar, meaning that over North-East of Europe the geopotential had very low values, looking like a vast trough, with a NE-SW axis. This structure assures the transport of polar air mass from the extreme north of the continent and Polar Seas toward center and South of Europe. Over the Mediterranean basin, the air mass enriched its moisture, afterward being drawn on a south-western component of the flow toward our country. The ultra-polar circulation is specific to cold season, when very cold arctic and polar air masses penetrate fast and easy until and over the Mediterranean basin. It is a less common situation for the warm season, especially because it persisted for three days. It should be noticed, too, the isolated cold nucleus in the Romanian region surface, the gradual decrease of pressure in the western part of the country, together with the extension and enforcement of the anticyclone in the NW, suggest the organization of a frontal system, the contrast in the air masses being secured by advection from the East of Mediterranean Sea. In these conditions, in Romania there was precipitation in all regions, more important quantitatively in the first day (11 July) in SE, center of the country and in the mountains, and in the second day in east of the country. The model overestimates the amounts of precipitation in NE, probably due to a faster advance to the east of the altitude nucleus.

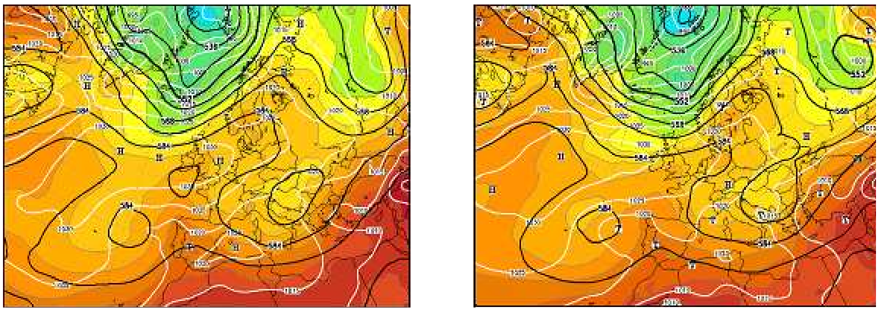

Figure 10: Synoptic situation (GME reanalysis) for 12.07.2005: 12 UTC (left) and 24 UTC (right).

The operational LM simulated precipitation field for 24 hour anticipation shows that for the SE and littoral area the amounts are in general overestimated, but not in a very high degree. Also an overestimation is found for the NW of the country, where the model shows up to 40 l/m^2, while in the observations there are amounts of 10 l/m^2 for this area. The general spatial distribution is well reproduced and also the center of maximum amounts near the Carpathians Bend. For the 48 hour anticipation there are more significant errors compared with the observed precipitation field: there are no precipitation in East of the country (in observations there are 10-60 l/m^2); the band of intense precipitation is located in the SW, in the model, while in reality it is on E-SE; West of the country is strongly overestimated. In LM standard version the precipitation amounts are underestimated in the Western part of the country and littoral area (1-2l/m^2 observed - 40-80 l/m^2 simulated). There are also two other regions (SW and SE of Romania) where the precipitation amounts are overestimated (100-150 l/m^2 observed - 10-20 l/m^2 simulated).

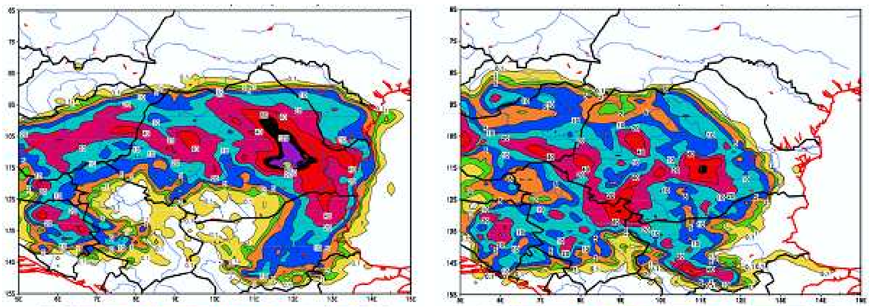

Figure 11: Operational Romanian version. 24 hour accumulated precipitation for 12.07.2005: 24 hour anticipation (left); 48 hour anticipation (right).

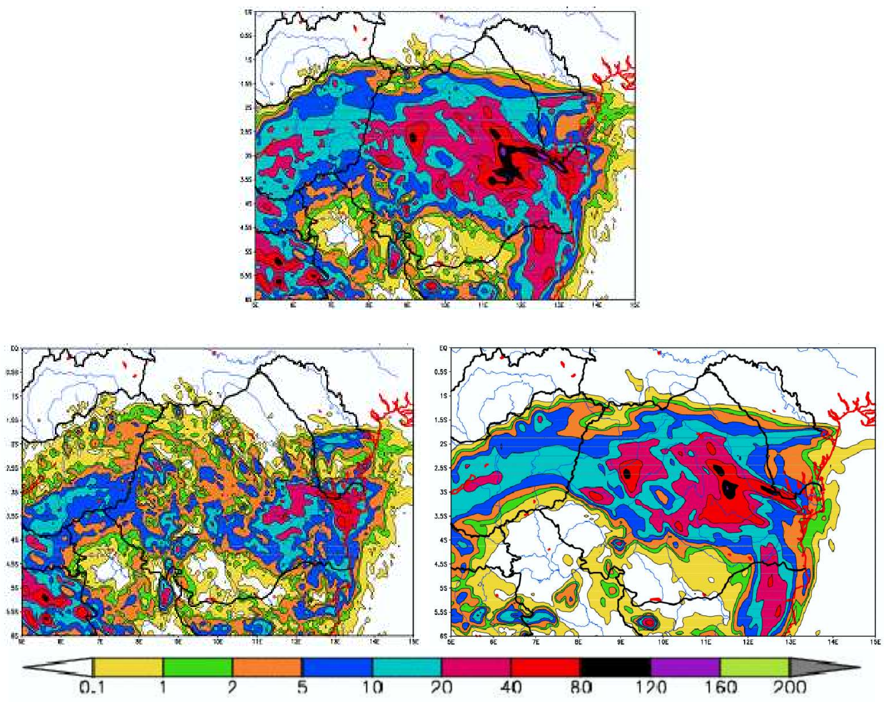

Figure 12: Standard version. 24 hour accumulated precipitation, for 12.07.2005: total precipitation (above); convective precipitation (below left); grid scale precipitation (below right).

3. Conclusion

A qualitative comparison between the observed and simulated precipitation field for both models, LM Romanian operational version and LM standard version, was done. For this kind of analysis 10 cases with poor QPF from February to September 2005 were selected. The choice of these cases was done using two main criteria:

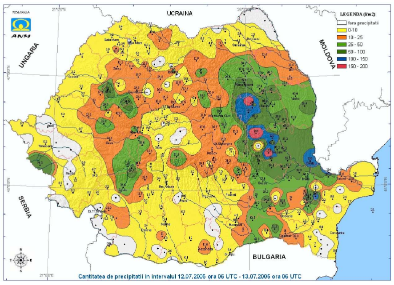

Figure 13: 24 accumulated observed precipitation for 12.07.2005.

- Errors in location of important amounts of precipitation and with regard to the extension of the area with intense precipitation.
- Significant over- or underestimation, especially of the heavy precipitation

Also, a qualitative comparison was done between the model forecast with 24 hours and 48 hours anticipation, for the same day. In all cases, the precipitation was determined mainly by frontal systems, being accentuated by convection in some areas for some situations (31 May, 19 July). In most of the cases the precipitations were quantitatively overestimated and regions with high amounts present only in the model (false maxima) are found in 5 cases (31.05, 23.06, 30.06, 2.07, 19.07), some determined by strong convection in the model (e.g. 23.06). However, there was one case with significant underestimation of observed precipitation, namely 19.07. Also, in few cases, errors in location of areas with important precipitations are found in the model. Comparing the results from the 24h and 48 h anticipation for Romanian operational version, it seems that possible causes for these errors in QPF forecast, for these cases, may be: a simulated large-scale circulation faster than in reality (e.g. for 04.05, 19.05, 02.07, 11.07); lows of geopotential at 500 mb are deeper in the model than in the German analysis (e.g. for 23.06); or improper estimation/simulation of specific humidity in the considered area (e.g. for 31.05, 19.07).

References

Baldauf, M. and J.-P. Schulz, 2004: Prognostic Precipitation in the Lokal Modell (LM) of DWD. *COSMO Newsletter*, No. 4, 177-180.

Doms, G. and J. Förstner, 2004: Development of a Kilometer-Scale NWP-System: LMK. *COSMO Newsletter*, No. 4, 159-167.

Gassmann, A., 2003: Case Studies with the 2-Timelevel Scheme and Prognostic Precipitation. *COSMO Newsletter*, No. 3, 173-176.

Klink, S. and K. Stephan, 2004: Assimilation of Radar Data in the LM at DWD. *COSMO Newsletter*, No. 4, 143-150.

Leuenberger, D. and A. Rossa, 2003: Assimilation of Radar Information in aLMo. *COSMO Newsletter*, No. 3, 164-172.

Evaluation of the Kain-Fritsch/Bechtold Convection Scheme

Silke Dierer and Francis Schubiger

Federal Office of Meteorology and Climatology, MeteoSwiss, Switzerland

1 Introduction

Horizontal resolution of today's operational weather prediction models is not yet high enough to resolve convection. Schemes to parameterize convection differ regarding the trigger function forcing the onset of convection, the closure assumption and the cloud model. The operational runs of the Swiss implementation of the COnsortium for Small-scale MOdeling (COSMO) model are performed using the mass-flux scheme developed by Tiedtke (1989). The scheme is based on a moisture convergence closure and was originally developed for applications on the global scale. For simulations with much smaller grid sizes (e.g. 7 km) a convection closure based on convective available potential energy (CAPE) - as used in the scheme by Bechtold et al. (2001) - might be more suitable.

Both convection schemes, the Tiedtke and the Kain-Fritsch/Bechtold (KF/B) scheme, are mass flux schemes. The main difference is the closure assumption that is based on moisture convergence in the Tiedtke scheme and on CAPE in the KF/B scheme. Besides, the two schemes differ regarding the trigger mechanism. In the Tiedtke scheme convection is triggered if the parcel's temperature exceeds the environment temperature by a fixed temperature threshold of 0.5 K. In the KF/B scheme the onset of convection depends on the large-scale vertical velocity. The Tiedtke and the KF/B scheme distinguish penetrative and shallow convection. The Tiedtke scheme additionally considers mid-level convection, convection starting above the planetary boundary layer. This is not separately considered in the KF/B scheme since the trigger criterion is also applied above the PBL. The major differences between the schemes are shown in Table 1.

The KF/B scheme was implemented in the COSMO model version 3.18. Preliminary tests were performed by simulating several cases of summer convection. The results are compared to results with Tiedtke scheme and to measurements. Compared to simulations with Tiedtke scheme the simulations with KF/B scheme tend to have higher average but lower maximum values of 24 hour precipitation. Both schemes overestimate precipitation, but the 12 hour sum of precipitation are slightly better with the KF/B scheme. The maximum of the daily precipitation cycle is delayed by about 2-3 hours resulting in a better agreement with the

	Tiedtke scheme	Bechtold scheme
Trigger	- near surface -updraft source layer $\sim$ model layer thickness - fixed value for ΔT	- near surface and upper levels - updraft source layer $\sim$ 60 hPa - ΔT = f(w)
Closure	- moisture convergence closure	- CAPE closure
En-/Detrainment	- turbulent mixing and organized inflow	- Turbulent mixing

Table 1: Major differences between the Tiedtke and the KF/B scheme.

measured precipitation cycle. A quasi-operational test chain using the KF/B scheme was set up end of May. The comparison of its results with measurements and results of the operational runs for wind, temperature, humidity, cloud cover and precipitation is described in Section 2. Conclusions and outlook are given in Section 3.

2 Results of the test chain with the Kain-Fritsch/Bechtold scheme

2.1 Description of the test chain with Kain-Fritsch/Bechtold scheme

The test chain using the KF/B scheme runs in a quasi-operational mode, equivalent to the operational runs for 00 UTC. Initial conditions are taken from the operational assimilation run using the Tiedtke scheme and lateral boundary values are interpolated from IFS data. The simulation period is 72 hours. The results of the operational runs and of the KF/B test chain are evaluated by comparison with the ANETZ measurements from 20 May to 31 October 2006.

2.2 Diurnal cycle of precipitation and cloud cover

The runs with Tiedtke and with KF/B scheme overestimate the measured precipitation. The overestimation is higher in the simulations using the KF/B scheme, mainly due to higher precipitation amounts in flat regions (Figure 1, lower panel, left). The frequency bias (Table 2) shows that the runs with KF/B scheme overestimate thresholds of 0.1 and 2 mm by 72% and 45%. The overestimation of light precipitation is lower for the operational run.

The percentage of observed cases with thresholds of 10 to 50 mm/6h is 2.3% and, thus, small.

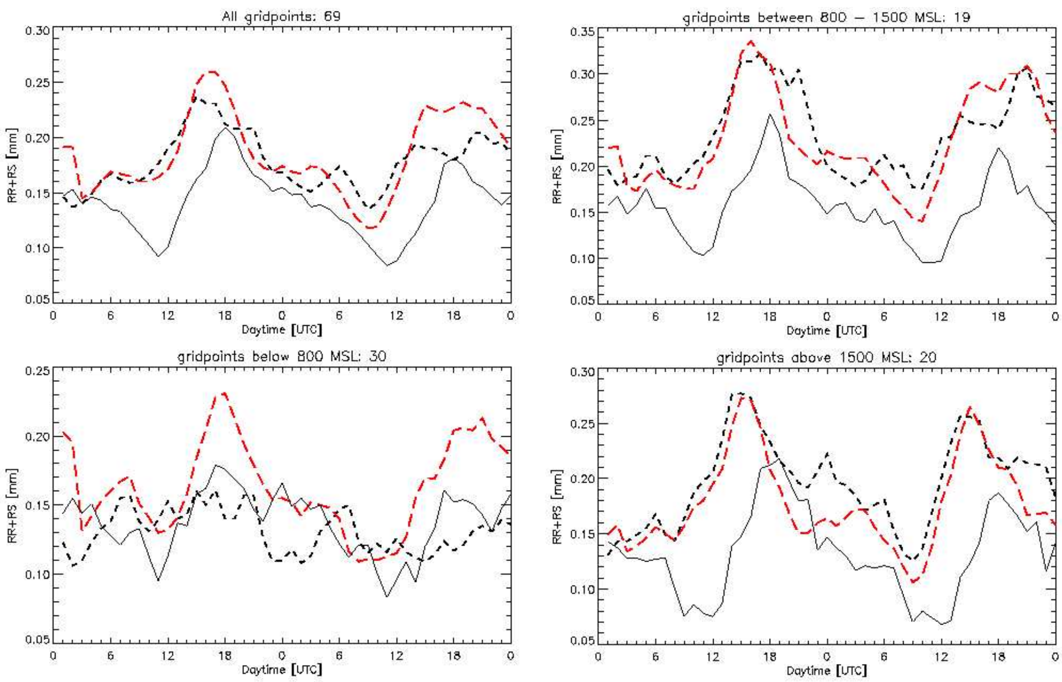

Figure 1: Diurnal cycle of precipitation of all stations (upper panel, left), stations below 800m (lower panel, left), stations between 800m and 1500m (upper panel, right) and above 1500m (lower panel, right). The figure shows measurements (black line), results with the Tiedtke scheme (black dashed line) and results with the KF/B scheme (red dashed line).

Frequency bias, threshold [mm/6h]	operational	Kain-Fritsch/Bechtold
0.1	148	172
2	123	145
10	112	100
30	230	84
50	362	54

Table 2: Frequency bias for the simulations with Tiedtke and KF/B scheme (mean of all 6h sums from +6h to +48 hours forecast time).

The operational runs strongly overestimate the amount of precipitation resulting from thresholds above 30 mm/6h (Table 2). The runs with KF/B scheme underestimate precipitation sums with thresholds above 10 mm (Table 2). The two schemes are more similar in regions where precipitation is strongly influenced by orography (Figure 1, lower panel, right).

The diurnal cycle of precipitation is too early in the operational runs and in the runs with KF/B: precipitation starts too early and reaches its maximum too early. The simulations with the KF/B scheme show a better agreement with the measurements, since the maximum of precipitation occurs about 2 hours later than in the operational runs. The time shift mainly occurs in flat areas, where the time of maximum precipitation is in good agreement with the measured one. The operational simulations with the Tiedtke scheme show hardly any diurnal cycle (Figure 1, lower panel, left). For stations above 1500 m the maximum of precipitation in the operational runs is about 4 hours too early, the KF/B scheme slightly improves the timing by delaying the maximum by 1 hour.

The simulations with KF/B scheme show enhanced precipitation during the first hours of the simulation (Figure 1, upper panel, left), mainly caused by precipitation in flat regions. The assumption that the spin up effect might be caused by taking initial conditions from the operational assimilation run using the Tiedtke scheme is investigated. A period with enhanced precipitation in the first few hours (5th to 7th of July 2006) is simulated. Taking the initial conditions from an assimilation run with KF/B scheme does not solve the problem of enhanced precipitation at the beginning of the simulation. Simulations are started at 00

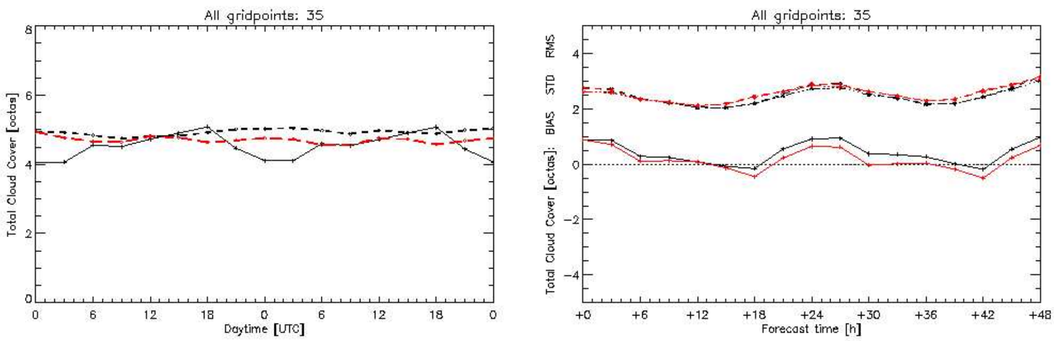

Figure 2: Diurnal cycle of cloud cover (left) and diurnal cycle of cloud cover bias, standard deviation and root mean square error (right). Left: the figure shows measurements (black line), results with Tiedtke scheme (black dashed line) and results with KF/B scheme (red dashed line). Right: the figure shows bias (full line), standard deviation (dashed dotted line) and root mean square error (dashed line) of results with Tiedtke scheme (black) and KF/B scheme (red).

UTC and 12 UTC. The spin up occurs in both simulations and, thus, rules out that the spin up is a consequence of night time meteorological conditions. Further investigations reveal that precipitation is strongly overestimated in regions that provide conditions for convection. Thus, the location of precipitation is correct, but the amount of precipitation is by far too high. After the first 3 hours the simulated precipitation amount is reasonable. Further investigations are carried out in order to prevent the spin-up effect.

The diurnal cycle of cloud cover is not reproduced by the operational run and neither by the run with KF/B scheme. With both schemes, the results show hardly any diurnal cycle. After 15 hours simulation time, when convection starts, the cloud cover in the runs with KF/B scheme gets about 0.3 octa smaller than in the operational runs. The deviation remains constant for the rest of the simulation. Both schemes show overestimation of cloudiness during night and a slight underestimation in the afternoon. The bias of cloud cover is slightly better with the KF/B scheme.

Preliminary investigations show that the main difference occurs for high clouds. For the results with KF/B the cloud ice tendency calculated within the convection scheme was not used for the prognostic cloud ice calculation. This deficiency was corrected and its impact was tested. The effect is very small and does not explain the difference between the runs with Tiedtke and KF/B scheme. Further investigations are carried out in order to understand the cloud cover differences.

2.3 Diurnal cycle of wind, temperature and dew point temperature

The 10m-wind speed is overestimated with Tiedtke and KF/B scheme. In the simulations with KF/B scheme the maximum of wind speed is about 0.15 m/s lower than in the operational runs reducing the overestimation of about 0.4 m/s. The overestimation of wind speed during night is about 0.1 m/s higher than in the operational run. The simulation of wind direction is hardly changed by the convection scheme.

The diurnal cycle of 2m-temperature shows negligible differences for the Tiedtke and the KF/B scheme. The daytime maximum overestimation is slightly reduced with the KF/B scheme (0.2-0.3 K), while the temperature underestimation during night is slightly increased (0.1 K).

The differences between the two schemes are small for 2m-humidity. Both schemes strongly overestimate humidity. The simulations with KF/B scheme slightly increase the overestimation during the day and slightly increase the underestimation during night. The reduction of night time values is mainly caused by the results for mountainous regions (stations higher than 1500m), while the higher values during the day are mainly caused by the results for flat regions (stations below 800 m).

3 Conclusions and outlook

The test chain using the KF/B scheme ran from 20 May to 31 October 2006. The results are compared to ANETZ measurements and results of the operational runs. Precipitation is overestimated in the simulations with both schemes. The KF/B test chain shows an even stronger overestimation than the operational run due to an overestimation of precipitation amounts below 2 mm/6h in flat regions. Further investigations will be performed in order to reduce this overestimation. The operational run strongly overestimates heavy precipitation events. The KF/B scheme significantly improves the diurnal cycle of precipitation in regions where precipitation is not predominantly affected by orography.

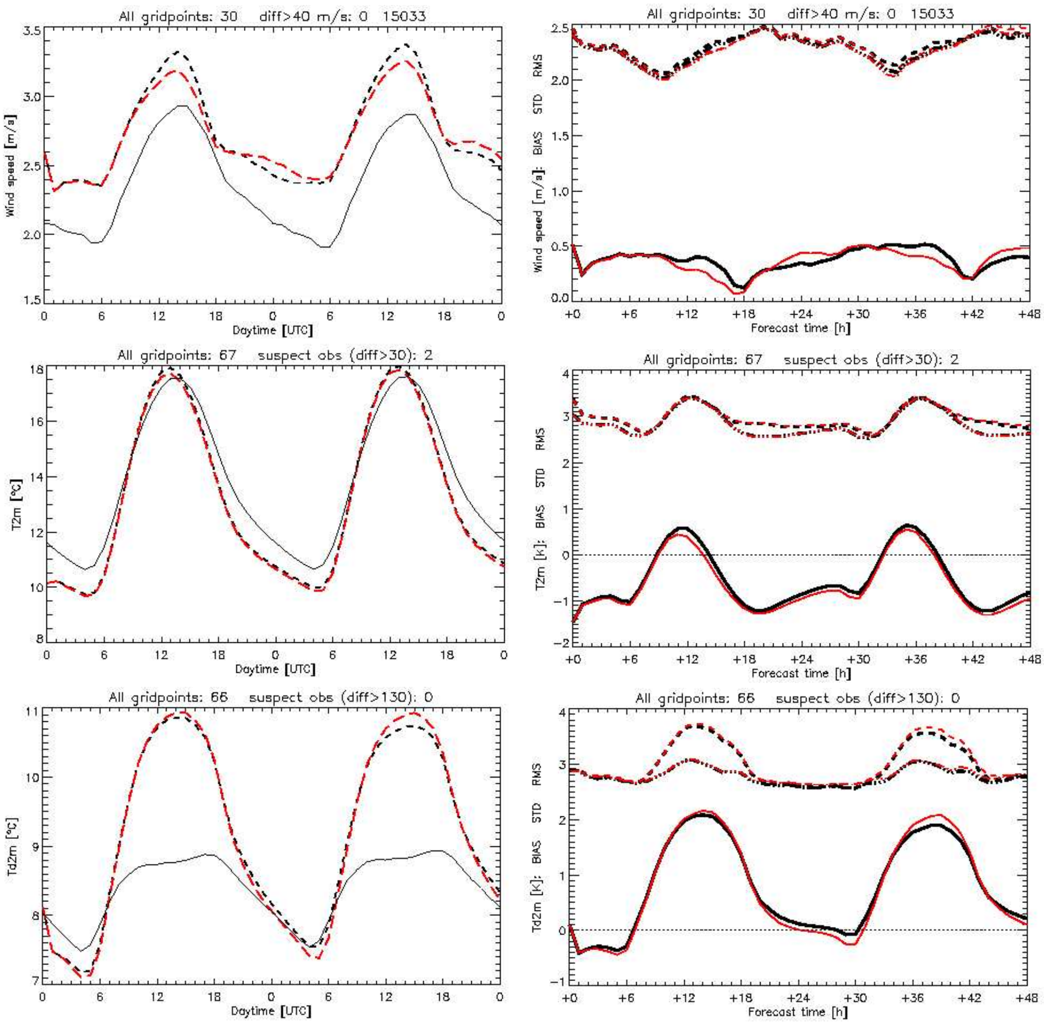

Figure 3: Like Figure 2, but for 10m-wind speed (upper panel), 2m-temperature (middle) and 2m-dew point (lower panel).

The quality of temperature, humidity and wind forecast is similar for the two convection schemes. Differences develop in cloud cover after 15 hours simulation time, when convection starts, and remain constant for the rest of the simulation. The simulation with KF/B has a cloud cover that is reduced by 0.3 octa compared to the operational runs. The bias compared to measured cloud cover is slightly lower with the KF/B scheme while standard deviation is slightly higher, thus, it's not possible to decide which cloud cover is more realistic. The strongest deviations occur for high clouds.

The simulations with the KF/B scheme show an overestimation of convective precipitation in the first 3 hours of the simulation. This spin up effect is not caused by the initial conditions taken from the assimilation with the Tiedtke convection scheme. It also occurs if initial conditions are taken from an assimilation run with KF/B scheme. The spatial distribution of precipitation is simulated correctly, but the amount of precipitation is too high in the first 3 hours. Further studies are carried out in order to investigate the cause of the spin up effect.

References

Tiedtke, M., 1989: A comprehensive mass flux scheme for cumulus parameterization in large-scale models. *Mon. Wea. Rev.*, Vol. 117, 1779-1800.

Bechtold, P.; Bazile, E.; Guichard, F.; Mascart, P. and E. Richard, 2001: A mass-flux convection scheme for regional and global models. *Q. R. J. Meteorol. Soc.*, Vol. 127, 869-886.

The Impact of the Alps on COSMO-LEPS Forecasts for the August 2005 Flood Event

André Walser and Mark A. Liniger

MeteoSwiss, Krähbühlstrasse 58, 8044 Zürich, Switzerland

Cathy Hohenegger

Institute for Atmospheric and Climate Science, ETH Zürich, Switzerland

1 Introduction

In August 2005, heavy precipitation for three days caused tremendous floods in Switzerland and in adjacent neighborhood countries (MeteoSwiss, 2006). A low pressure system over Italy transported warm and very moist air at the eastern edge of the Alps to the northern side where the air impinged on the northern slopes of the Alpine ridge (the mesoscale flow is shown later in Fig. 5). The heavy precipitation period started on August 20. During the following 72 hours, more than 100 mm precipitation occurred in a large area from the western Alps to the north-eastern Alpine foreland. In central Switzerland, more than 150 mm were observed and at some locations even more than 300 mm. Fig. 1 shows a precipitation analysis for the event, derived from about 400 rain gauges and a high-resolution precipitation climatology.

The global ensemble prediction system (EPS) of the European Centre for Medium-Range Weather Forecasts (ECMWF) missed the intensity of this event, while the COSMO-LEPS forecast with initialization time 19.8.2005 1200 UTC provided a very appropriate warning (Walser, 2006). COSMO-LEPS is the limited-area EPS of COSMO. It makes high-resolution ensemble forecast available for central and southern Europe by a dynamical downscaling of selected ECMWF EPS members (see Marsigli et al., 2005) and is particularly benefical for the prediction of extreme weather events (e.g. Walser et al., 2006).

The aims of this study are twofold. First, we investigate the impact of the Alps on the amount and spatial distribution of precipitation for this extreme event. Second, we asses

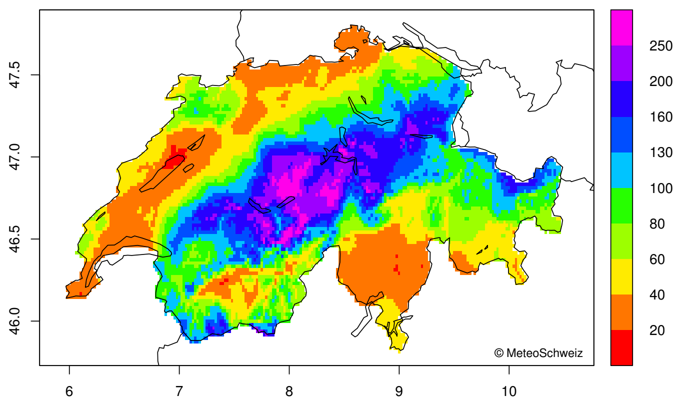

Figure 1: Accumulated precipitation from 20 Aug 2005 0600 UTC to 23 Aug 2005 0600 UTC (courtesy C. Frei, MeteoSwiss).

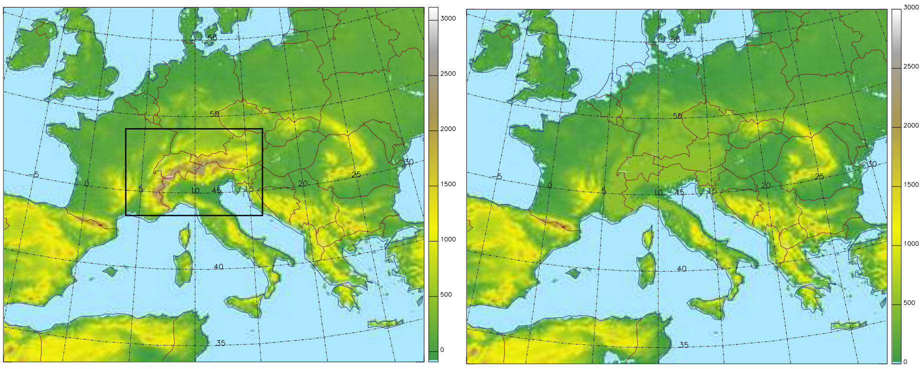

Figure 2: COSMO-LEPS model domain for experiments with (left) operational orography for the OPR experiment and (right) orography limited to 500 m in a rectangle including the Alpine arc for the FLAT experiment. The domain for the HR experiment with 2.2 km horizontal grid-spacing is indicated in the right panel.

the benefit of using a cloud-resolving EPS with a very detailed orography compared to the driving COSMO-LEPS forecast. The outline is as follows: Section 2 presents the experimental set-up of the experiments. Section 3 compares the probabilistic precipitation forecasts for the event with different settings, while Section 4 further analyzes the experiments on the basis of one specific member. Finally, the conclusions are provided in Section 5.

2 Experimental setup

COSMO-LEPS experiments are performed using three different configurations. The first setting corresponds to the operational set-up of COSMO-LEPS with a horizontal grid-spacing of 10 km, hereafter referred to as OPR[2]. For the second setting, referred to as FLAT, the orography is limited to 500 m a.s.l. in a rectangle encompassing the Alpine arc (which includes also the Jura, the Vosges, and the Black Forest). This change in orography required also adaptations of the roughness length. For grid points with reduced orography, the roughness length is set to 0.5 m which is a typical value for the Swiss plateau. The third setting provides a cloud-resolving ensemble for the Alpine region with a grid-spacing of 2.2 km driven by the OPR experiment. The model domains including the orography for the OPR and FLAT experiments are illustrated in Fig. 2. All experiments are based on version 3.19 of the non-hydrostatic limited-area COSMO model (formerly LM; see Steppeler et al. 2003) using the leapfrog kernel.

3 Comparison of probabilistic precipitation forecasts

In this section, probabilistic precipitation forecasts of the three ensemble experiments are compared. We first focus on the experiments OPR and FLAT. Fig. 3 shows probability maps for precipitation between August 20, 0600 UTC and August 23, 0600 UTC, which corresponds to the period with the largest observed 72-h precipitation amounts. The different panels indicate the probability to exceed 50 mm, 100 mm, and 150 mm, respectively. The OPR experiment (panels in middle row) shows high probabilities for large precipitation amounts for the region in which large values were observed (cf. Fig. 1), e.g. more than 60% probability

[2] This ensemble is based on a ECMWF EPS forecast with initial time 19.8.2005 1200 UTC while the operational COSMO-LEPS ensemble for this initial time was based on the ECMWF EPS forecasts for 0000 UTC and 1200 UTC.

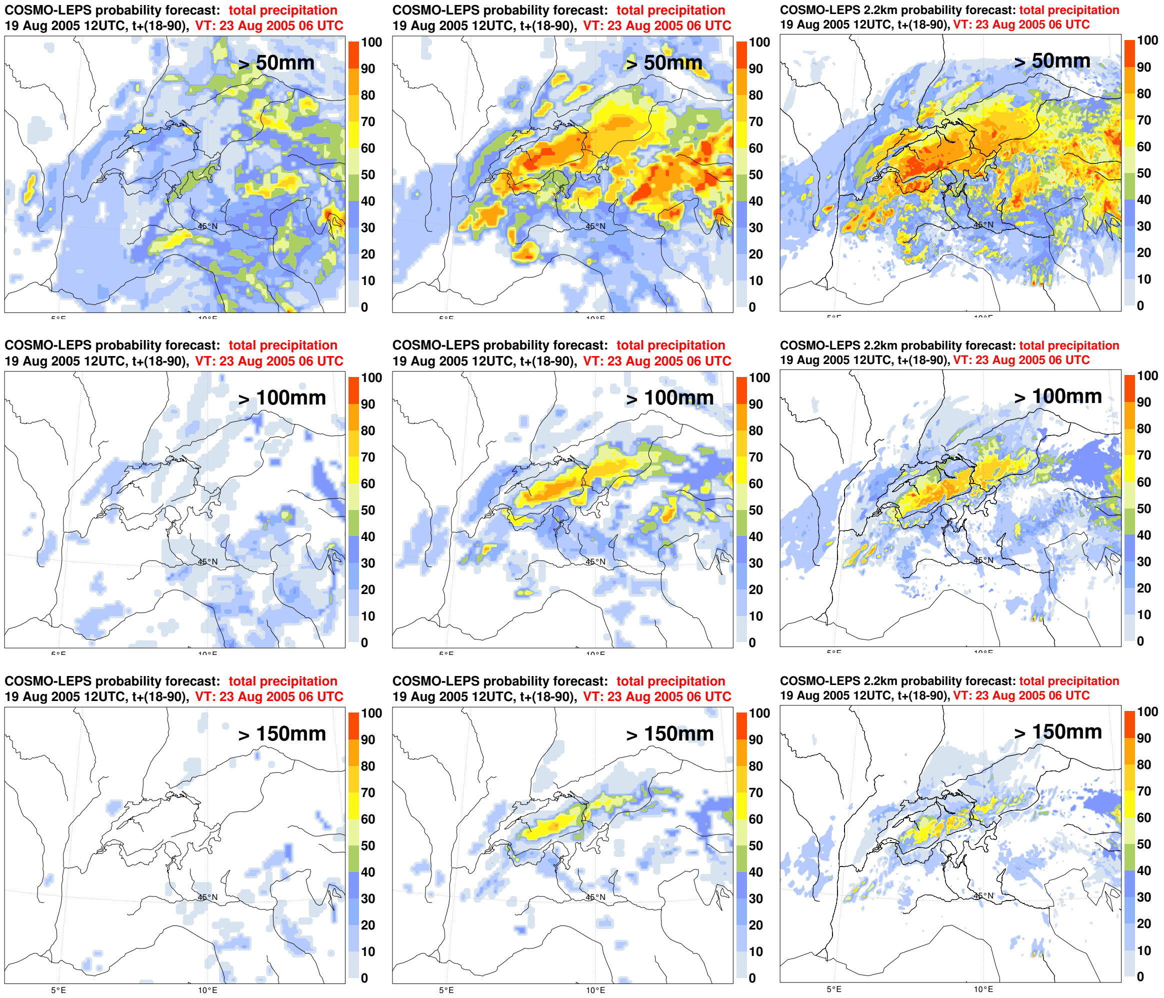

Figure 3: Ensemble experiments for initial time 19.8.2005 1200 UTC. The panels indicate the probability for accumulated precipitation between forecast hours 18-90 exceeding the thresholds 50 mm, 100 mm, and 150 mm, for the FLAT (left), the OPR (middle), and the HR (right) experiments, respectively (see text).

for precipitation exceeding 150 mm on the northern slopes of the Alps. In contrast, the FLAT experiment reveals probabilities of less than 40% for most parts of Switzerland even for the lowest threshold of 50 mm. In addition, the probabilities in this experiment are only marginal or even zero for amounts of more than 100 mm and in particular for more than 150 mm. Only for the Appenine, the FLAT ensemble predicts higher probabilities than the OPR ensemble with the threshold 50 mm.

The FLAT members produce clearly less precipitation compared to the OPR members, and the FLAT members do not compensate the large deficit on the northern slopes with higher precipitation amounts in other regions, although a comparison of the humidity transport does not show significant differences between the two experiments (not shown). Hence, the precipitation efficiency is clearly lower in the FLAT experiment.

For all three thresholds, the HR experiments provides, as expected, probability pattern with higher spatial variability than the OPR experiments, but the larger-scale pattern are very similar with similar amplitudes. This study cannot objectively evaluate the benefit of these local probability information provide by the HR experiments. However, we note some appropriate fine-scale features with regard to the observations (Fig. 1), e.g. no warning for

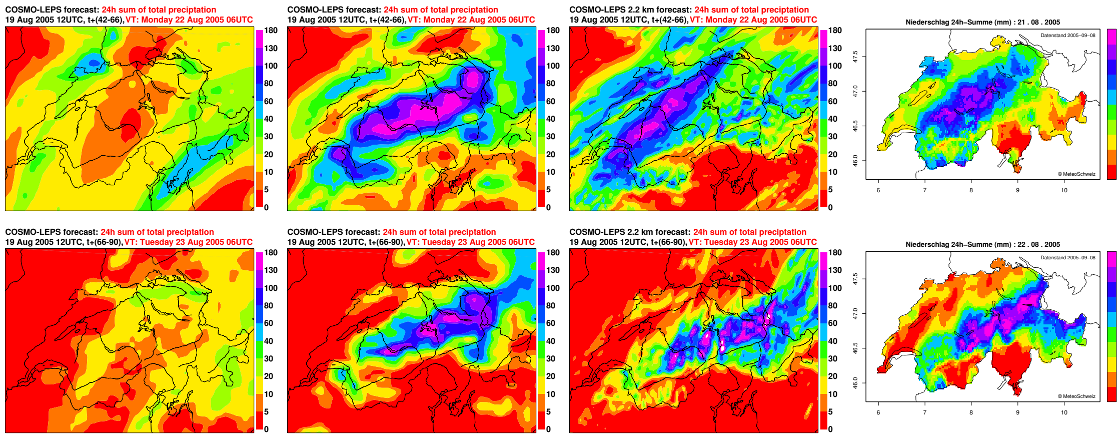

Figure 4: Member representing the largest cluster of the experiments FLAT (left), OPR (second row) and HR (third row), as well as a precipitation analysis (right) for 24-h precipitation sums valid at August 22 (top) and August 23, 2005 0600 UTC (bottom). The ensemble experiments have initial time 19.8.2005 1200 UTC.

the comparatively dry inneralpine Rhone valley.

4 Further analysis

The three experiments are investigated regarding the spatial distribution and timely evolution of the precipitation on the basis of one individual ensemble member. The member representing the largest cluster is chosen. It has a weight of 31% in the probabilistic products. Detailed information for the clustering procedure of COSMO-LEPS are given in Montani et al. (2003).

Figure 4 shows the observed and predicted 24-h precipitation sums for August 21 and August 22 (0600 - 0600 UTC on the following day), respectively. On August 21, the convective precipitation systems moved from northeast to southwest over the Swiss plateau and the northern Alpine slopes. In the morning of the following day, the flow changed to north, leading to prolonged heavy precipitation on the northern Alpine slopes. The OPR member simulates the evolution of this event well, while the FLAT member shows the same flow patterns (see below) but clearly lower precipitation amounts on the northern side of the Alps for both days. The precipitation systems occurring in the OPR member are also simulated in the FLAT member but they are typically less intense and cross Switzerland on tracks shifted somewhat to the south, indicated by the precipitation maxima in the south-eastern part of Switzerland. On the second day, the precipitation systems move quickly to the south and loose rapidly their intensity during the course of the day.

The flow characteristic on the northern side of the Alps is hardly changed due to the missing Alps. This is consistent with the very similar synoptic in the two members. Figure 5 shows the geopotential at 700 hPa of both members for August 22, 0000 UTC. In the FLAT member the cyclone is slightly shifted to the north. Hence, the mesoscale flow is only marginally affected by the elimination of the Alpine barrier. However, for such an analysis the simulation period may be too short. In addition, it should be noted, that the driving global simulation (providing initial and lateral boundary conditions) is the same for both experiments and hence includes the Alpine barrier, even though with the coarse resolution T255 (about 80 km horizontal grid-spacing) used by the ECMWF EPS.

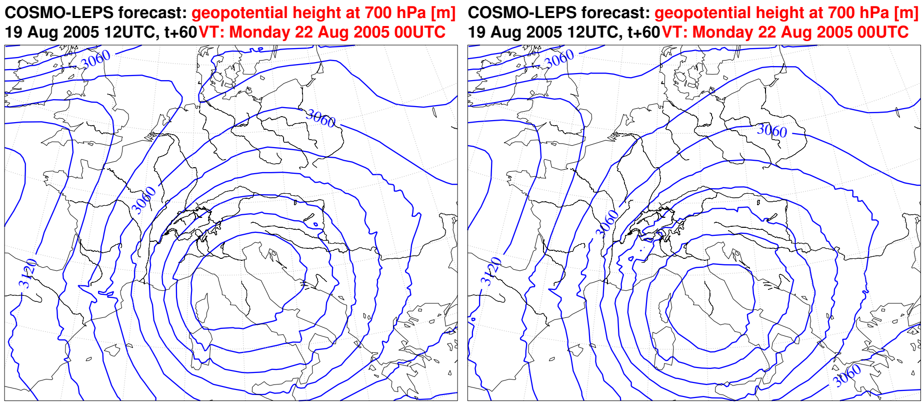

Figure 5: Geopotential at 700 hPa for 22.8.2005 0000 UTC of one selected member from the FLAT (left) and the OPR (right) experiment with initial time 19.8.2005 1200 UTC.

In contrast to the probability maps, the comparison of the HR and the OPR member points out a discrepancy between the two experiments for the validation time August 22 0600 UTC. The precipitation in the south-western Alps seems to be better captured by the HR member. However, this member predicts the band with the highest precipitation amounts in central and eastern Switzerland not along the Alpine slopes, but clearly shifted to the north. The OPR member, on the other hand, produces the highest amounts in the central Switzerland rather shifted to the south with respect to the analysis. The precipitation peaks are clearly overestimated in the OPR member, while they agree quite well with the analysis in the HR member. Further inspections revealed, that the unexpected large difference between the two HR and the OPR member, in particular for the eastern Alps, are related to the Tiedtke convection scheme which produces in the OPR member the large overestimation in the eastern Alps. In the HR experiment the scheme is switched off due to the explicit treatment of convection using a 2.2 km horizontal grid. On the following day, the differences between the HR and the OPR member are much smaller. The fine-scale structures provided in the HR member matches well the observed pattern, but the exact location of the maxima is just partly captured.

5 Conclusion

The sensitivity experiment points out, that the complex orography of the Alpine area was a key ingredient for the large precipitation amounts in this event. The ensemble forecast without the Alpine barrier did not produce an extreme precipitation event. The missing precipitation on the northern and central Alpine region is not distributed to other regions. The deficit is obvious for both flow regime, the north-easterly flow on August 21 and for the northerly flow on August 22, respectively. Hence, the lifting of air masses impinging on the Alpine slopes as well as convection triggering in the complex orography in the first phase of the heavy precipitation period played a major role. The application of an ensemble with a 2.2 km horizontal grid-spacing for this event highlighted the potential of convection-resolving numerical weather predictions. While the probability forecasts with 2.2 km and with its driving 10 km ensemble provided appropriate and similar results, large differences are found between corresponding members pointing out also distinct failures with regard to the observations. These results support the necessity of high-resolution ensemble forecasting systems which are able to consider the complex orography of the Alpine area and take into account the predictability limits of such an extreme event, in order to achieve further progresses in the prediction of heavy precipitation at a local scales.

Acknowledgments

This study was supported by the Swiss NSF through the National Centre for Competence in Research Climate (NCCR-Climate).

References

Marsigli, C., F. Boccanera, A. Montani, and T. Paccagnella, 2005: The COSMO-LEPS mesoscale ensemble system: validation of the methodology and verification. *Nonlinear Processes in Geophysics*, 12, 527-536.

MeteoSwiss, 2006: Starkniederschlagsereignis August 2005. Arbeitsbericht MeteoSchweiz, 211, 63 pp. Available from the Federal Office of *Meteorology and Climatology MeteoSwiss*, Zürich, Switzerland.

Montani, A., M. Capaldo, D. Cesari, C. Marsigli, U. Modigliani, F. Nerozzi, T. Paccagnella, P. Patruno, and S. Tibaldi, 2003: Operational limited-area ensemble forecasts based on the Lokal Modell. *ECMWF Newsletter*, No. 98, 2-7.

Steppeler, J., G. Doms, U. Schättler, H.-W. Bitzer, A. Gassmann, U. Damrath, and G. Gregoric, 2003: Meso-gamma scale forecasts using the nonhydrostatic model LM. *Meteorol. Atmos. Phys.*, 82, 75-96.

Walser, A., 2006: COSMO-LEPS forecasts for the August 2005 floods in Switzerland. *COSMO Newsletter*, No. 6, available from http://www.cosmo-model.org.

Walser, A., M. Arpagaus, M. Leutbecher, and C. Appenzeller, 2006: The impact of moist singular vectors and horizontal resolution on short-range limited-area ensemble forecasts for two European winter storms. *Mon. Wea. Rev.*, 134, 2877-2887.

Probabilistic Verification of COSMO-LEPS Forecasts with SYNOP Stations

André Walser and Mark A. Liniger

MeteoSwiss, Krähbühlstrasse 58, 8044 Zürich, Switzerland

1 Introduction

A probabilistic verification of the limited-area ensemble prediction system COSMO-LEPS is carried out for spring and summer precipitation. COSMO-LEPS is the operational limited-area ensemble prediction system (EPS) of the Consortium for Small-Scale Modeling (COSMO) running daily at ECMWF since November 2002. Since February 2006, COSMO-LEPS is a 16-member ensemble based on version 3.17 of the non-hydrostatic limited-area COSMO model (formerly LM; see Steppeler et al., 2003) using a horizontal grid-spacing of 10 km. Previous verification efforts of ARPA-SIM, Bologna (Marsigli et al., 2005; Marsigli et al., 2006) compare upscaled high-density observations of the COSMO member states Germany, Greece, Italy, Poland and Switzerland with forecasts of COSMO-LEPS and the European Centre for Medium-Range Weather Forecasting (ECMWF) EPS on boxes of 1.5×1.5 degrees.

This study assesses the COSMO-LEPS against observation of European SYNOP stations. The skill of COSMO-LEPS precipitation forecasts at a local scale is evaluated and analyzed with regard to the overall skill, the skill in complex topography and the spatial variability. This report is organized as follows: Section 2 presents the verification strategy including a brief introduction to the verification metric used. The results are given in Section 3 including a detailed skill analysis for spring 2006 (3.1), a comparison with the skill of deterministic forecasts using a higher resolution (3.2), a comparison with other verification periods (3.3), and finally an analysis of the skill in the complex topography of the Alpine area (3.4). Conclusions are provided in Section 4.

2 Verification method

The verification is based on accumulated precipitation between 0600-1800 UTC and 1800-0600 UTC, referred to as daytime and nighttime precipitation hereafter. It is carried out on the common model domain of COSMO-LEPS and the Swiss implementation of the COSMO model using a horizontal grid-spacing of 7 km, referred to hereafter as aLMo. The model domains are illustrated in Fig. 1. The thresholds considered are 1 mm, 5 mm, 10 mm and 25 mm precipitation, respectively. For the results presented here, the predicted probabilities are derived from the average precipitation of the five grid points closest to the station location. Investigations reveal no significant differences in overall scores using an average of five, nine or just the closest grid point. COSMO-LEPS probabilities are derived by equally weighting the ensemble members, since earlier verification studies for precipitation pointed out slightly worse scores for probabilities derived by weighting the members according to the size of the cluster they represent (Marsigli 2004, personal communication). This might be related to the bias of the Brier Skill Score (see below) for weighted ensembles (Weigel et al., 2007b).

In order to evaluate the predicted probabilities for an event, we use the Brier score (BS) as proposed by Brier (1950) which measures the square of the differences between predicted

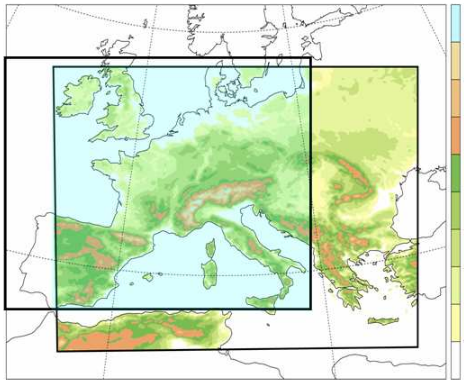

Figure 1: COSMO-LEPS domain with topography (color coded) and aLMo domain. The verification is performed on the common area (transparent light blue).

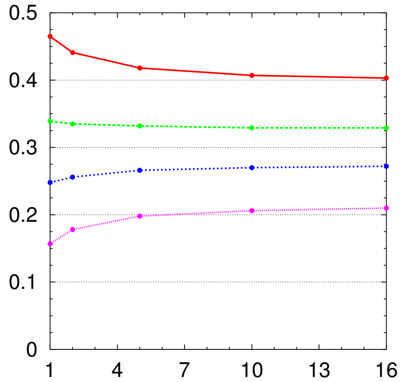

Figure 2: Debiased Brier skill score for 12h-accumulated precipitation exceeding 1 mm for spring 2006 as a function of ensemble size for lead-time +18h (red line), +42h (green), +66h (blue), and +90h (purple), respectively.

and observed probabilities. The BS can be decomposed into the scalar attributes reliability, resolution, and uncertainty (Murphy 1973):

$$\mathrm{BS} = \underbrace{\frac{1}{N}\sum_{k=1}^{J} N_k \left(y_k - \overline{o_k}\right)^2}_{reliability} - \underbrace{\frac{1}{N}\sum_{k=1}^{J} N_k \left(\overline{o_k} - \overline{o}\right)^2}_{resolution} + \underbrace{\overline{o}\left(1-\overline{o}\right)}_{uncertainty} \tag{1}$$

where N is the number of forecast-observation pairs, J the number of probability classes k, y the predicted probability, and $\overline{o}$ the relative frequency of the event in the verification period. The reliability (REL) term indicates how closely the forecast probability matches the observed event frequency as a function of forecast probability; the smaller the reliability value, the better. The resolution (RES) term measures the ability of the forecasting system to resolve the set of events into subsets with characteristically different observed frequencies. The third term, uncertainty (UNC), is independent from the forecasting system and only a function of the event frequency.

Forecast skill is measured by a comparison of forecast score with the score from a reference forecast. Therefore, the Brier Skill Score (BSS) is defined as $BSS = 1 - BS/BS_{ref}$. The BSS has a maximum of one (if BS equals zero). A BSS value below zero means no skill, i.e. the forecast is worse than the reference forecast. As reference forecast we use climatology. A climatological forecast has no resolution by definition and if the event frequency in the verification period is equal to the climatological probability, then the reliability terms becomes also zero, and hence $BSS = (RES - REL)/UNC$, i.e. the forecasts have skill if $RES > REL$. The station climatology is estimated from the observations in the correspond-

	MAM	JJA
1800-0600 UTC	735	810
0600-1800 UTC	680	806

Table 1: Number of SYNOP stations used for the verification from totally 1273 stations with a sufficient availability to build a climatology.

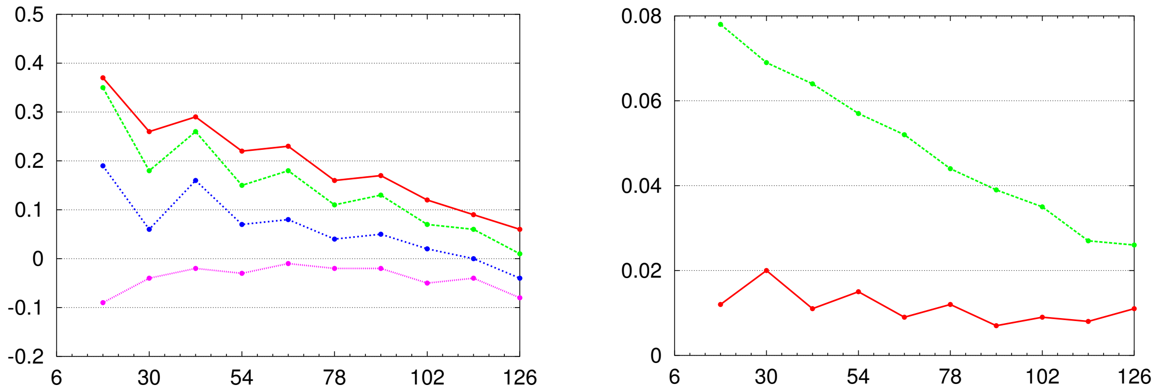

Figure 3: Verification results of COSMO-LEPS 12-h-accumulated precipitation forecasts for spring 2006 as a function of forecast range [h]. The left panel shows the Brier skill score for thresholds 1 mm (red solid line), 5 mm (green), 10 mm (blue), and 25 mm (purple), respectively. The right panel shows reliability (red solid line) and resolution (green) for the 1 mm threshold.

ing season of the past 10 years (1997-2006) for both verification times, requesting a minimal availability of 50% of the SYNOP messages. This reduces the total number of stations from 1273 inside the verification domain to about 750 depending on the season and the verification time. The exact numbers are summarized in Table 1.

From Müller et al. (2005) it is known that the BSS is negatively biased for EPSs with small ensemble sizes. Weigel et al. (2007a) gives an analytical formula to derive a biased corrected version

$$BSS_D = 1 - \frac{BS}{BS_{Clim} + D} \quad \text{with a correction term} \quad D = \frac{1}{M}\overline{o}(1-\overline{o}) \tag{2}$$

identified as the intrinsic unreliability of the forecasting system due to the limited number of ensemble members M. Figure 2 shows the BSS_D as a function of ensemble size for the 1 mm thresholds for different lead-times. The values are a result of 100 random samples. The skill decreases considerably with lead-time but is positive for all lead-times and ensemble sizes. In addition to the bias discussed above for the BSS, we note a secondary bias for small ensemble size, which is positive for short lead-times and negative for long lead-times. The positive bias for lead-time +18h indicates, that the ensemble is overconfident for that lead-time as explained in Weigel et al. (2007b).

3 Results

3.1 Verification for spring 2006

We begin the discussion of the verification results with spring 2006 (March, April and May). Fig. 3a presents the BSS as a function of forecast range for the thresholds 1 mm, 5 mm, 10 mm, and 25 mm, respectively. For the two lowest thresholds, the forecasts have skill until the end of the forecast range which is also valid for the 10 mm threshold except for the very end of the range. While the skill decreases as expected with increasing lead-time, we note a significant diurnal cycle for these lowest three thresholds reflecting a higher skill for precipitation during nighttime. This behavior is most probably related to the limited

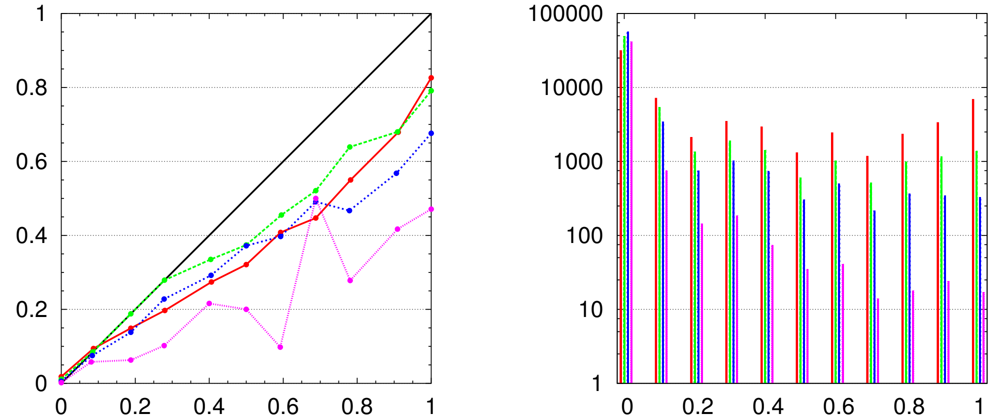

Figure 4: COSMO-LEPS 12h-accumulated precipitation in spring 2006 for the forecast range +18h for precipitation exceeding 1mm (red solid line), 5 mm (green), 10 mm (blue), and 25 mm (purple). The left panel shows the reliability diagram with forecast probability on the x-axis and observed frequency on the y-axis. The right panel indicates the number of forecast-observation pairs in each probability class (note the logarithmic scale).

predictability of convection (e.g. Walser et al., 2004) which occurs more frequently during daytime. Finally, the panel reveals a negative BSS, i.e. no skill, for precipitation exceeding 25mm/12h for all lead-times which is further discussed later on.

The reliability and the resolution term are shown in Figure 3b as a function of forecast range for the 1 mm threshold. While the reliability is quite small and rather constant with lead time, the resolution decreases almost linearly with increasing forecast range, which is the normal behavior of every weather forecasting system due to decrease in predictability with increasing forecast range.

A so-called reliability diagram for the lead-time +18h is derived presenting the reliability qualitatively for the four thresholds considered (Fig. 4a). The predicted probabilities are divided into 11 probability classes (<5%, 5-15%, 15-25%,..., >95%). The sample size for each class and threshold is given in Fig. 4b. For all thresholds, the curves lie below the diagonal (black line), in particular for classes with high predicted probabilities. Hence, COSMO-LEPS overestimates the occurrence of precipitation events when it predicts rather high probabilities, particularly for the highest threshold 25 mm. However, it should be noted that the sample sizes are small for this threshold (except for the first class of course), in particular for probabilities higher than 60% (see Fig. 4b). The reliability diagrams look similar for other lead-times except for classes with high probabilities due to the decrease of sample size for those classes with increasing forecast range.

In addition, Fig. 4 shows event resolution for all four thresholds, even for the 25 mm threshold which reveals no skill. This points to a weakness of the BSS with climatological forecasts as reference forecast as discussed in Mason (2004): if the BSS is negative, the forecasts are assumed unskillful, but there might nevertheless be some useful event resolution in the forecast that can be used after a calibration (a simple example is discussed later in section 3.4). In our case, the forecast for precipitation exceeding 25 mm would be nevertheless more valuable than a climatological forecast for a customer with a rather low cost-loss ratio (Richardson 2000) taking action already at rather low predicted probabilities.

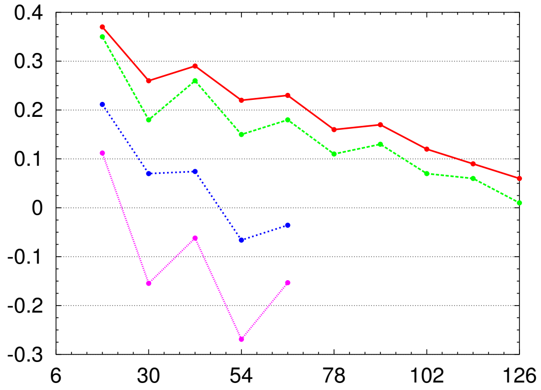

Figure 5: As Fig. 3a, but a comparison between skill for COSMO-LEPS (red and green lines) and aLMo (blue and purple) forecasts for precipitation exceeding 1 mm (red and blue) and 5 mm (green and purple), respectively.

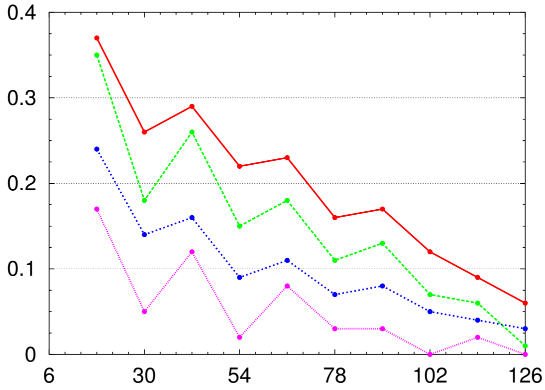

Figure 6: Comparison of skill for 12h-accumulated precipitation between spring and summer 2006 in terms of Brier skill score. Red and green lines indicate skill for threshold 1 mm and 10 mm, respectively, for spring, blue and purple lines indicate skill for the same thresholds for summer.

3.2 Comparison with aLMo forecasts

The deterministic model aLMo can be considered as one-member ensemble predicting the probabilities 0% or 100%, respectively, for up to +72h. The BSS of aLMo for spring 2006 and thresholds 1 and 5 mm, respectively, is compared with COSMO-LEPS in Fig. 5. The skill of the aLMo forecasts is clearly lower for all lead-times with skill only in the short-range for the 5 mm threshold and up to +42h for the 1 mm threshold. Considering BSS_D, then aLMo clearly outperforms COSMO-LEPS (not shown). For the 1 mm thresholds, BSS_D for aLMo is in the range 0.58 (+18h) and 0.44 (+54h). The largest differences in the COSMO setup between aLMo and COSMO-LEPS is the assimilation cycle of aLMo (relevant for short lead-times) and the horizontal resolution as mentioned above. The clearly higher skill of aLMo in terms of the BSS_D highlights a potential to significantly improve COSMO-LEPS forecast with a higher horizontal resolution.

3.3 Comparison with different verification periods

In this section, we compare the verification results for spring 2006 with those for summer 2006 and spring 2005. Figure 6 presents the BSS for the thresholds 1 mm and 5 mm for spring and summer 2006, respectively. For both thresholds, the skill is clearly higher for spring, which is most probably related to the larger fraction of convective precipitation events in summer than in spring.

Investigating spring 2005 and 2006, two different setups of COSMO-LEPS can be compared. Before February 2006, the COSMO-LEPS ensemble was a 10-member ensemble using COSMO version 3.15 and a coarser vertical resolution (32 levels, new setup has 40). At the same time a new cycle of the driving EPS was introduced at ECMWF with a higher horizontal (from T255 to T399) and vertical resolution (from 45 to 61 levels). Figure 7 shows a comparison in terms of BSS (left) and BSS_D (right) for the thresholds 1 mm and 10 mm, respectively. In general, the BSS is higher for spring 2006, while the BSS_D shows only marginal differences. Thus, the better skill for spring 2006 is mainly a result of the larger

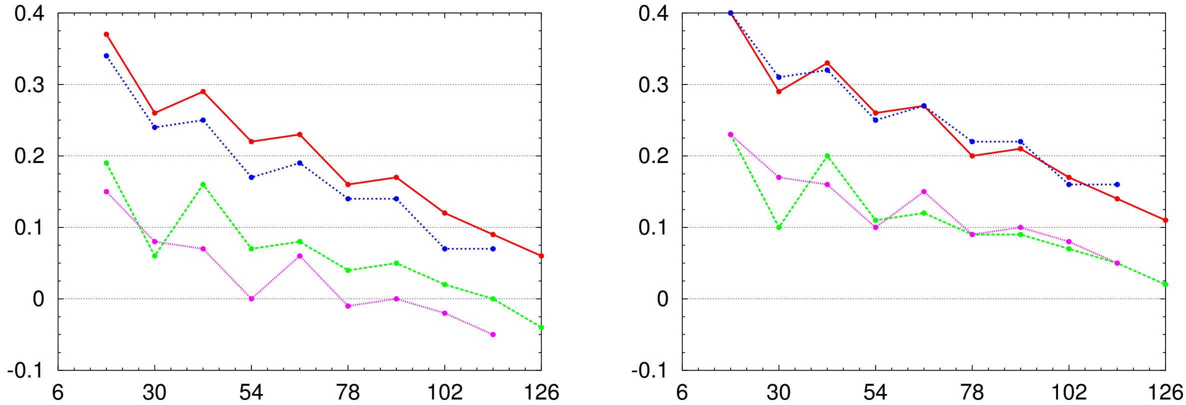

Figure 7: Comparison of skill for 12h-accumulated precipitation between spring 2006 and 2005 in terms of Brier skill score (left) and debiased Brier skill score (right). Red and green lines indicates skill for threshold 1 mm and 10 mm, respectively, for 2006, blue and purple lines indicates skill for the same thresholds for 2005.

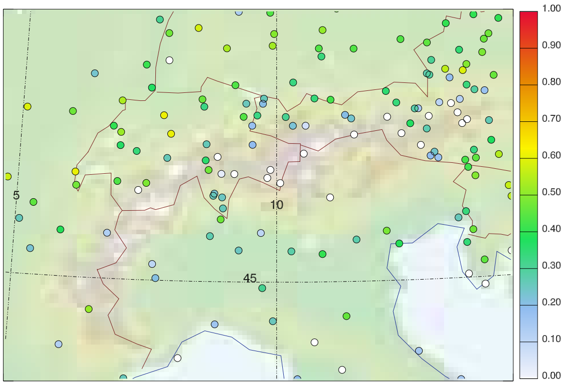

Figure 8: Brier skill score for 12h-accumulated precipitation exceeding 1 mm for spring 2006 and lead-time +42h at SYNOP stations in the Alpine region.

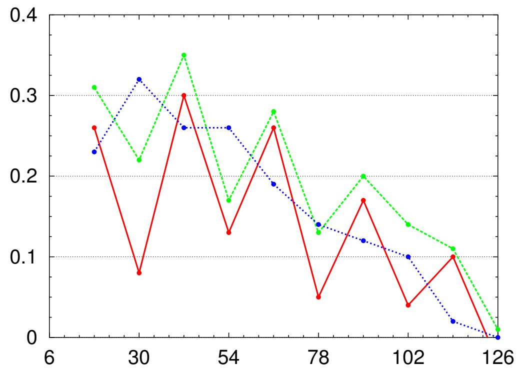

Figure 9: Same as Fig. 3a, but for Swiss stations only and without 25 mm threshold (sample size too small).

ensemble and not due to the improvements of the model setups of COSMO-LEPS and the driving ECMWF EPS.

3.4 Forecast skill in the complex topography of the Alps

In this section, we focus on COSMO-LEPS forecast skill in the complex topography of the Alpine region. The spatial variability of the skill is very large in this region (Fig. 8). Some stations show very good skill with BSS higher than 0.5, while a few stations, mainly located in inneralpine valleys, show no skill (white circles). The BSS derived with Swiss stations only (39) is presented in Fig. 9. As for the entire verification domain, we found skill until the end of the forecasting range for the thresholds 1 mm, 5mm, and 10 mm, but the skill for the different thresholds are closer together with a better skill for 5 mm than for 1 mm for all lead-times. Due to the small sample size, the 25 mm threshold is not investigated for this limited number of stations.

In the following, we analyze the skill for station Sion in the Rhone valley which reveals no

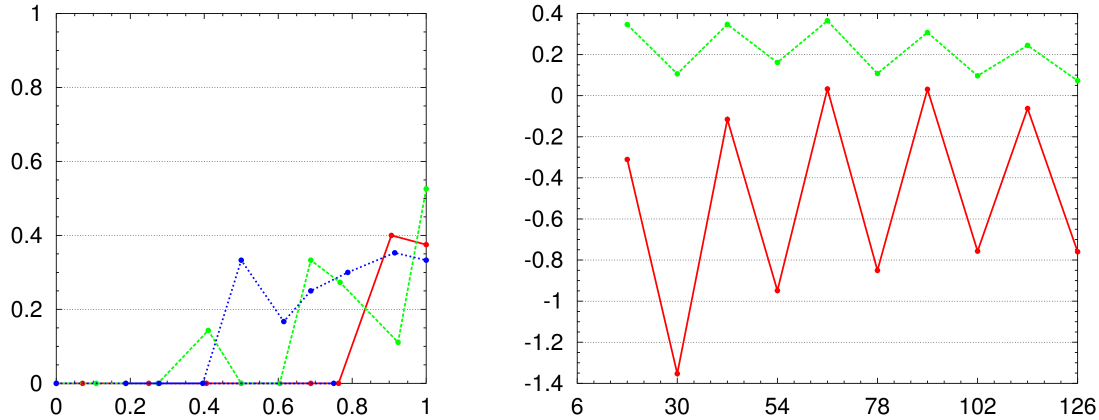

Figure 10: Verification for SYNOP station Sion in the Swiss Rhone valley for 12h-accumulated precipitation exceeding 1mm. The left panel shows the reliability diagram for lead-time +30h (red), +54h (green), and +78h (blue). Brier skill score (red) and Brier skill score of the calibrated forecast (green) is indicated in the right panel.

skill for daytime precipitation exceeding 1 mm for all lead-times and no or very low skill for nighttime precipitation, indicated as red solid line in Fig. 10b. The reliability diagram in Fig. 10a for lead-times +30h, +54h, and +78h shows that COSMO-LEPS dramatically overestimates the probability for all classes, resulting in a very low reliability. In order to investigate the impact of a postprocessing on the skill, an ad-hoc calibration is applied by multiplying the predicted probabilities: $y^* = 0.5y$. The factor 0.5 is chosen according to the reliability diagram that indicates slopes of about 0.5 for the three lead-times. The BSS using the calibrated probabilities y^* for the 1 mm threshold is indicated in Fig. 10b as green line. It is not only positive for all lead-time, it is even higher than the average skill for the Swiss stations (cf. Fig. 9).

4 Conclusion

An objective and comprehensive probabilistic verification of COSMO-LEPS 12h-accumulated precipitation has been carried out for spring and summer 2006. Overall, the results show forecast skill in terms of the Brier skill score until the end of the 5.5 days forecasting range for precipitation exceeding 1 mm, 5 mm, and 10 mm, respectively, while the BSS for 25 mm turned out to be negative for all lead-times. A comparison with results for 2005 reveals that the scores have been improved since 2005, but mainly due to the increase of ensemble size from 10 to 16 members in February 2006, while changes in the model setups do not show a significant impact on the scores. In addition, skill for spring is considerably higher than for summer precipitation, most probably related to the limited predictability of convective events.

Further investigations indicate that the ensemble is overconfident for short-lead times, i.e. has a too small spread. The skill scores exhibit a high spatial variability, in particular in complex topography where a few stations with very low or no skill are found. It is demonstrated that even an ad-hoc calibration of the predicted probabilities has a large potential to improve the skill for such stations.

This study has some notable limitations. It focuses only on weak to moderate precipitation since the sample size using seasonal verification periods is too small for larger thresholds than

25mm/12h. In addition, the verification is based only on spring and summer precipitation. In a follow-up study, the other seasons will be investigated too, including the interannual variability. In addition, the use of larger time-series will allow to examine the skill of COSMO-LEPS forecasts for extreme events which is of particular interest.

Acknowledgments

This study was supported by the Swiss NSF through the National Centre for Competence in Research Climate (NCCR-Climate).

References

Brier, G. W., 1950: Verification of forecasts expressed in terms of probability. *J. Atmos. Sci.*, 78, 1–3.

Marsigli, C., F. Boccanera, A. Montani, and T. Paccagnella, 2005: The COSMO-LEPS mesoscale ensemble system: Validation of the methodology and verification. *Nonlinear Processes in Geophysics.*, 12, 527–536.

Marsigli, C., A. Montani, and T. Paccagnella, 2006: Verification of the COMO-LEPS new suite in terms of precipitation distribution. *COSMO Newsletter*, No. 6, 143–141.

Mason, S. J., 2004: On using climatology as a reference strategy in the Brier and ranked probability skill scores. *Mon. Wea. Rev.*, 132, 1891-1895.

Müller, W., C. Appenzeller, F. Doblas-Reyes, and M. A. Liniger, 2005: The impact of horizontal resolution and ensemble size on probabilistic forecasts of precipitation by the ECMWF ensemble prediction system. *Weather and Forecasting*, 17, 173–191.

Murphy, A. H., 1973: A new vector partition of the probability score. *J. of Appl. Meteor.*, 12, 595–600.

Richardson, D. S., 2000: Skill and relative economic value of the ECMWF ensemble prediction system. *Quart. J. Roy. Meteor. Soc.*, 126, 649–667.

Steppeler, J., G. Doms, U. Schättler, H.-W. Bitzer, A. Gassmann, U. Damrath, and G. Gregoric, 2003: Meso-gamma Scale Forecasts using the Nonhydrostatic Model LM. *Meteorol. Atmos. Phys.*, 82, 75–96.

Walser, A., D. Lüthi, and C. Schär, 2004: Predictability of Precipitation in a Cloud-Resolving Model. *Mon. Wea. Rev.*, 132, 560–577.

Weigel, A. P., M. A. Liniger, and C. Appenzeller, 2007a: The discrete Brier and ranked probability skill scores. *Mon. Wea. Rev.*, accepted.

—, 2007b: Generalization of the discrete Brier and ranked probability skill scores for weighted multi-model ensemble forecasts. *Mon. Wea. Rev.*, accepted.

Postprocessing of the aLMo Precipitation with the Neighborhood Method

Pirmin Kaufmann

MeteoSwiss, Zürich, Switzerland

1 Introduction

The resolution of numerical weather prediction models is advancing to finer scales. With increasingly smaller scales, the predictability is decreasing due to the sensitivity of the forecasts to errors in the initial state and in the model formulation. This is especially true for precipitation, a meteorological field with a high temporal and spatial variability. The exact time of onset and location of a single convective cell for example cannot be predicted even with the highest-resolving models. The uncertainty in time and space should be accounted for when using model output fields on the grid scale.

The neighborhood method (Theis *et al.*, 2005) accounts for the probability related to local-scale spatial and temporal model uncertainty. It solves for the above-mentioned predictability problem by sampling a temporal and spatial neighborhood around each grid cell to derive a probabilistic forecast. Doing this, the neighborhood method provides a way to derive a probabilistic forecast from a deterministic model.

In the present study, precipitation forecasts of the Swiss set-up of the COSMO model with a grid spacing of 7 km, the Alpine Model (aLMo), are used as input.

2 Optimizing the neighborhood size

Method

The neighborhood size has an important impact on the magnitude of the predicted probabilities. It is, however, difficult if not impossible to determine an optimal neighborhood size based on objective verification alone (Theis 2005). With this unpromising prospect, I chose to base the optimization on a graphical comparison of the forecast probabilities with actual precipitation measurements of August – October 2006. Of course, an objective evaluation of the neighborhood determined in this way must follow later.

Spatial radius of neighborhood

Theis *et al.* (2005) tested three different sizes for the neighborhood. A small, a medium and a large neighborhood with a spatial radius of 3, 6 and 10 grid points, respectively, were used. Here, four sizes of 3, 5, 10 and 20 grid point radius are compared graphically (Figure 1). While the smallest radius gives more detail than is meaningful for a probabilistic method, the largest radius on the other hand blurs the information too strongly.

Shape of the neighborhood

Theis *et al.* (2005) tested different spatial shapes. The impact proved to be quite small and at times even detrimental. Therefore, a circular neighborhood was chosen here, without further experimenting with spatial shape. In the time dimension, they chose a spatial radius depending on the temporal distance to the central point. This implies a space-time dependency. Here, it is assumed that the time and space dimensions are independent. This

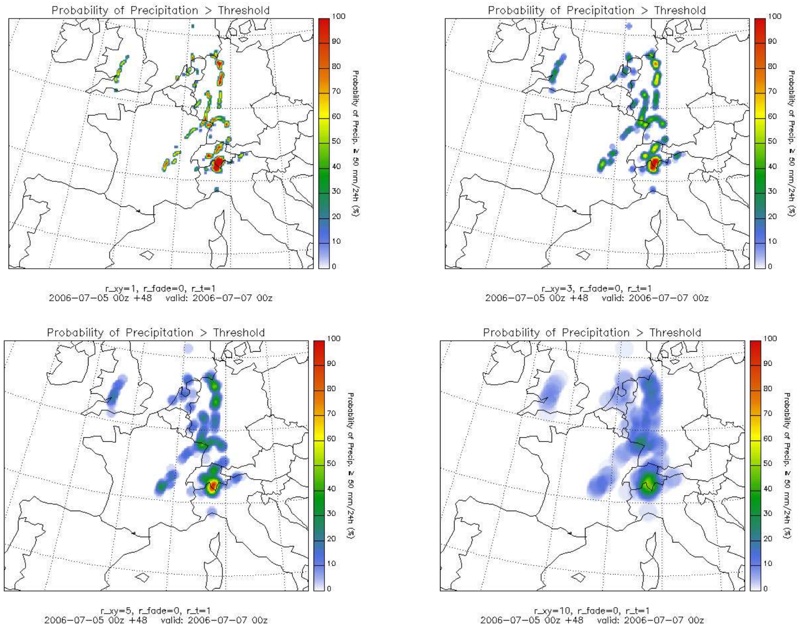

Figure 1: Probabilities of precipitation for spatial neighborhood radius of 1, 3, 5, and 10 grid points, in this order.

assumption is true if the ambient wind is nearly zero, and becomes increasingly inaccurate with increasing advection. The resulting neighborhood is cylindrical as opposed to the ellipsoidal neighborhood of Theis *et al.* (2005).

Linearly fading weights

The circular neighborhood shape in space, in combination with localized strong precipitation peaks, leads to a dotted plot of probabilities, with a circular dot surrounding each major precipitation peak (Figure 1). Such an unwanted feature could be smoothed out in a next step, but it is more meaningful to do this as part of the neighborhood processing by adding an additional zone around the neighborhood with decreasing weights. For simplicity, the weights were chosen to decrease linearly. The physical reasoning behind such a zone, or sponge-layer, as it could be called, is that given a forecast at the central point, a thunderstorm is equally likely to appear within a certain radius, but that beyond this radius the likelihood decreases and finally reaches zero at some larger distance. Figure 2 shows the weight depending on the spatial distance of a grid cell to the neighborhood center for two neighborhood sizes.

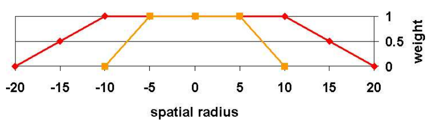

Figure 2: Weights for two different spatial sizes of the neighborhood. Red: Zone of equal weight and fading zone of 10 gridpoint radius each. Orange: 5 gridpoint radius each.

Temporal radius

The temporal radius of the neighborhood finally represents the uncertainty in time of a rainfall prediction. For convective precipitation, it is known to span several hours. However, tests with temporal radius of 0, 1, 3, and 6 hours showed relatively little influence for a case

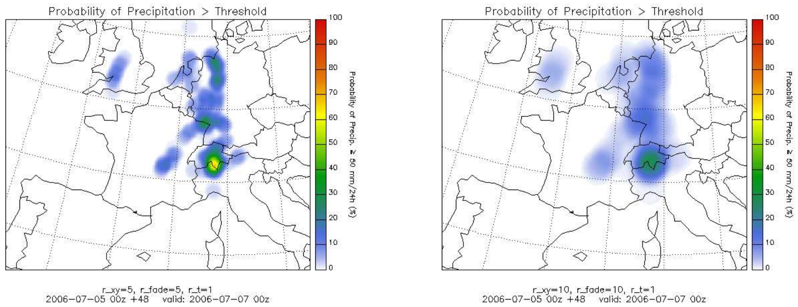

Figure 3: Same as Figure 1 but with a fading zone of same width as the spatial radius added, for 5 (left) and 10 (right) gridpoint radius.

with frontally induced thunderstorms. This might be different if no front is involved, but the rainfall accumulation of 6 hours or even more of 24 hours already has a smoothing effect on the time scale, rendering the temporal extent of the neighborhood less critical.

3 Cases

Threshold 25 mm / 6 h

Figure 4 displays a case last summer with a small region of strong precipitation over southern Switzerland. The probabilities for precipitation above the threshold level of 25 mm / 6 h reach 50% in that region. Although probabilities and single precipitation events cannot be compared directly, large probabilities should coincide with rainfall above the threshold for a majority of cases. The probabilities generally decrease with increasing neighborhood size, thus the frequent occurence of moderate probabilities with actual rainfall above the threshold as in Figure 4 indicates that the chosen neighborhood size might still be slightly larger than optimal.

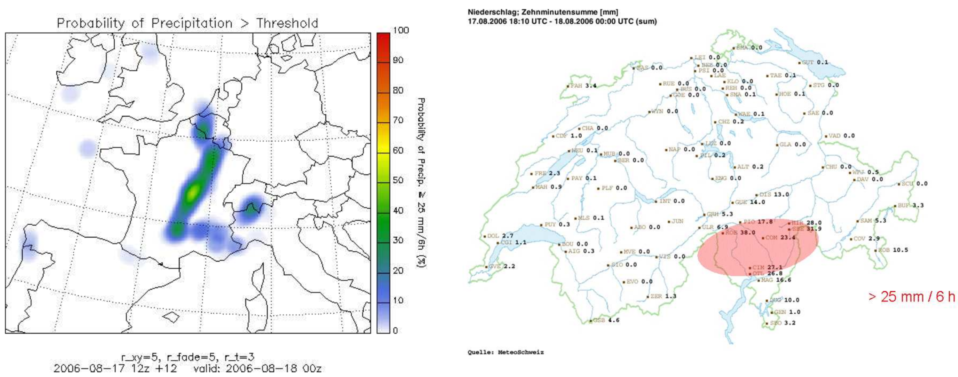

Figure 4: Probabilities predicted by the neighborhood method (left) and actual rainfall sum (right) for 2006-08-18 00:00 UTC

Threshold 50 mm / 24 h

Figure 5 shows a case with strong precipitation over northern Switzerland. The region of probabilities of 50% and more for precipitation above the threshold level of 50 mm / 24 h nicely fits with the observed precipitation.

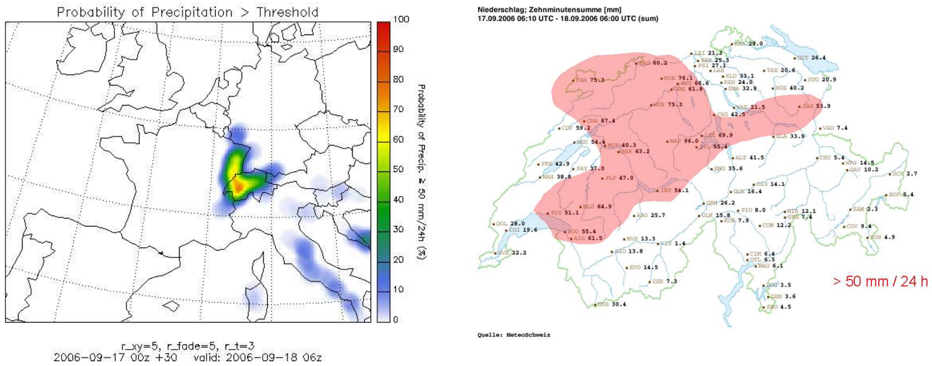

Figure 5: Probabilities predicted by the neighborhood method (left) and actual rainfall sum (right) for 2006-09-18 06:00 UTC

4 Conclusions and Outlook

The neighborhood method is used to derive a probabilistic forecast from a deterministic model. The probability is related to local-scale spatial and temporal model uncertainty. The resulting plots are compared to real cases and are optimized in this way. A spatial radius of five grid cells with an additional zone of decreasing weights with the same width gives probabilities which are in accordance with the observed events and non-events. The spatial radius is kept constant within the temporal radius of 3 hours, however the extent of the neighborhood in time is of lesser importance. This choice seems to be near the optimal size judging from the graphical comparison with the effective precipitation. A throughout validation however, using objective verification, will have to follow to prove the quality of the probability forecast with the chosen neighborhood.

The neighborhood method is able to represent the local uncertainty concerning the prediction of the exact position and onset of precipitation. It does not account for the uncertainty related to synoptic forcing, which can be done using a model ensemble forecast. A combination of the ensemble and the neighborhood methods would combine both synoptic-scale and small-scale uncertainties.

References

Theis, S., 2005: Deriving probabilistic short-range forecasts from a deterministic high-resolution model. Ph. D. thesis, Univerisity Bonn, Germany.

Theis, S. E., A. Hense, and U. Damrath, 2005: Probabilistic precipitation forecasts from a deterministic model: a pragmatic approach. *Meteorol. Appl.*, **12**, 257 – 268, doi:10.1017/S1350482705001763

Sensitivity Tests for LPDM

T. Popova and P. Kaufmann

MeteoSwiss, Zürich, Switzerland

Abstract

A sensitivity analysis is performed with a Lagrangian Particle Dispersion Model (LPDM). The meteorological input for the LPDM is provided from the limited-area model of MeteoSwiss, the Alpine Model (aLMo), which is the Swiss operational set-up of the COSMO Model (COSMO: Consortium for Small-Scale Modelling). The LPDM concentrations output have been analyzed in order to study the influence of the following parameters: Turbulent kinetic energy, sedimentation velocity, thickness of averaging layer for concentrations, and horizontal drift correction.

The results are evaluated in the present report: An unexpected result was the large impact that the parameterisation of the turbulent kinetic energy, depending on the meteorological conditions, may have. The choice of the parameter "height of the averaged concentration layer" is significant in the beginning of the release: The maximal values of the concentration are factors higher. The other parameters do not affect significantly or not at all the results.

1 Introduction

MeteoSwiss uses the Lagrangian Particle Dispersion Model (LPDM) of the German Weather Service (DWD) for emergency preparedness. In this study, a sensitivity analysis was performed in order to study the influence of some of the steering parameters. The usage of diagnostic turbulent kinetic energy (TKE) from LPDM instead of the prognostic TKE from the numerical weather prediction model is one of the tested steering parameters. A second tested steering parameter is the taking into accout of a sedimentation velocity, which has only recently been added. The output concentrations are averaged over some height above the ground; three choices of the averaging layer have been examined. The influence of a horizontal drift correction term is studied. A steering parameter for the additional output of cross-sections was additionally tested to see whether it has no undesired side effects.

The LPDM was developed by Glaab (1986) at DWD. It is also in use at MeteoSwiss. It may be used operationally for simulating radioactive accidental releases. LPDM predicts the long-range transport, dispersion, sedimentation, wet and dry deposition and the atmospheric concentration of radioactive material.

It has been tested and evaluated several times during different tracer experiments and Inter- comparisons, such as ETEX (Glaab, Fay, and Jacobsen, 1998), ANATEX , CAPTEX, ATMES II, and ENSEMBLE, and the quality of the performance has been demonstrated. Simulations with a LPDM have successfully been established as a useful tool for emergency response requirement in case of accidental releases.

The calculation of trajectories of tracer particles is based on wind fields derived from the limited-area COSMO model at MeteoSwiss, the Alpine Model (aLMo), at hourly intervals. The superimposed turbulent fluctuations (Monte Carlo method) depend on TKE that is either provided by the COSMO model or can be diagnosed within LPDM. The processes of radioactive decay and convective mixing are included. The atmospheric concentration is calculated by counting the particle masses in arbitrary grids (Schättler and Montani, 2005).

The COSMO model was developed within the framework of the Consortium for Small-Scale Modelling. It has been designed for both operational weather prediction and various scientific applications on the meso-β and meso-γ scale (spatial scales where non-hydrostatic effects play an essential role). It is based on the primitive hydro-thermodynamical equations describing compressible non-hydrostatic flow in a moist atmosphere (Doms and Schättler, 2002).

The model equations are solved numerically on a rotated latitude-longitude grid with terrain-following coordinates in the vertical, using an Eulerian finite difference method. A variety of subgrid-scale physical processes is taken into account by parameterization schemes (Doms *et al.*, 2005).

One of the parameterization schemes adopted and implemented for optional use in the COSMO model, related to the fact that it is a non-hydrostatic model, is a scheme for vertical diffusion, based on prognostic treatment of TKE.

2 Method

The sensitivity tests consisted of changing or switching off five LPDM steering parameters, and analyzing the LPDM outputs.

The parameters that are modified and tested in the sensitivity study are the following: Turbulent kinetic energy (parameter LTKE), sedimentation velocity (LSED), output of vertical cross-section (LVERT), averaging of a layer with constant thickness (LIAEA), height of the averaged concentration layer (HMEAN), horizontal drift correction (LDRIFTCH).

The tests, depending on the setting of one of the above-mentioned parameters are named as follows:

- Ref: Reference
- Tst1: LTKE = FALSE
- Tst2: LSED = FALSE
- Tst3: LVERT = FALSE
- Tst4: LIAEA = TRUE, HMEAN = 200
- Tst4a: LIAEA = FALSE
- Tst5: LDRIFTCH = TRUE

The parameter values attributed to the reference are the following:

- LTKE = TRUE
- LSED = TRUE
- LVERT = TRUE
- LIAEA = TRUE, HMEAN = 500
- LDRIFTCH = FALSE

The LPDM analyses have been launched with three separated periods of two days each of meteorological data. Object of the analyses are the near-surface concentration (Bq m^{-3}) outputs from the LPDM. The three days of the dispersion simulation were represented graphically. Theses results have been compared with the reference, and between the sensitivity tests.

3 Data

INPUT DATA: The LPDM sensivity analyses have been launched with three separated two-day periods of meteorological data, provided by aLMo forecast. The meteorological input to LPDM was chosen to represent different wind directions. The aLMo forecasts were from 6/7 October, 12/13 October, and 1/2 November 2006, always starting at 00:00 UTC.

SOURCE TERM: The simulated hypothetical source is located in Beznau, Switzerland (47°33' N, 8°13' E) with the following release characteristics: Release height 30 m above ground level (AGL), emitted substance Cs-137, emission rate 46290 MBq s^{-1}, and duration of the emission 6 hours.

OUTUP DATA: For this study, we used the LPDM concentration output, represented graphically every 6 hours after the release. For each time period, the maximal value of the concentration is given in the Tables 1 – 3.

4 Results

Maxima of the near-surface concentration fields (Bq m^{-3}) obtained for a source localized in Beznau, are given in Table 1, Table 2, and Table 3, with the meteorology for 6/7 October, 12/13 October, and 1/2 November 2006 respectively.

Diagnostic turbulent kinetic energy (Tst1)

The LPDM uses in the reference run the prognostic TKE provided by the COSMO model. For this test, LPDM has been set to use its own, built-in diagnostic scheme to calculate TKE.

Test of 6/7 October
At 6 hours after the event, the propagation of the concentration cloud is slower in Tst1 than in the reference. The surface occupied by the cloud for Tst1 is much larger and more frayed and becomes increasingly large in time. The shape of the cloud in Tst1 is more circular and larger at the beginning. It becomes very quickly larger with time (Fig. 1). The propagation velocity diminishes compared to the reference propagation velocity.

	T_0+06 h	T_0+12 h	T_0+18 h	T_0+24 h	T_0+30 h	T_0+36 h	T_0+42 h	T_0+48 h
Ref	3959.3	551.4	40.054	14.795	13.055	7.3482	4.2925	1.6906
Tst1	4275.9	657.14	20.161	7.4244	5.8462	4.173	1.7024	0.9379
Tst2	3961.2	551.24	40.1671	14.783	12.707	7.0984	4.4746	1.722
Tst3	3959.3	551.4	40.054	14.795	13.055	7.3482	4.2925	1.6906
Tst4	9854.7	1202.7	53.819	15.111	13.842	6.515	6.0063	2.2615
Tst4a	25988.	2547.9	79.642	31.131	25.252	8.5324	9.099	2.6271
Tst5	3960.7	552.17	40.485	14.824	13.033	7.3095	4.6299	1.711

Table 1: Maximal values of concentration obtained by LPDM for the period (T_0 + XX hours) after the release, based on 06 October 2006 aLMo forecast. Blue: minimal value, red: maximal value for the given time.

	T_0+06 h	T_0+12 h	T_0+18 h	T_0+24 h	T_0+30 h	T_0+36 h	T_0+42 h	T_0+48 h
Ref	8269.4	6055.9	1614.1	322.96	136.11	45.916	32.518	19.599
Tst1	8617.4	6665.4	1020.	312.61	86.164	81.412	19.376	11.825
Tst2	8269	6061.8	1618.5	325.15	134.19	42.002	32.911	20.247
Tst3	8269.4	6055.9	1614.1	322.96	136.11	45.916	32.518	19.599
Tst4	20542	12521	1321	199.78	105.31	56.097	29.449	29.6
Tst4a	53430	12636	1378	255.56	140.9	97.408	36.657	71.715
Tst5	8281.3	6070.2	1619.2	319.72	135.54	43.512	32.349	19.276

Table 2: Maximal values of concentration obtained by LPDM for the period (T_0 + XX hours) after the release, based on 12 October 2006 aLMo forecast. Blue: minimal value, red: maximal value for the given time.

	T_0+06 h	T_0+12 h	T_0+18 h	T_0+24 h	T_0+30 h	T_0+36 h	T_0+42 h	T_0+48 h
Ref	1309	147.69	3.6425	0.3639	0.173	0.095	0.074	0.0508
Tst1	1390	145.39	4.427	0.866	0.378	0.141	0.0773	0.058
Tst2	1309	147.67	3.2447	3.3294	0.1672	0.086	0.0069	0.0518
Tst3	1309	147.69	3.6425	0.3639	0.173	0.095	0.074	0.0508
Tst4	2882.7	181.36	5.797	0.523	0.202	0.129	0.1147	0.0765
Tst4a	4695.9	308.74	8.569	0.952	0.367	0.217	0.176	0.124
Tst5	1308.2	147.33	3.3865	0.38962	0.1599	0.0841	0.0670	0.0477

Table 3: Maximal values of concentration obtained by LPDM for the period (T_0 + XX hours) after the release, based on 1 November 2006 aLMo forecast. Blue: minimal value, red: maximal value for the given time.

From the maximum values point of view, maximum concentrations are slightly higher for Tst1 for hours 6 and 12. The situation is reversed the following hours, but in general, the values are not very different thereafter between test and reference.

Test of 12/13 October
For the Tst1 hours 6 and 12, the area of equal concentrations is smaller, the cloud shape is better limited with smoother boundaries, whereas for the 18, 24, 30, 36, and 42 hour following the event, the situation is reversed, the cloud shape is more diffuse and larger.

Test of 1/2 November
The cloud is much larger from the beginning, and more diffuse. The surface covered by the entire cloud is almost doubled, but the surplus of the covered surface is only within the lowest concentration level. The surfaces occupied by the other concentration levels are practically identical with the reference.

The position of the maximum value for tests and reference is the same the first day. From the second day the position is shifted. No great differences between all maximum concentration values are observed. The concentration values are in the same range.

Sedimentation off (Tst2)

The LPMD includes the sedimentation in the modeled processes. This has been turned off for this test.

Tests of 6/7 October, 12/13 October, 1/2 November
Both simulations, reference and Tst2, are identical for each day in form, surface occupied by the same concentration level, and have nearly identical maximum values.

ASCII diagnostic output reduced (Tst3)

Some diagnostic ASCII output is turned off in this test. This should of course not have any

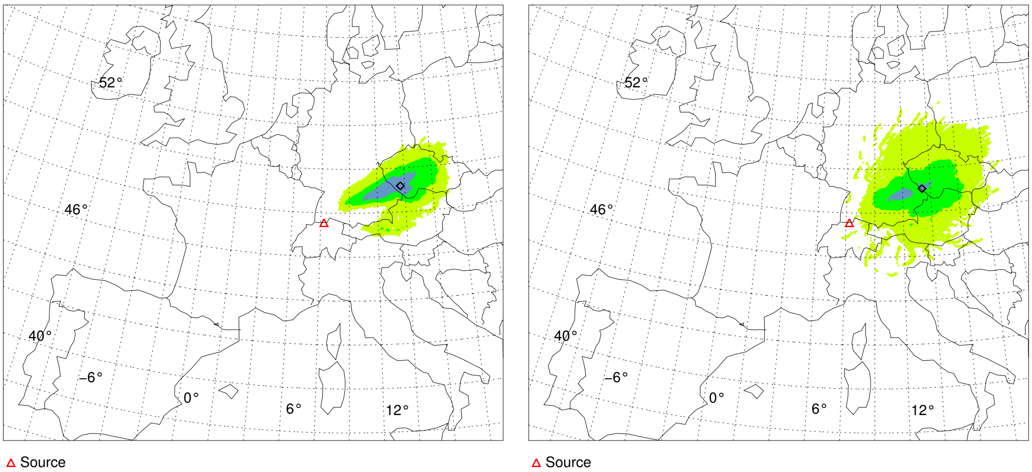

Figure 1: Reference (left; prognostic turbulent kinetic energy from aLMo) and Tst1 (right; diagnostic turbulent kinetic energy) of 6 October 2006. The filled isolines show the near-surface concentrations expressed in Bq m^{-3} of the ranges <1, 1 – 10, 10 – 100 (not visible: 100 – 1000, 1000 – 10000, >10000). The black diamond marks the location of the maximum value.

effect on the concentrations. Nevertheless it is tested here because we will operationally use a different setting than that of the DWD.

Test of 6/7 October, 12/13 October, 1/2 November
The tests repeat in an identical way the results of reference (same surface occupied by the same concentration level, equal maxima values), as expected.

Averaging layer reduced to 200 m (Tst4)

In emergency response systems, the average concentration over the lowest 500 m AGL is normally used for decision support. In this test, the concentration is averaged over the lowest 200 m AGL only.

Test of 6/7 October
The form and the surface of the concentration isolines are almost identical for both tests. On T_0+24, the position of the concentration peak is moved towards the North-East for the Tst4, and then starts to decrease slowly compared with the reference test. The maxima of concentrations are higher by factors for the Tst4 at the beginning (first 6 and 12 hours) of the event. Later on, the values become almost identical.

Test of 12/13 October
Referring to the first 6, 12, 18 and 24 hours, the form and the surface of the concentration isolines are identical for test and reference. For the remaining hours, the surface taken from the contaminated territory is slightly lower for the Tst4. The maxima of concentrations are largely higher than in the beginning (first 6 and 12 hours) of the event for the Tst4. The situation is reversed during the next 18, 24 and the 30 hours.

Test of 1/2 November
The shape of the surfaces covered by the same level of concentration is the same. Maximum values are increasingly higher compared to the test of reference.

Concentration of lowest model layer (Tst4a)

In this test, the concentration is averaged over the lowest aLMo layer only (approx. 60 m

AGL).

Test of 6/7 October
For the reference, the concentration levels are more concise. The form and the surface of the concentration are almost identical for test and reference. At the time T_0 + 24 h, the surface occupied by the Tst4a cloud is slightly smaller than the one in the reference and more limited from the north-east side.

The maxima of the concentrations for Tst4a are much higher than the reference at the beginning of the event (at 6 and 12 hours, roughly 5 and 4 times, respectively). It remains always higher at later times, but not as much as at the beginning.

Test of 12/13 October
In the reference, the levels of concentration are more concise. For the test Tst4a, after 24 hours, the surface occupied is smaller compared to the reference (Fig. 2) and becomes increasingly limited with time toward the north. The maxima of concentrations are much higher than in the reference at the beginning of the event (at 6 and 12 hours, almost by a factor of 6 and 2, respectively) for the Tst4a. The situation is reversed at 18 and 24 hours. It is in Tst4a that we find the highest peaks among all tests, except for the hours 18 and 24.

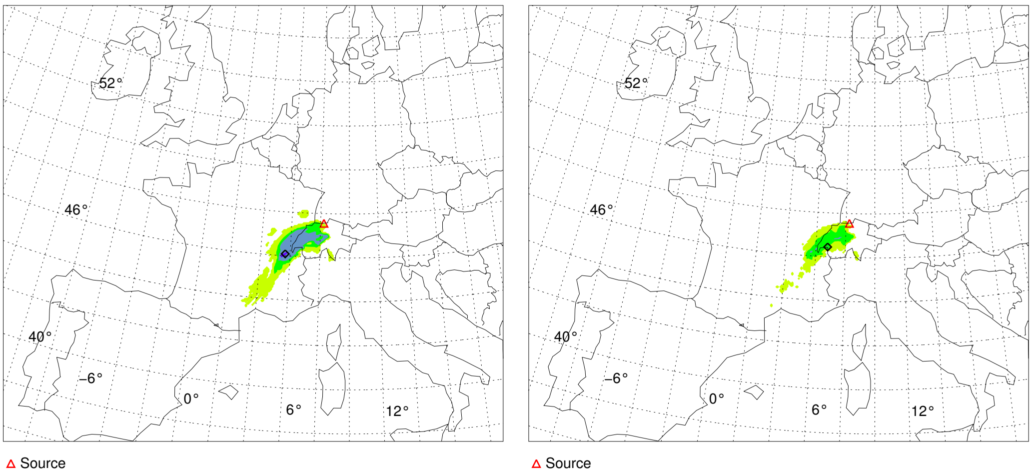

Figure 2: Reference (left; concentration in lowest 500 m above ground) and Tst4a (right; concentration in the lowest aLMo model layer) of 12 October 2006. Scale as in Figure 1.

Test of 1/2 November
The contours are less frayed; the form is much more restricted, and with higher concentrations during the simulation period. Higher maximum values occur during the whole period. The maximum value is more than 3 times bigger at the end of the first 6 hours.

Horizontal drift correction (Tst5)

The horizontal drift correction term in the equation of motion is turned on for this test. Its effect is usually small, so that it can be neglected.

Test of 6/7 October, Test of 12/13 October, Test of 1/2 November
The maximum concentrations values, the shape of the cloud as well as the surfaces occupied are identical for both reference and Tst5. Only for the test from 1/2 November, maximum values are very slightly lower.

5 Generalization in terms of cloud properties

Cloud shape: The shapes are identical (plume shape) for all tests, except for Tst1. For Tst1 with the meteorological data from the 6/7 October 2006, the cloud appears larger; round shaped, and later becomes rather circular and much dispersed (Fig. 1). For the tests with the meteorology from the 12/13 October 2006, Tst1 is much more dispersed. For the tests with the meteorology from the 1/2 Novermber 2006, the cloud shape for the Tst1 is larger and more diffuse. For this time period, the Tst4 and 4a cloud becomes smaller starting at 18 hours.

Covered surface: The occupied surface from the same level of concentrations is identical for all tests, except for the Tst1, where the cloud appears larger and occupies a very broad territory at the end of the period of observation.

Direction of cloud propagation: As intended, according to the variing weather data inputs, the directions of the pollutant cloud propagation are different: On October 6/7 the cloud is directed towards east-north-east, on October 12, the direction is towards south-west, while on November 1/2 the direction is towards south-est.

Maximum values of concentration:
The Tst3 results match completely with those of the reference. The values obtained for the maxima concentration are equal.

The Tst2, Tst3 and Tst5 results are not very different from each other, as well as compared with the references. In the first 6 hours after the release, the differences between the maximum concentrations values are very large, corresponding to different parameterizations: almost 5 times.

We can generalize that the test Tst4a has the most increased concentration among all tests.

6 Conclusions

1. Depending on the meteorological input, the parameterization of the turbulent kinetic energy may play an important role (Fig. 1). Although some change was to be expected, the extent of the change was not expected, because diagnostic and prognostic TKE describe the same physical measure of the turbulence.

2. The height of the constant-height averaging layer influences the results strongly (Fig. 2) with various duration depending on the examined meteorological conditions.

3. The influence of the sedimentation velocity and the correction of the horizontal drift are negligible for the in-air concentration under the considered meteorological conditions.

4. The printout of vertical cross-sections does not affect the results at all. This is as it should be.

References

Glaab, G., 1986: Lagrangesche Simulation der Ausbreitung passiver Luftbeimengungen in inhomogener atmosphärischer Turbulenz. Ph. D. thesis, Technische Hochschule Darmstadt, Germany.

Glaab, G., B. Fay, I. Jacobsen, 1998: Evaluation of the emergency dispersion model at the Deutscher Wetterdienst using ETEX data, *Atmos. environ.*, **32**, No 24, 4359 – 4366.

Schättler, U., A. Montani, 2005: Model System Overview. In: *COSMO Newsletter*, No. 5, 7–23. Available from http://www.cosmo-model.org.

Doms, G., U. Schättler, 2002: A Description of the Nonhydrostatic Regional Model LM. Part I: Dynamics and Numerics. *Deutscher Wetterdienst*, Offenbach, 134 pages. Available at: www.cosmo-model.org.

Doms G., J. Förstner, E. Heise., H.-J. Herzog, M. Raschendorfer, R. Schrodin, T. Reinhardt, G. Vogel, 2005: A Description of the Nonhydrostatic Regional Model LM. Part II: Physical Parameterizations, *Deutscher Wetterdienst*, Offenbach, 139 pages. Available at: www.cosmo-model.org.

Verification of LAMI at Synop Stations

A. Raspanti - A. Celozzi

CNMCA, Pratica di Mare - Italy

1 Introduction

A synthesis of COSMO-I7 (the Italian version of the COSMO-Model) verification results for winter, spring, summer and autumn 2006 is presented. In this paper only the following surface parameters are analysed: 2m Temperature (2m T), 2m Dew Point Temperature(2m TD), 10m Wind Speed (10m WS), Mean sea Level Pressure (MSLP) and precipitation (PP). Further information concerning verification of upper-air parameters can be found in the COSMO web site, along with several stratifications for weather parameters.

The observations forming the control data set were collected on 3-hourly basis from synoptic Italian network, including 91 manned stations and distributed over the Italian area (soon this sample will increase with the use of all synoptic Italian stations). Stations were subdivided into three classes according to geographical location; mountain stations ($>$ 700 m), valley stations or inner lowland stations and coastal stations. Stations subdivision in different classes has been chosen in order to check systematic errors related with different geographical and surface conditions. This approach can give two type of results: information about models ability in reproducing correct surface processes through a correct climatology in different geographical areas and indication of possible error sources through error comparison in different areas. For this reason, the results obtained in the verification of daily cycle for 2m T, 2m TD, 10m WS, MSLP and for categorical rainfall verification are presented.

2 Daily Cycle

In order to verify the diurnal behaviour of the model, the couples observation-forecast were stratified according to the hour of the day (3-hourly frequency), the season of the year and the forecast range (day 1 and day 2). Synchronous and co-located couples observation-forecast independently from the station position then form each sample. For each of the obtained samples the mean error (ME, forecast-obs) and mean absolute error (MAE) were computed.

3 2m Temperature

Figure 1 shows the behaviour of 2m-Temperature forecast error for all the set of Italian stations. A clear diurnal cycle is present for all months with the amplitude increasing form spring, through summer, to autumn. About the error pattern the figures show a strong cold Bias in winter becoming a warm one in the other seasons until 12 UTC with a fast decreasing between 15-18 UTC. Low absolute accuracy in the early morning and around midday, maybe a signal of an early warming.

Figures 2 and 3, the seasonal 2m-Temperature for coastal and valley stations, show, of course, the same behaviour of the previous graphs, with some more interesting characteristics. For example for coastal stations the model seems to be colder during afternoon, as even more for valley stations except for summer when it is a bit warmer. Again for valley stations MAE seems to be always lower (higher accuracy) and the Bias in summer shows us a model warmer for almost all the day (except at the sunset).

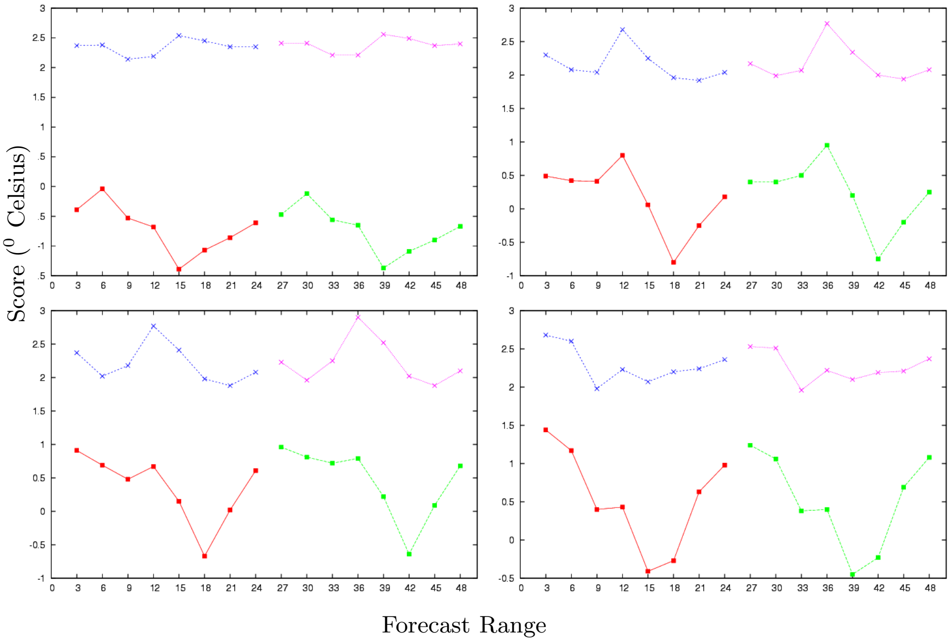

Figure 1: 2m-Temperature forecast error for 2006 (all stations): winter (upper left), spring (upper right), summer (lower left) and autumn (lower right).
Mean Error: day 1, day 2; Mean Absolute Error: day 1, day 2

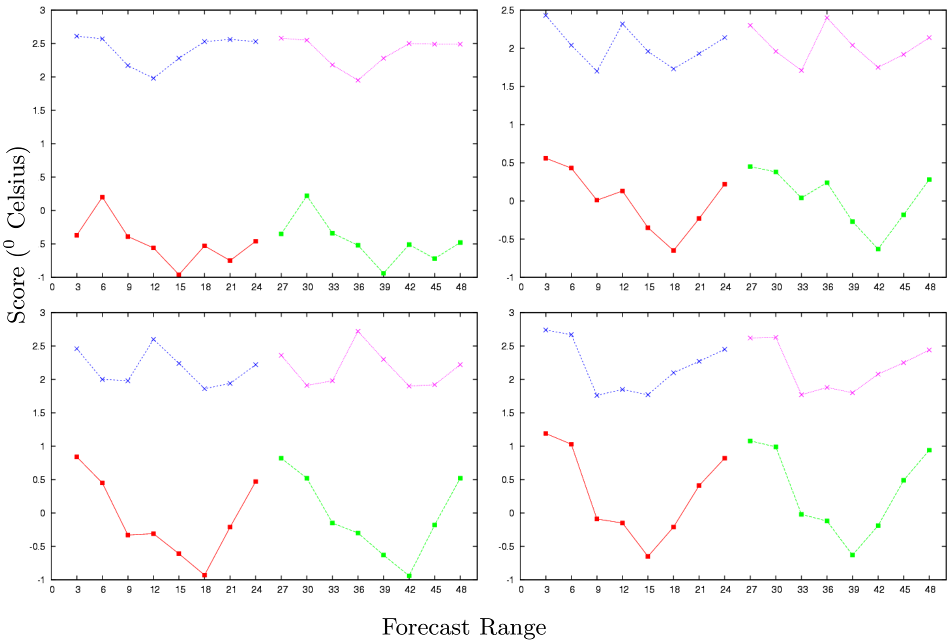

Figure 2: Seasonal 2m-Temperature for coastal stations: winter (upper left), spring (upper right), summer (lower left) and autumn (lower right).
Mean Error: day 1, day 2; Mean Absolute Error: day 1, day 2

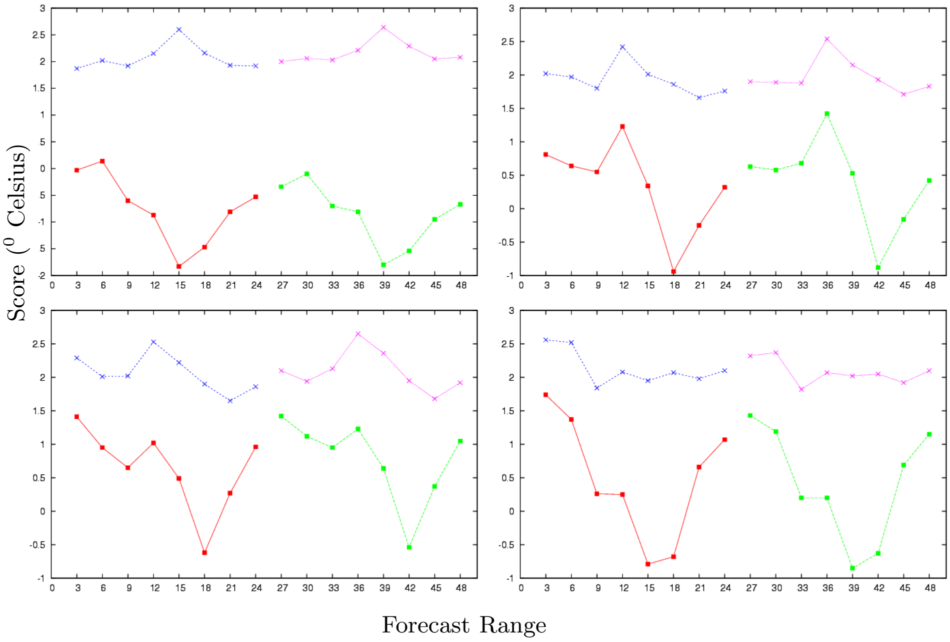

Figure 3: Seasonal 2m-Temperature for valley stations: winter (upper left), spring (upper right), summer (lower left) and autumn (lower right).
Mean Error: day 1, day 2; Mean Absolute Error: day 1, day 2

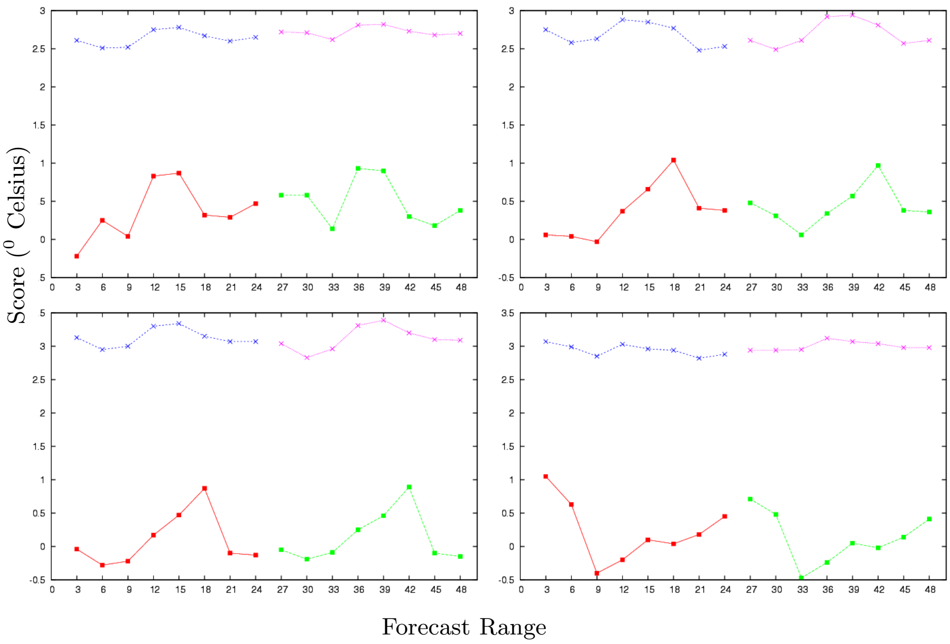

Figure 4: 2m Dew Point Temperature for all stations: winter (upper left), spring (upper right), summer (lower left) and autumn (lower right).
Mean Error: day 1, day 2; Mean Absolute Error: day 1, day 2

4 2m Dew Point Temperature

A diurnal cycle is also present in ME curves of 2m Dew Point Temperature, see Figure 4 for all Italian stations. In general, from the MAE or Bias point of view, it can be said the model has a better behaviour compared with temperature; in fact the mean is around 0/0.5 except for 15-18 UTC when it reaches the maxima values. An interesting behaviour can be found during autumn when the maxima are reached during the night. The absolute accuracy (MAE) values remain relatively high with maxima in summer, while a diurnal cycle is less evident.

5 10m wind speed

In Figure 5, the curves relative to mean error and mean absolute error of 10m wind speed for all Italian stations, are shown. Even if the amplitude is small a diurnal cycle is present in ME curves. An overestimation of wind speed, positive Bias, occurs especially during the cold months when dynamical circulation is dominant. It is interesting to point the attention to low ME and MEA values in spring and summer seasons: it could be interpreted as a good model interpretation of local breeze circulation.

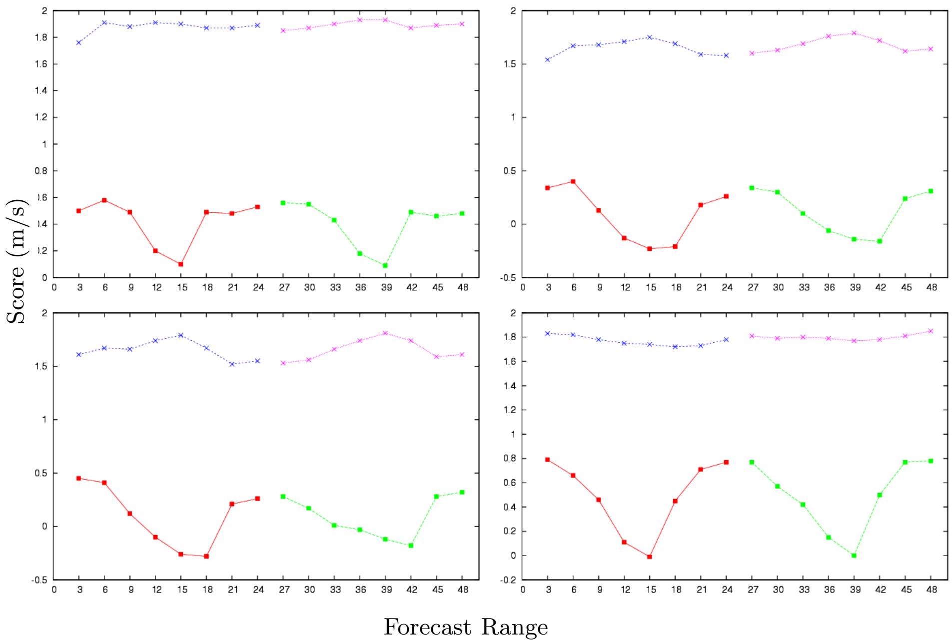

Figure 5: 10m wind speed for all stations: winter (upper left), spring (upper right), summer (lower left) and autumn (lower right).
Mean Error: day 1, day 2; Mean Absolute Error: day 1, day 2

6 Mean Sea level Pressure

Figure 6 shows MSLP mean error and mean absolute error for 2006 seasons all over Italy. Mean error curves do not show a clear diurnal cycle, also there is a quite good phase agreement between ME D+1 curve and ME D+2 curve, except for summer when a large positive Bias can be found during early morning at D+1 and decreasing with ranges. MAE curves shows how the mean sea level pressure is less affected by local circulations or by model physics and is dominated by atmosphere dynamics; in fact, MAE increases quasi-linearly in function of forecast with a degradation in MAE during the winter and autumn (characterised by stronger atmospheric motions). Besides, in summer, there is a clear negative Bias for D+2 (a loss of mass?).

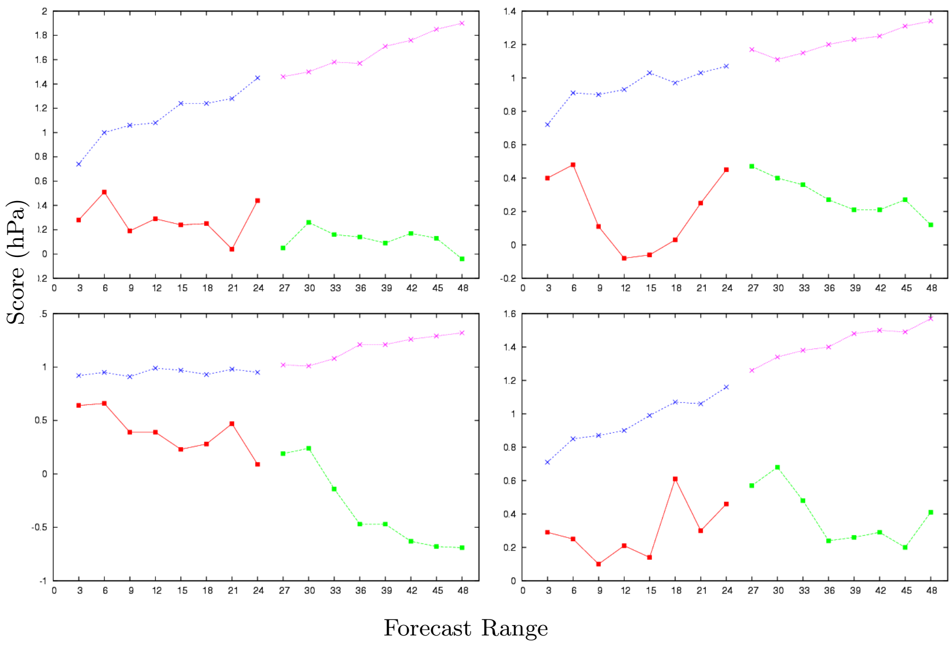

Figure 6: MSLP mean error and mean absolute error for all stations: winter (upper left), spring (upper right), summer (lower left) and autumn (lower right).
Mean Error: day 1, day 2; Mean Absolute Error: day 1, day 2

7 Precipitation

The results for 2006 seasons are summarised in Figures 7 and 8 where FBIAS, ETS scores are presented, respectively, for all Italian stations stratified for 12h accumulated precipitations, without any morphological or regional stratifications (for details about stratified precipitation scores see COSMO web site). Figure 7 (FBIAS) shows in winter (and less in spring) a better model performance, probably due to the type of precipitations (mainly large scale vs. convective) up to 4mm/12h, while in summer the shift in convective daily precipitations (model anticipates the occurrence) can be seen as a clear link with the same kind of signal in 2m-Temperature; in fact there are clear larger FBIAS scores for the morning ranges (00-12 and 24-36). In spring the signals are more complicated and, probably, a mix of the previous two. Equitable Threat Score plots for 12 hours accumulated rainfall, reported in Figure 8 show that the model performance decrease with the season and only 12 and 36 range remains acceptable, also in summer.

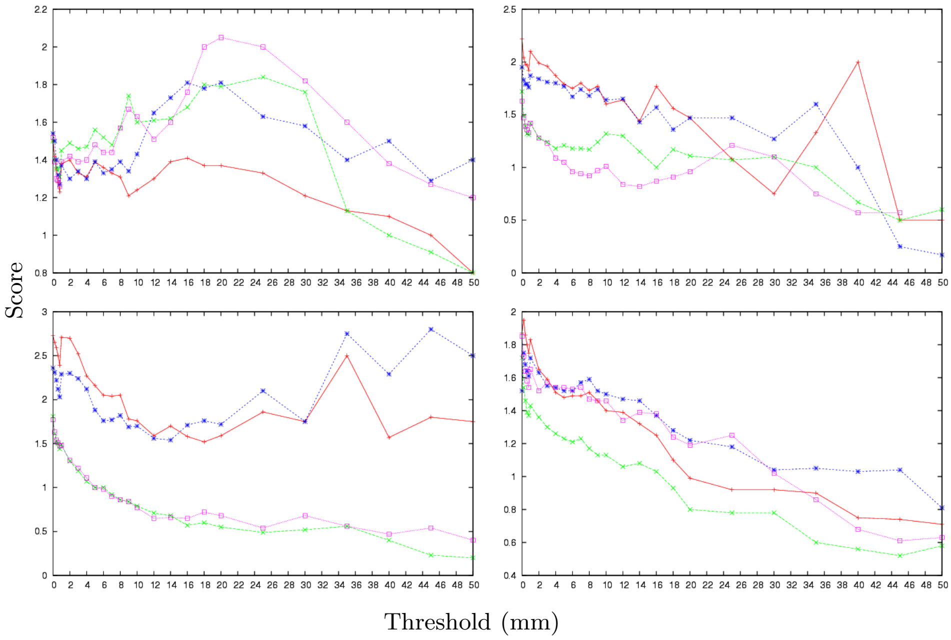

Figure 7: FBIAS for 12h accumulated precipitations for all stations: winter (upper left), spring (upper right), summer (lower left) and autumn (lower right).
FBI +12, FBI +24, FBI +36, FBI +48

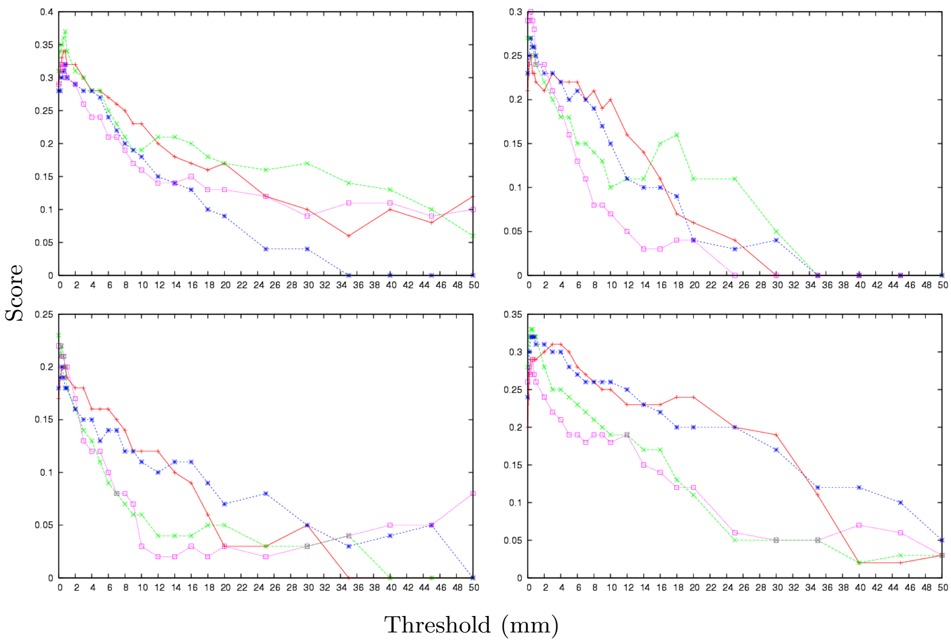

Figure 8: ETS for 12h accumulated precipitations for all stations: winter (upper left), spring (upper right), summer (lower left) and autumn (lower right).
ETS +12, ETS +24, ETS +36, ETS +48

Latest Results of the Meteorological Elements Verification over Poland

(Short note)

Katarzyna Starosta, Joanna Linkowska, Andrzej Mazur

Institute of Meteorology and Water Management
Centre of Numerical Weather Forecasts
61 Podlesna str., PL-01673 Warsaw, Poland

1 Introduction

The results of the verification of surface continuous parameters, of 24-h accumulated precipitation and upper-air parameters from January 2006 to December 2006 are presented in this article. We compared the data from SYNOP stations, rain gauges and TEMP stations vs. data from model version 3.5.

Verification of surface parameters using 56 SYNOP stations:

- Monthly verification for the following meteorological elements: 2m temperature, 2m dew point temperature, sea level pressure, 10m wind speed
- Operational verification of selected continuous parameters for chosen synoptic stations

The meteorological variables forecasted by the model were compared with synoptic data from 56 Polish synoptic stations. Mean error (ME) and root mean square error (RMSE) were calculated using the 12 forecast ranges (every 6 hours) for a 72 hour forecast starting at 00 UTC. The error estimators were calculated for all stations and for the whole country.

Verification of the 24-h accumulated precipitation using 308 rain gauges:

- Verification of the 24-hour accumulated precipitation using 7 indices from the contingency table for the 3 forecast ranges (1-day, 2-day, 3-day)
- The following precipitation thresholds were used: 0.5, 1, 2.5, 5, 10, 20, 25, 30 mm. For each threshold we calculated the following indices: FBI, POD, PON, FAR, TSS, HSS, ETS

Verification of upper-air parameters using 3 TEMP stations:

- Operational verification of the selected continuous parameters for Polish sounding stations
- Off-line verification of the selected continuous parameters. The quality of forecasts was verified against measurements of air temperature, relative humidity, air pressure and wind velocity at standard pressure levels conducted at three Polish upper-air stations

Selection and description of cases with poor QPF:

- Selection of single cases with a poor QPF but a reasonably well predicted large-scale flow from all the COSMO model implementations

- Conditional verification with predefined criteria: different vertical stability, stratiform vs. convective (model) precipitation, weather situation, etc.
- Collection of the cases with the largest QPF errors or greatest importance
- Running model reference version (3.19) for the test cases

2 The temperature at 2 m above ground level

A monthly and seasonal variation for the RMSE and ME occurred. The mean error is negative in the winter and positive in the summer. We observed a clear diurnal cycle during the spring (April - June). In the spring and the summer we noticed a large diurnal amplitude of both indices. The biggest amplitude of the ME and RMSE occurred in April and May with maximum value during the day. The smallest value of the ME was in November. See Figures 1 and 2.

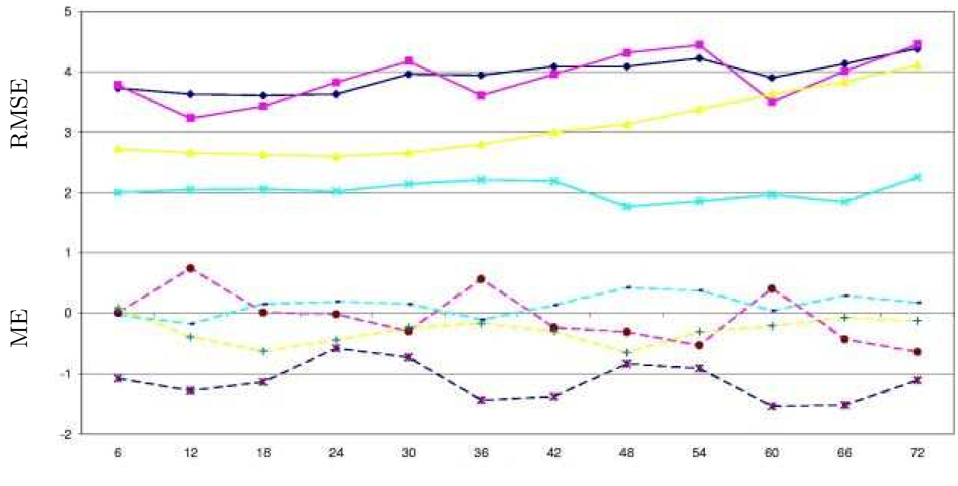

Figure 1: RMSE (full lines) and ME (dashed lines) for Polish SYNOP station measurements (February 2006). Colors are: Temperature, Dew point temperature, Wind, Pressure

3 The dew point temperature at 2m a.g.l.

The monthly variation of the mean error can be observed. The ME for March is negative at night time and positive during the day. The clear diurnal cycle of the RMSE and ME occurred in the summer. For the first half of the year the RMSE increases with the forecast time. The amplitude of RMSE is small from November to December. See Figures 1 and 2.

4 The wind speed at 10 m a.g.l.

The ME is mostly positive from 0 m/s to 1 m/s. The ME increases during the forecast time. The RMSE is quite similar for every month and different forecast ranges (first day, second day and third day). See Figures 1 and 2.

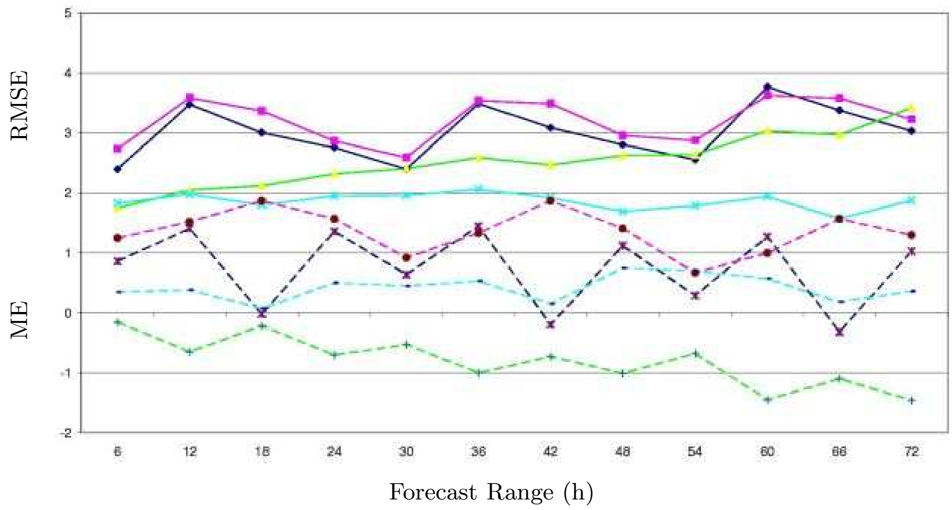

Figure 2: RMSE (full lines) and ME (dashed lines) for Polish SYNOP station measurements (June 2006). Colors are: Temperature, Dew point temperature, Wind, Pressure

4 Sea level pressure.

The RMSE and ME increase with the forecast time. The range of ME is from -1 hPa to +1 hPa. Only in August the ME value is below the above-mentioned range. The RMSE is smaller in the spring and summer and higher in the winter. See Figures 1 and 2.

5 Precipitation.

The model predicts more precipitation than actually occurred. The forecast is better for the first day and for smaller thresholds of precipitation. The best result of the precipitation prediction is in November. See Figures 3-8.

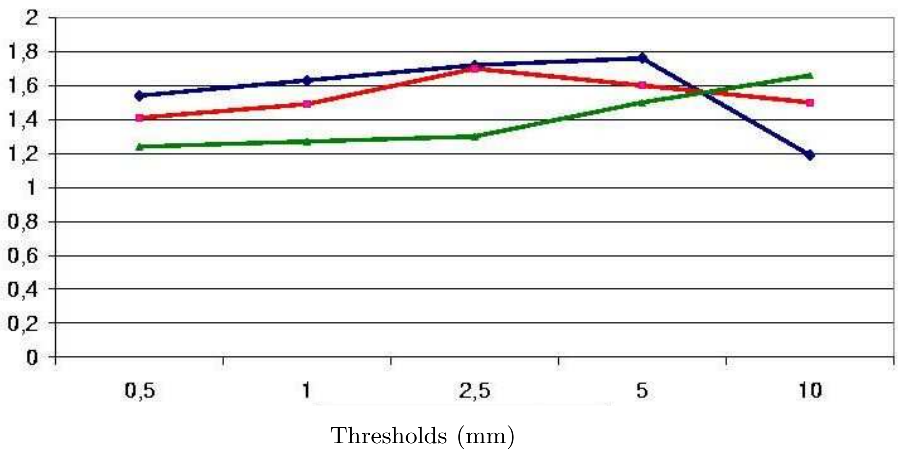

Figure 3: FBI index, precipitation measured with rain gauge network (February 2006). Colors are: day 1, day 2, day 3

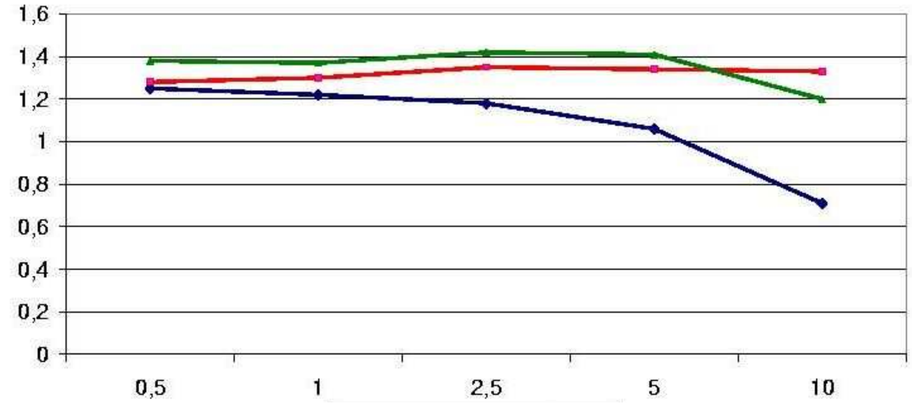

Figure 4: FBI index, precipitation measured with rain gauge network (June 2006). Colors are: day 1, day 2, day 3

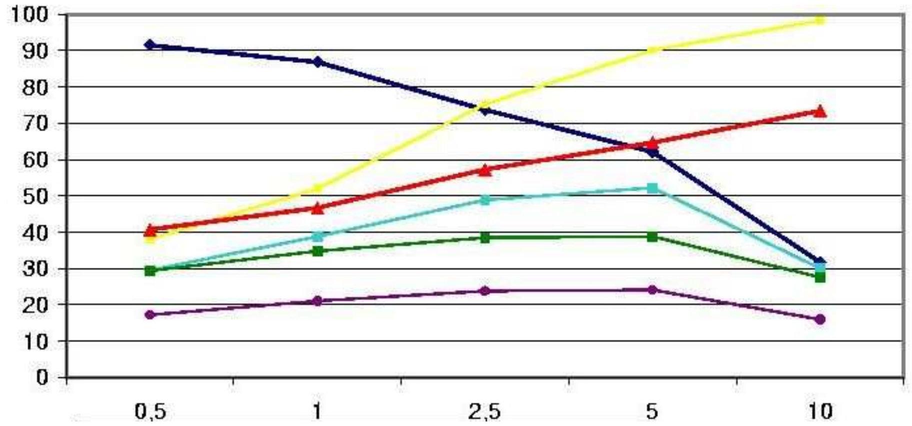

Figure 5: Indices for 24h precipitation, first day of forecast (February 2006). Colors are: POD, PON, FAR, TSS, HSS, ETS

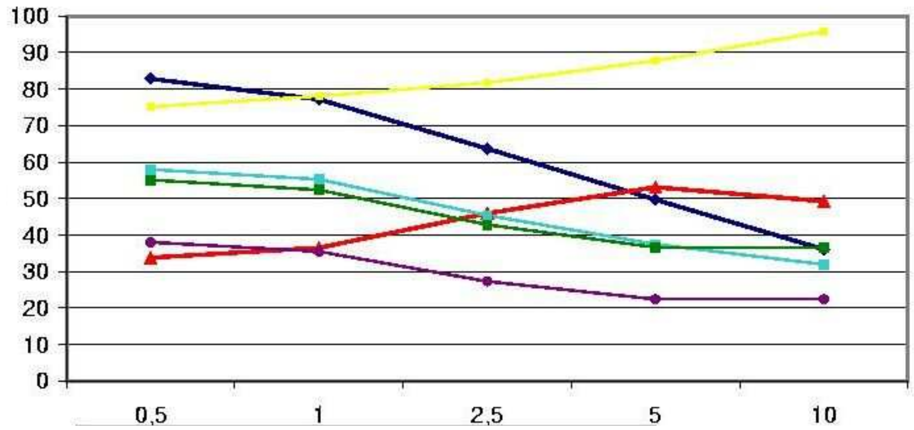

Figure 6: Indices for 24h precipitation, first day of forecast (June 2006). Colors are: POD, PON, FAR, TSS, HSS, ETS

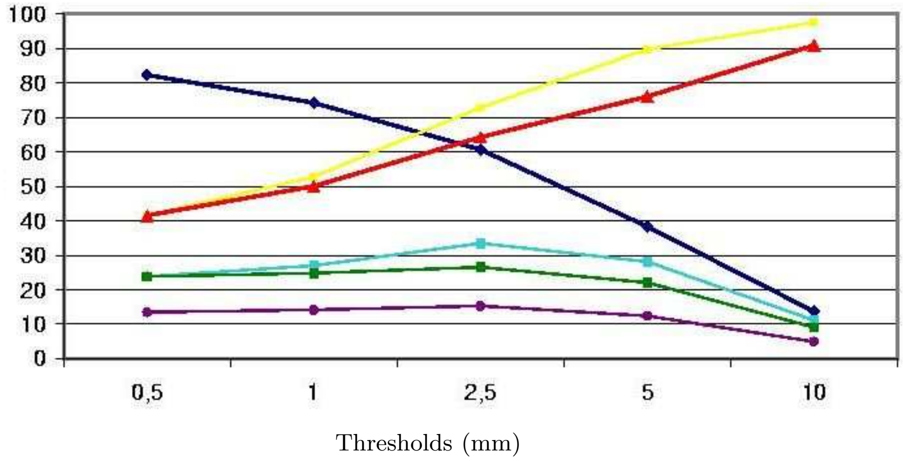

Figure 7: Indices for 24h precipitation, second day of forecast (February 2006). Colors are: POD, PON, FAR, TSS, HSS, ETS

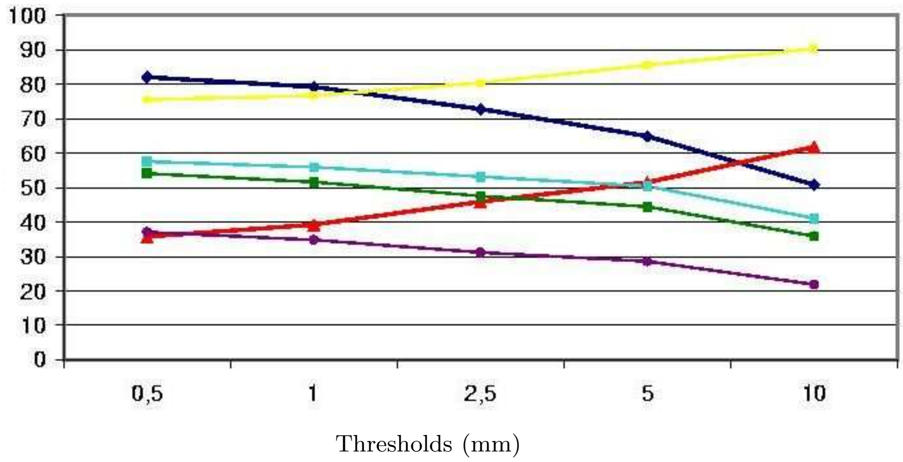

Figure 8: Indices for 24h precipitation, second day of forecast (June 2006). Colors are: POD, PON, FAR, TSS, HSS, ETS

6 Verification of upper - air parameters

Errors (especially RMSE) increase with forecast time. That is clearly seen mainly for wind velocity and air temperature, still, relative error (i.e. ratio error to value) for these two parameters is actually very low. Comparing sequential years, improved parametrisation results in enhancement of quality of forecasts. See Figures 9-12.

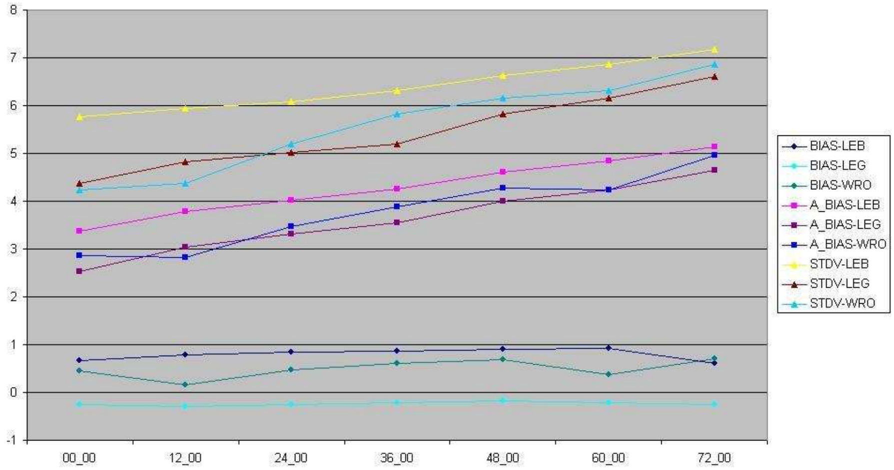

Figure 9: Bias, absolute bias and standard deviation of wind velocity at pressure levels, Polish upper-air stations, vs. forecast hours (January 2005 - June 2006).

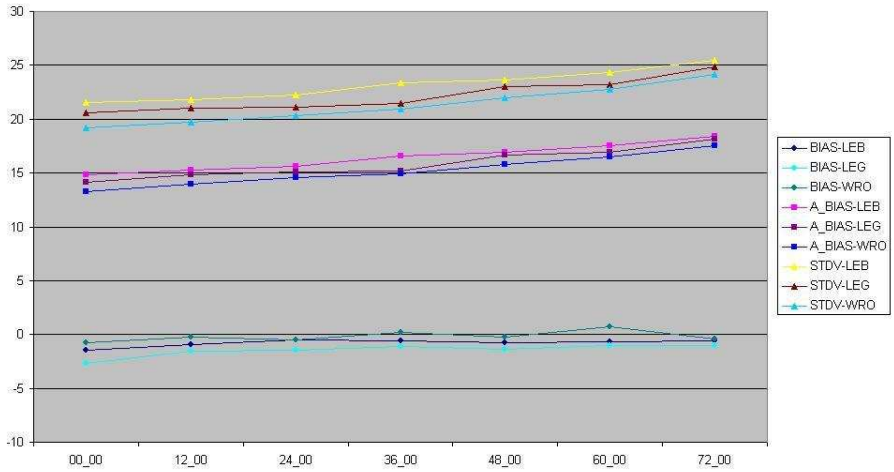

Figure 10: Bias, absolute bias and standard deviation of relative humidity at pressure levels, Polish upper-air stations, vs. forecast hours (January 2005 - June 2006).

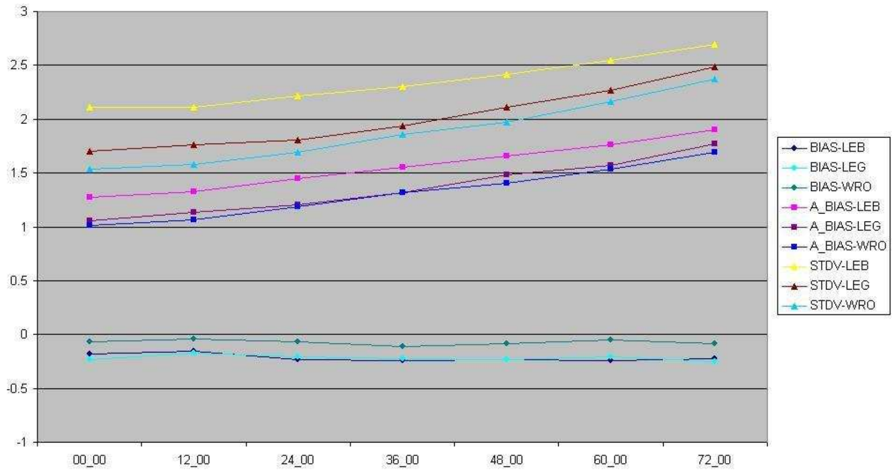

Figure 11: Bias, absolute bias and standard deviation of temperature at pressure levels, Polish upper-air stations, vs. forecast hours (January 2005 - June 2006).

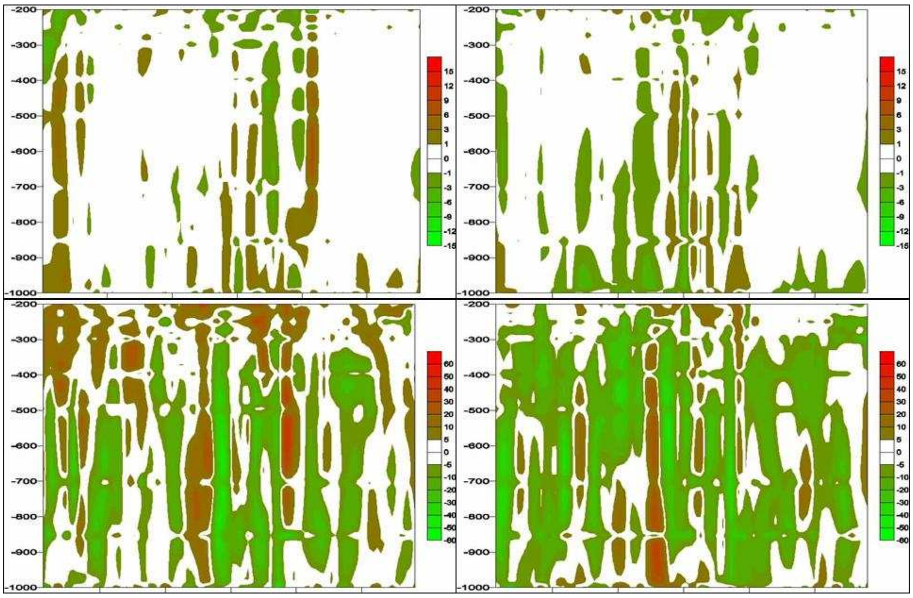

Figure 12: Mean error of air temperature (upper charts) and relative humidity (lower charts) at standard pressure levels for model run at 00 UTC (left charts) and at 12 UTC (right charts), (Leba station, 2005-2006).

7 Case study of QPF.

To choose test cases being dominated by stratiform or convective precipitation we used every day model results (3h forecast and accumulated 24 h), surface data from 56 SYNOP stations and 308 rain gauge stations and radar network. We received reference version of the model 3.19 with grid scale 7 km. This version was used for sensitivity studies by changing the initial condition, numerics, and physical parametrisations. Following example demonstrates model's behaviour in selected meteorological situation(s) and presents the results of precipitation forecast derived from two different runs of the operational version and reference version of the model. As an example we show here the results for 24-hours accumulated precipitation, 4 May 2005. See Figures 13-16.

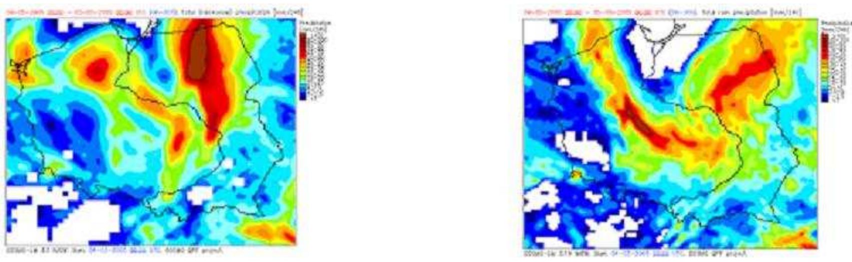

Figure 13: Total precipitation (left: COSMO model v. 3.05, right: COSMO model v. 3.19).

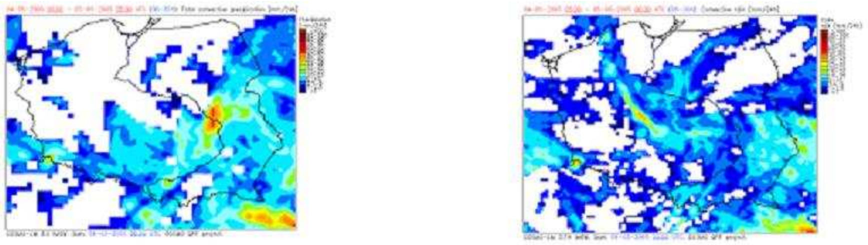

Figure 14: Convective precipitation (left: COSMO model v. 3.05, right: COSMO model v. 3.19).

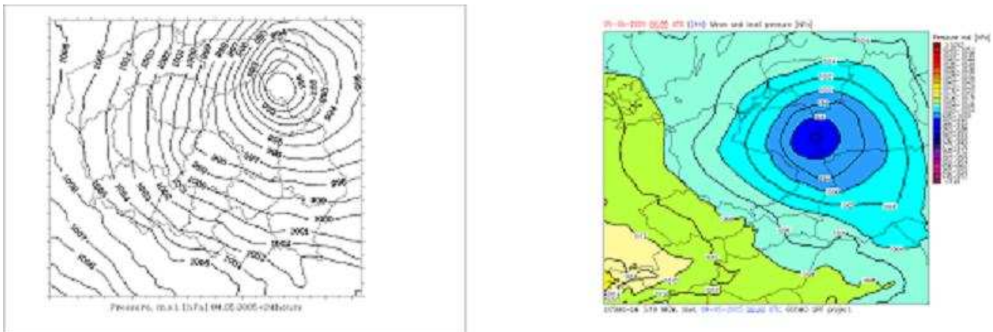

Figure 15: Pressure chart (left: COSMO model v. 3.05, right: COSMO model v. 3.19).

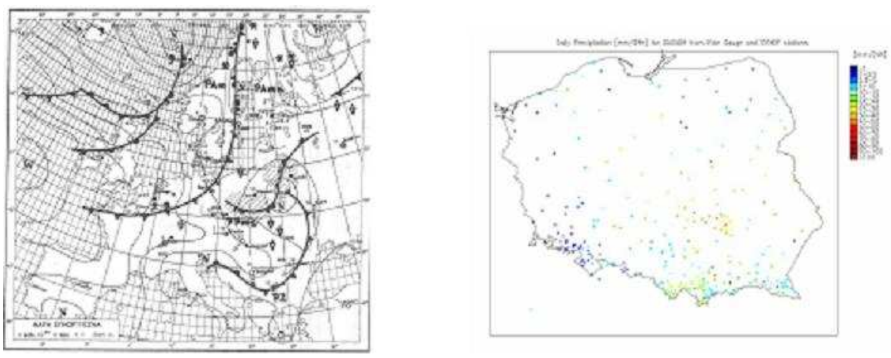

Figure 16: Synoptic chart and precipitation measured at Polish stations network.

Results on Precipitation Verification over Italy

Elena Oberto, Marco Turco, Paolo Bertolotto

ARPA PIEMONTE, Torino, Italy

1 Introduction

In this report we sum up the most significant results on QPF verification of the three COSMO model versions (German, Swiss and Italian, hereafter called LME, aLMo and LAMI respectively for sake of comprehension) over Italy. The considered observation dataset is composed by a collection of high resolution rain gauges network coming from the Civil Protection Department (about 1300 stations have been taken into account due to their high performance in term of data quality, see Fig. 1). It has to be noted that about 400 of these stations are already shared in the COSMO common database. The considered verification period depends on the archived models availability: in fact we have got a common and complete dataset for the three versions only from January 2006. So, we carry out the skills and scores comparison among them for the first half of 2006 (200601 - 200606) considering 24h cumulated precipitation (forecasted and observed) averaged over the meteo-hydrological Italian basins.

Figure 1: Italian observation network (1300 rain gauges distributed over the most part of the territory).

2 Scatter plot of QPF

We performed a direct comparison between observed and forecasted 24h cumulated precipitation (D+1) averaged over Italian basins for the first 6 months of the year 2006 considering 00UTC runs of the three model versions (Fig. 2).

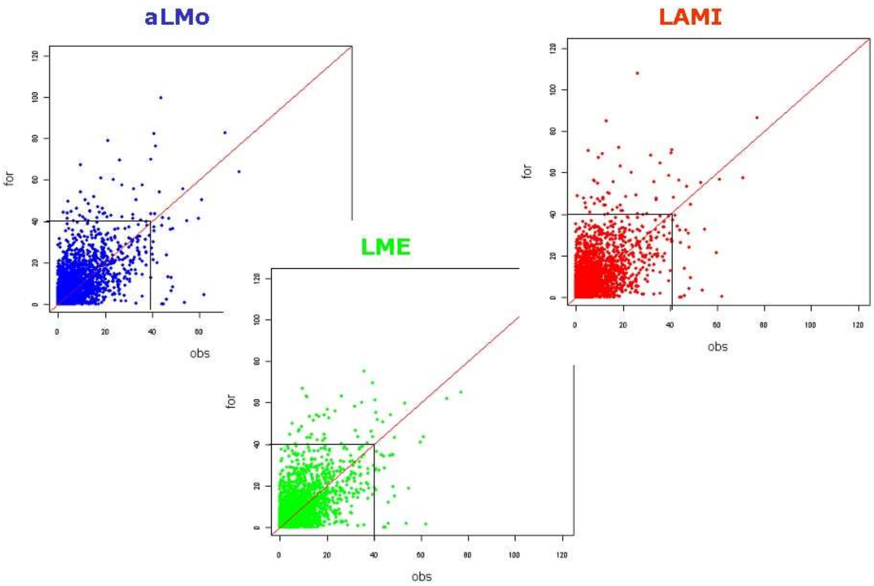

Figure 2: Scatter plot of QPF averaged over Italian basins D+1: 200601 - 200606.

There is a general overestimation in all the versions, especially for LAMI. Then, fixed a threshold at 40 mm (for both observations and forecasts), we can see that: most of the points above the threshold are situated in the upper left part of the box that means the model has more false alarms than misses. LME seems to have a better agreement between observed and forecasted data with a dispersion less pronounced than the other ones.

3 Statistical indices

We calculate the statistical indices (BIAS and ETS), considering the period from 200601 to 200606, over each Italian meteo-hydrological basins to evaluate the different behaviour of the three model versions (00UTC runs) with respect to the territory and orography (Fig. 3).

In order to reach a good statistics we fixed a low threshold of 2 mm in 24h. Remarkable comments:

- The BIAS has a similar pattern for the three versions (with a general more noticeable overestimation for LAMI). There is an overestimation over the alpine chain with a peak on the Ticino area (probably due to a strong impact of the orography) and over central Italy; slight underestimation over south Italy. On the other hand, we obtain a different performance over the Po valley, with good results on average for aLMo and LME but a higher BIAS for LAMI over the eastern part.
- The ETS has a good performance for aLMo and LME; in general the lowest scores are over the alpine chain and Liguria (the lowest ETS values in the Abruzzo region maybe are due to observed data problems).

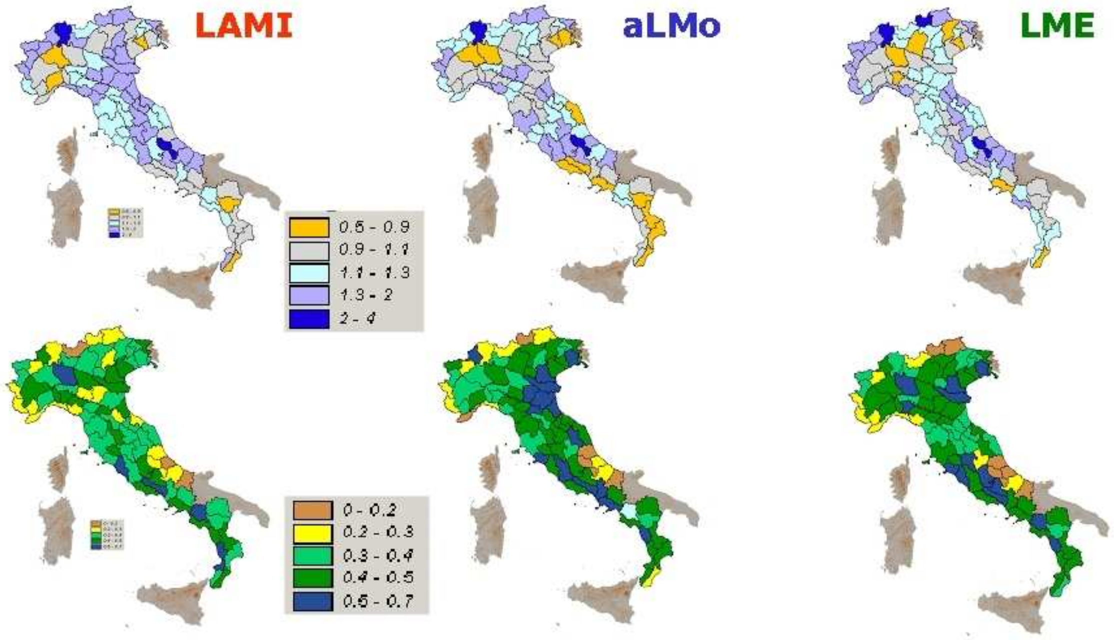

Figure 3: BIAS and ETS over each meteo-hydrological basins for 2 mm/24h: 200601 - 200606.

On the other hand, to evaluate a statistically significant difference among the versions we plot again (over the same period 200601 - 200606) the scores with a sample made by all the 24h cumulated precipitation average over the basins (Figs. 4, 5, 6).

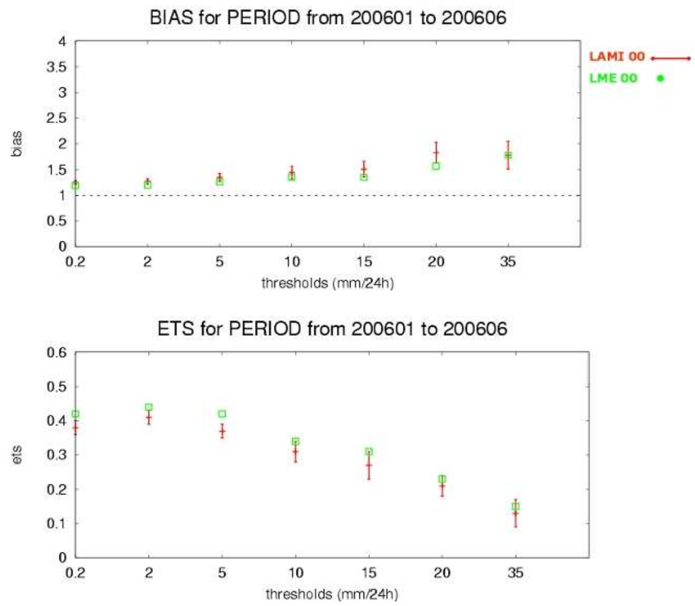

Figure 4: Scores at D+1: cumulated average precipitation over Italian basins (200601 - 200606) for LME and LAMI.

In this case, the Hamill Hypothesis test (bootstrap resampling technique, see Hamill, 1999) is used to calculate a confidence interval to evaluate if the model performance differences are statistically significant. The error bars indicate 2.5th and 97.5th percentiles of resampled distribution, applied to the "reference" model (see Turco et al., 2005). In Fig. 4 is plotted

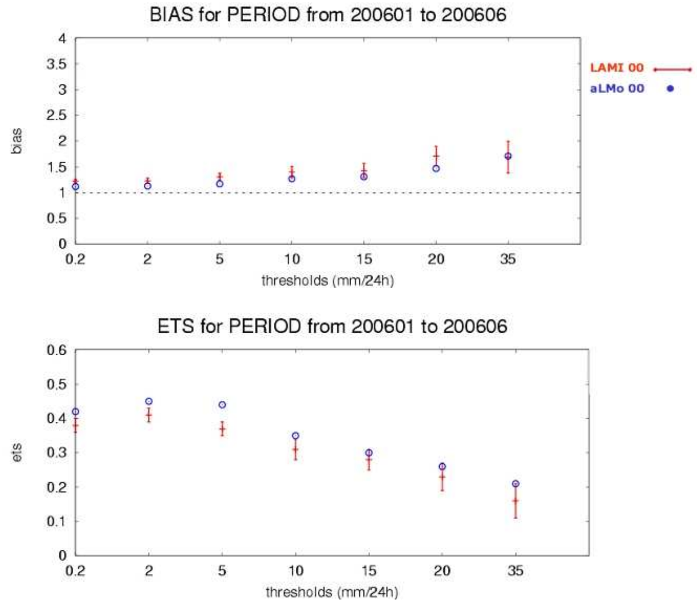

Figure 5: Scores at D+1: cumulated average precipitation over Italian basins (200601 - 200606) for aLMo and LAMI.

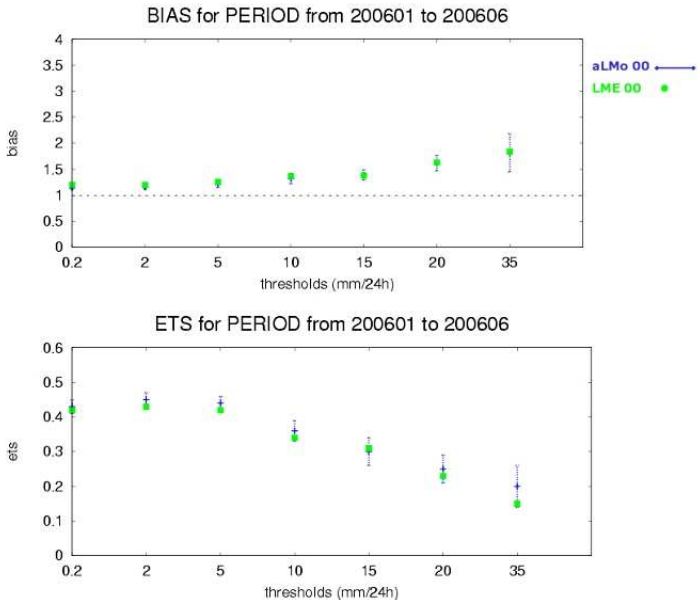

Figure 6: Scores at D+1: cumulated average precipitation over Italian basins (200601 - 200606) for aLMo and LME.

the comparison between LAMI and LME: we obtain quite similar values with respect to the BIAS (except for 20 mm) for all the thresholds, but there is a little statistically significant improvement for LME in terms of overestimation, on the other hand we obtain a significant better ETS for LME for thresholds below 20 mm. In Fig. 5 is plotted the comparison between LAMI and aLMo: we obtain a statistically significant improvement in the BIAS of aLMo with respect to LAMI for almost all the thresholds (except 15 mm and 35 mm) and better ETS below 15 mm. In Fig. 6 is plotted the comparison between aLMo and LME: except for very low thresholds, where aLMo BIAS is better then LME BIAS, both versions are comparable.

In the following figures we plotted BIAS and ETS for the three versions considering 6h average cumulated QPF over Italian basins for a fixed thresholds (10 mm) to evaluate the models behavior versus the forecast time. In this case we could not apply the bootstrap technique due to the data time correlation (Fig. 7).

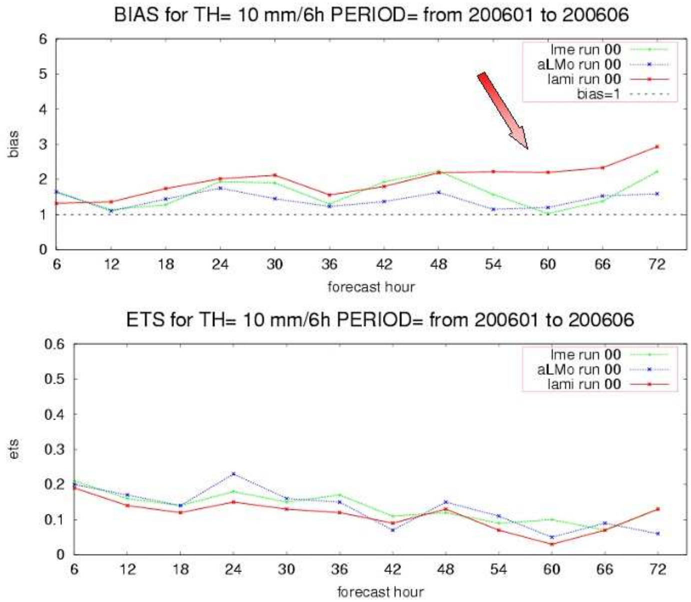

Figure 7: Daily trend over Italian basins.

Anyway, some important observations can be summarized:

- LAMI has the worst skill with a sharp worsening after D+2.
- Similar results for aLMo and LME, with a slightly better skills for aLMo.
- There is an evident diurnal cycle for the BIAS index: lower values at midday and greater at night.

4 Focus on LAMI

In this part we consider a longer data period to study the long term LAMI performances and features. So, in Fig. 8 we show the seasonal trend for BIAS and ETS starting from winter 2003 to spring 2006, both for the first (red line in the plot) and the second day (green line in the plot), having chosen a fixed thresholds of 20 mm: a worsening with respect to the forecast day is evident. There is no significant trend in time but there is a seasonal trend, in which the higher overestimation occurs during the summer and the better performance is obtained in autumn.

It is interesting to study the spatial error distribution for LAMI, on average over a long period. So, starting from winter 2003 to spring 2006 we calculated and plotted BIAS, ETS, POD and FAR over each of the Italian meteo-hydrological basins with respect to a fixed thresholds of 10 mm (the minimum to have a sufficient statistics). In Fig. 9 we show the BIAS for D+1 and D+2: there is an overestimation over most of the basins, especially over the mountains and Central Italy, with a noticeable deterioration for D+2 (the higher BIAS values in the Abruzzo region maybe are due to observed data problems).

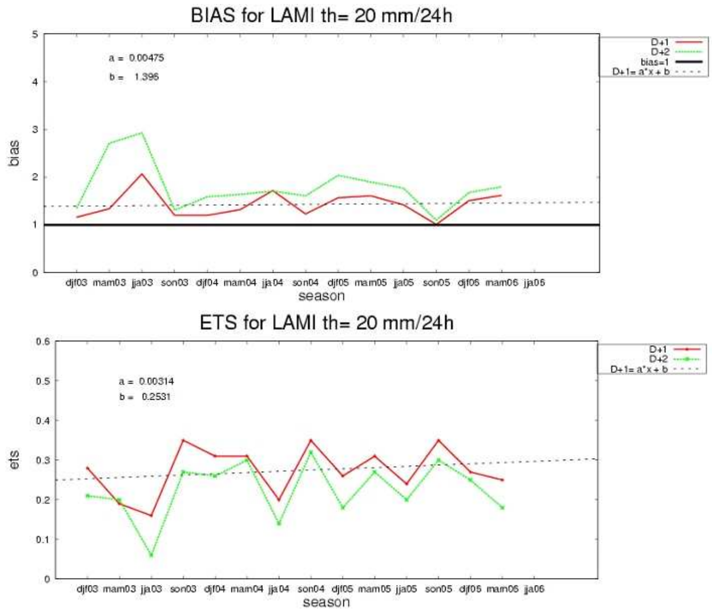

Figure 8: Seasonal trend for LAMI for 20 mm starting from DJF03 to MAM06: the red line refers to the first 24h and the green line to the second one.

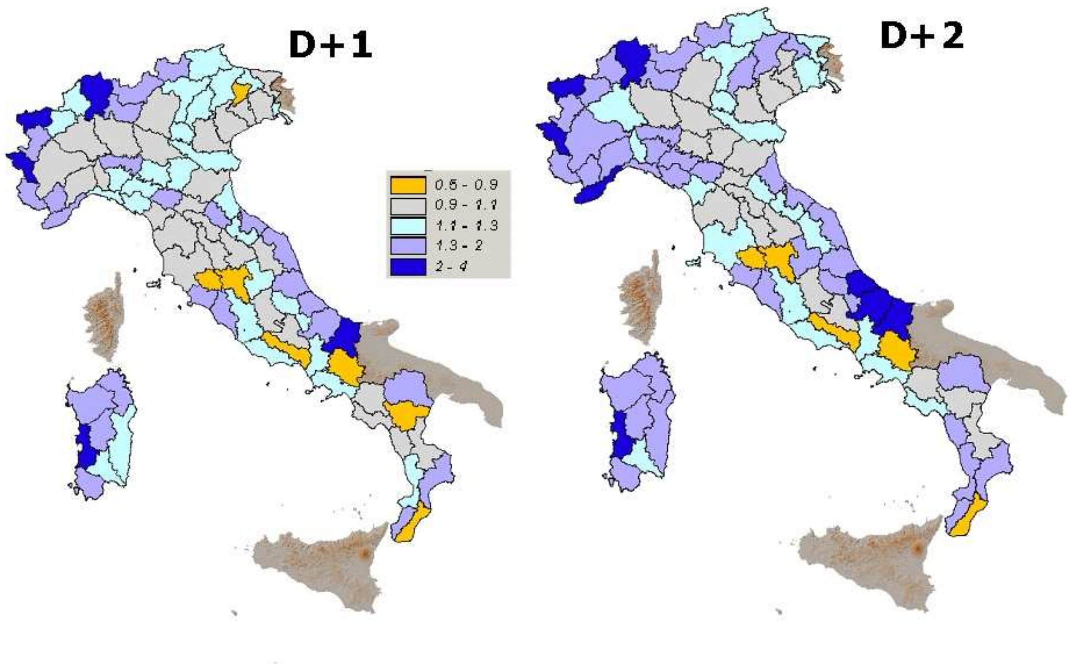

Figure 9: D+1 and D+2 BIAS over each basin (200212 - 200606).

In the same way, in Fig. 10 we show the ETS for D+1 and D+2: we find a rather good performance for the first 24h especially in Northern Italy and Tyrrhenian regions and worse performance over Sardinia and Adriatic regions (the low ETS values in the Abruzzo region maybe are due to observed data problems).

In Fig. 11 we show the POD for D+1 and D+2 and we can see a good performance for D+1 especially in north-western Italy; the worst performance is over Sardinia and central-south Italy.

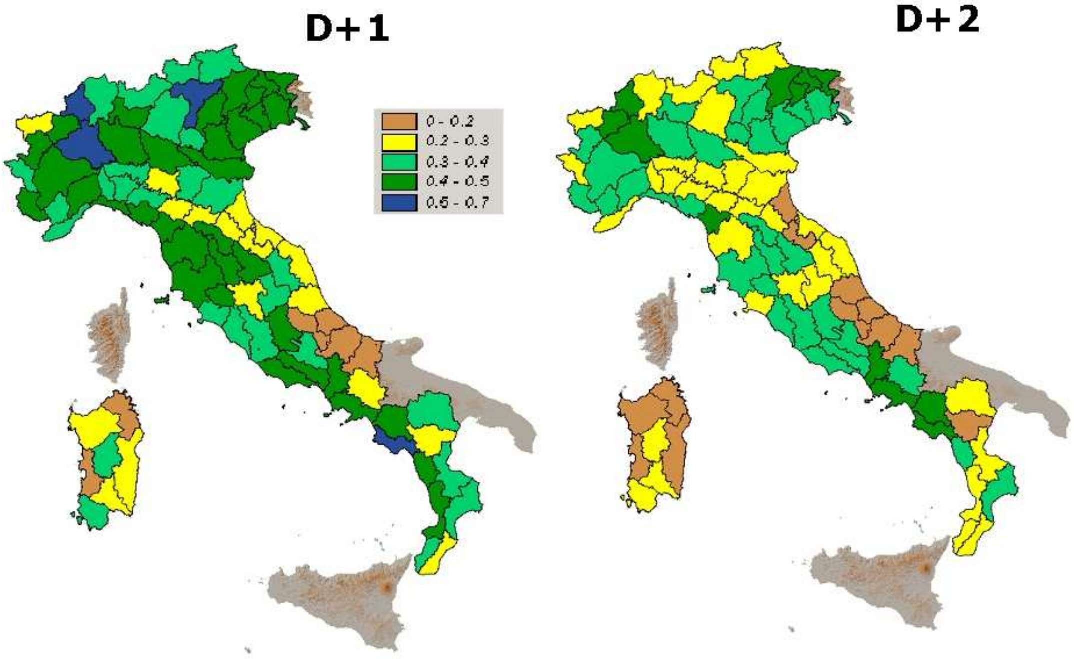

Figure 10: D+1 and D+2 ETS over each basin (200212 - 200606).

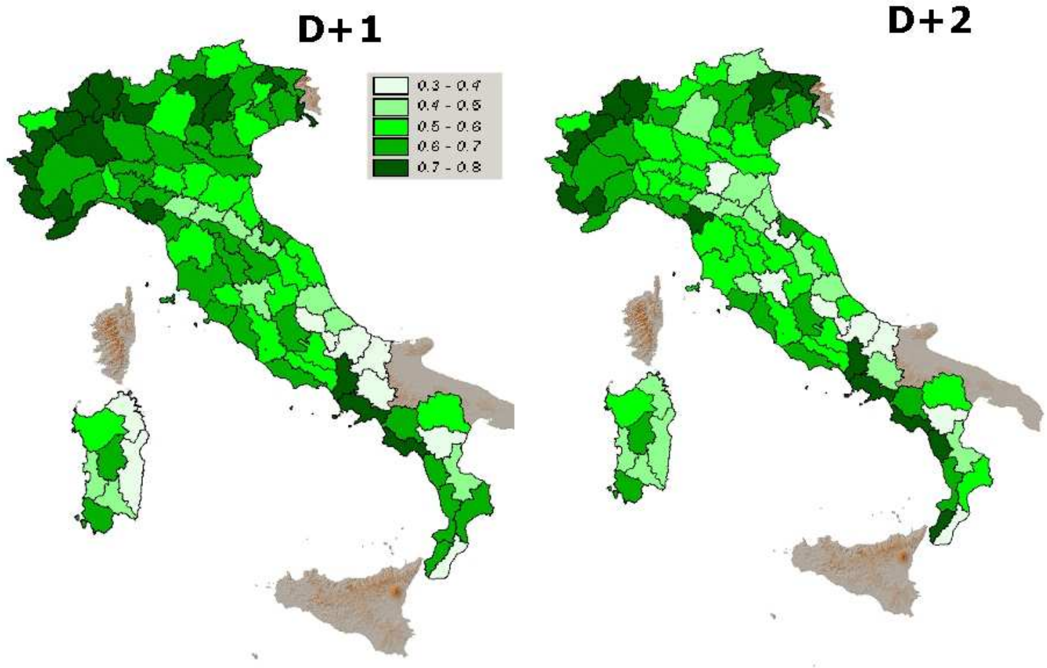

Figure 11: D+1 and D+2 POD over each basin (200212 - 200606).

Finally, the FAR in Fig. 12 shows a strong worsening with the forecast time and higher values over mountainous regions (the alpine chain and the Apennines) and Sardinia.

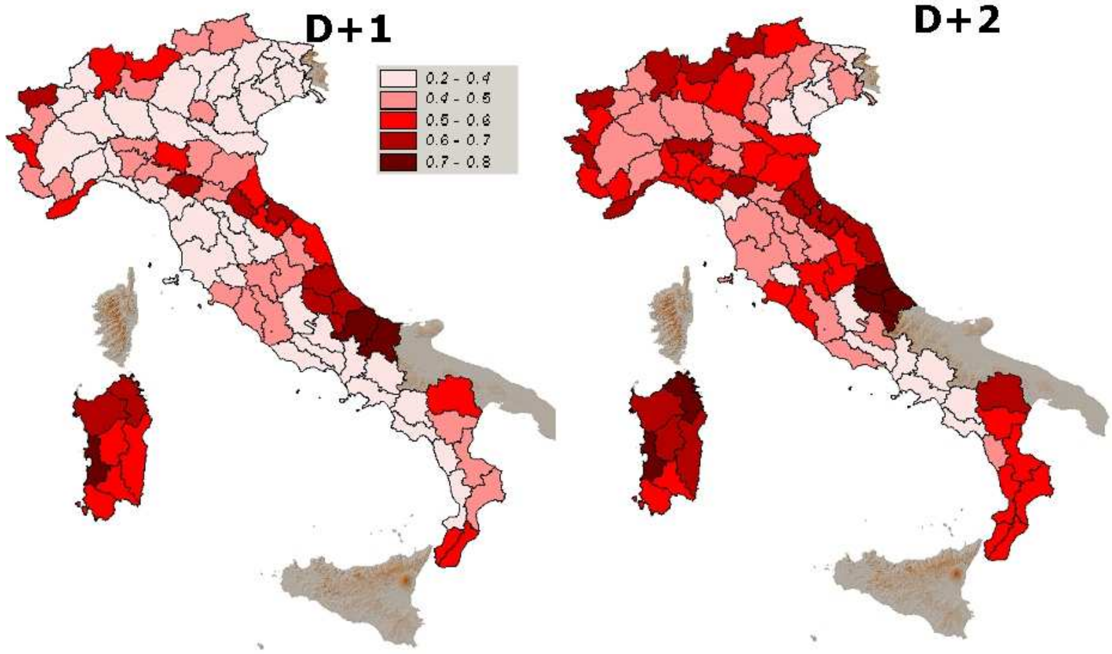

Figure 12: D+1 and D+2 FAR over each basin (200212 - 200606).

References

Hamill, T. M., 1999: Hypothesis tests for evaluating numerical precipitation forecasts. Wea. Forecasting, 14, 155-167.

Turco, M., Oberto, E. and Bertolotto, P., 2005: Progresses on LAMI, LM-DWD, aLMo verification over Northern Italy. COSMO Newsletter 5.

WG5-Report from Switzerland: Verification of the COSMO Model in the Year 2006

Francis Schubiger, Pirmin Kaufmann, André Walser, Emanuele Zala

MeteoSwiss, Zürich

1 Operational Verification

1.1 Verification with European SYNOP [*Pirmin Kaufmann*]

The operational verification of the COSMO model has been extended to include the diurnal cycle in 6h-steps. For the verification of wind direction (DD_10M), the winds with observed speeds below 3 m/s are filtered out starting spring 2006. The effect of this filtering is largest on the standard deviation, which is strongly reduced. Unfortunately, some stations in valleys even as broad as the Po valley have too little data left after filtering, so that the number of stations is somewhat decreased.

Some highlights of the seasonal verification:

Autumn 2005 (September, October, November)

- The verification results are in the same range as for all previous autumns. The one exception however is worth mentioning: the standard deviation of the pressure error (both PMSL and PS) is lower than in any previous autumn.

Winter 2005/2006 (December, January, February)

- The standard deviation of the pressure error (both PMSL and PS) is considerably lower in the last two winters (2004/2005 and 2005/2006) than in all the winters before. This includes the first winter with IFS boundary conditions (winter 2004/2005), so that this likely cause does not seem to determine the drop.
- The strong dry bias of the previous winters in the dewpoint temperature (TD_2M) has disappeared this winter due to the introduction of the prognostic TKE scheme on 1 December 2005.

Spring 2006 (March, April, May)

- The standard deviation of the pressure error (both PMSL and PS) of 1 - 2 hPa is slightly lower than the results for spring last year and is considerably smaller than during the three springs (2001 - 2003) prior to the usage of IFS boundary conditions.
- The general cold bias in T_2M has disappeared.
- This spring, a wet bias instead of the usual dry bias is visible in TD_2M (due to the introduction of the prognostic TKE scheme on 1 December 2005).
- The precipitation bias (TOT_PREC) and the frequency bias for the 0.1 mm/12h threshold are both larger than in all previous spring seasons except spring 2001.

- Some stations are missing due to the frequent occurrence of wind below 3 m/s (observed), for which the corresponding wind direction is filtered out. Note that a comparison of the wind direction results with previous years, for which no such filtering was done, is meaningless !

Summer 2006 (June, July, August)

- A positive model pressure bias of 0.5 - 1.5 hPa prevails in the model domain, but in the reduced pressure (PMSL) only (see Figure 1). This bias seems to correspond to increasing altitude and is not seen in the station pressure (PS), which indicates that the error of the pressure reduction is considerably larger than the model error. Stations along the eastern boundary have negative biases. This pattern has now been repeated during 3 summers (2004, 2005, 2006).

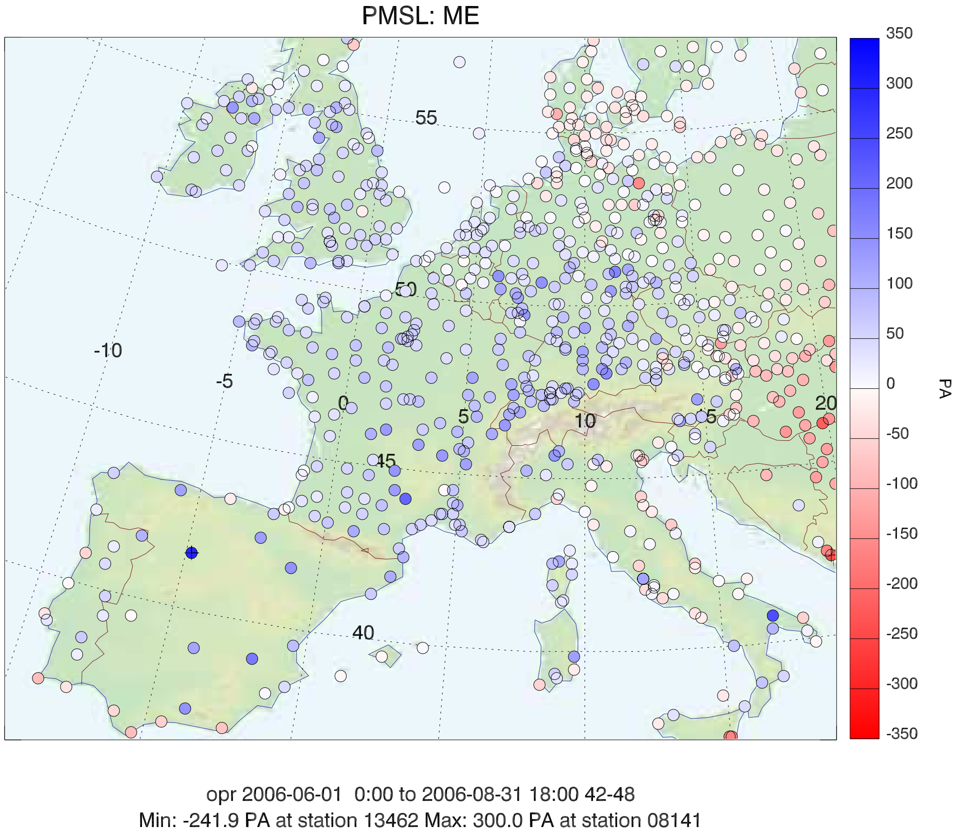

Figure 1: Bias of reduced pressure (PMSL) in Summer 2006 at the SYNOP locations for all 00 UTC and 12 UTC forecasts at +42h and +48h.

- The cold bias in T_2M of the previous summers has almost vanished. The average standard deviation has slightly increased from last summer and is between 2 and 2.5 K.
- A dry bias in TD_2M around -1 K occurs over the coastal areas and Italy. At the inland stations of all other countries, the bias is positive, indicating a wet bias, with values of 1 to 3 K. This is the strongest wet bias of all summers 2001 - 2006.
- There is a clear tendency for negative wind speed (FF_10M) biases along the coast,

up to 3 m/s. In contrast, at many inland stations the model has a positive bias with values up to +3 m/s, especially over north-eastern Austria.

- The precipitation bias generally ranges from 0 to 1 mm/12h at most stations, but increases considerably over the complex terrain of the Alps. It is somewhat higher than in the previous summer. The frequency bias for the thresholds 0.1 mm/12h and 1 mm/12h is larger than 1 at most stations and reaches very large numbers in the Alps (see Figure 2).

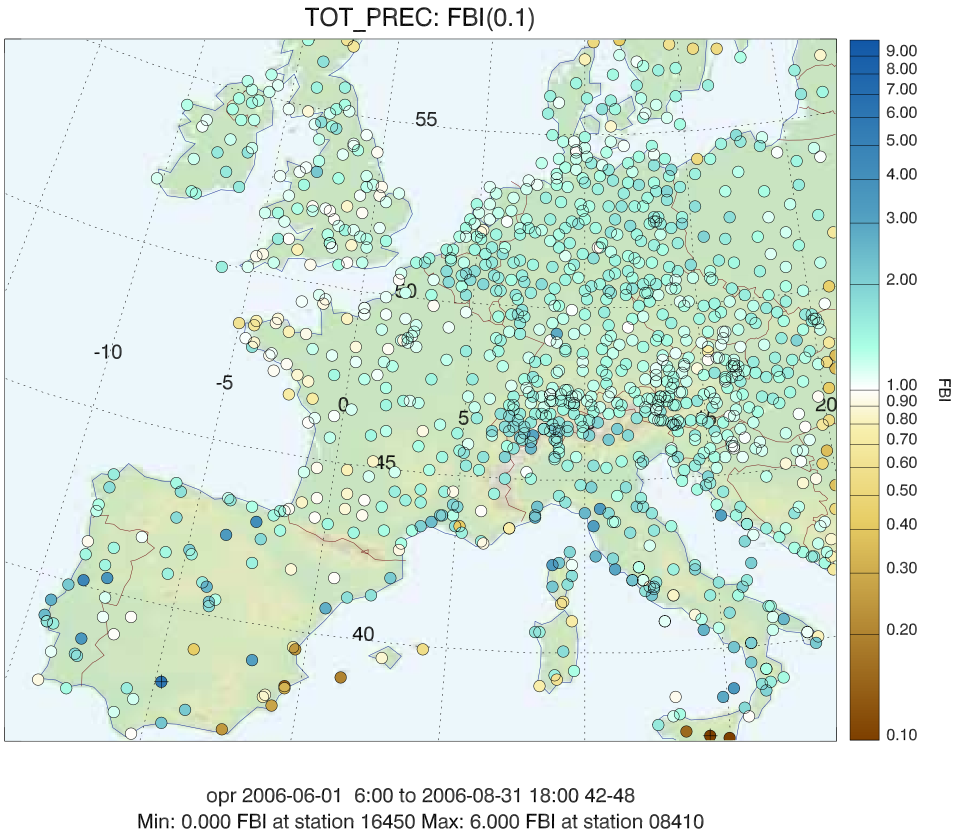

Figure 2: Frequency bias total precipitation for the threshold 0.1 mm/12h in Summer 2006 at the SYNOP locations for all 00 UTC and 12 UTC forecasts at +42h.

Autumn 2006 (September, October, November)

- The cold/dry bias in temperature (T_2M) and dewpoint temperature (TD_2M) is much smaller than for all preceding autumns due to the prognostic TKE scheme introduced in late 2005.

- The precipitation (TOT_PREC) bias and the frequency bias for the 1 mm/12h threshold are both larger than in all previous autumns except autumn 2001.

1.2 Verification of daily cycle over Switzerland [*Francis Schubiger*]

We give here some highlights of the seasonal verification in a hourly resolution with the automatic network of MeteoSwiss.

Precipitation

- During Winter 05/06 precipitation are overestimated, especially for gridpoints > 800 m (due to a strong overestimation of amounts < 2 mm/6h). The low amounts [0.1 mm/6h] show an overestimation at all height ranges: 65% for gridpoints < 800 m and up to 90% for gridpoints > 1500 m. The high amounts [10 mm/6h] are underestimated by 20% for gridpoints < 800 m and overestimated by 30-35% for gridpoints > 1500 m.
- In Spring, Summer and Autumn 06 precipitation amounts have almost no bias for gridpoints < 800 m but are overestimated at gridpoints > 800 m by 30-40% (and up to more than 50% in Autumn). The low amounts [0.1 mm/6h] show an overestimation at all height ranges: for gridpoints < 800 m 15-20% (Spring and Autumn) - 30% (in Summer) and for gridpoins > 1500 m up to 60% (even 90% in Autumn). The high amounts [10 mm/6h, about 2-3% of all cases] are underestimated for gridpoints < 800 m by 20-30% and overestimated for gridpoints > 800 m by 30-40% (even 50-60% in Autumn).
- In Summer 06 the diurnal cycle is too pronounced over mountains (especially in the height range 800-1500 m) and the maximum is reached 4h too early (15 UTC instead of 19 UTC).

2m-temperature

- In Winter 05/06 there is a negative bias during night-time of the order of 2K for gridpoints < 800 m and up to 5 K for gridpoints > 1500 m. The daily amplitude is exaggerated by 2 K for gridpoints < 800 m.
- Spring 06 shows (as compared to Spring 05) a stronger daily cycle and higher values for gridpoints < 800 m (i.e. already in Spring [and not only Summer] too high maxima). The daily cycle is exaggerated for gridpoints < 800 m by 2K: 1K too cold during the night and maxima of 1K too high. For gridpoints > 800 m, there is a negative bias of 2K in the height range of 800-1500 m and even 4K for gridpoints > 1500 m.
- In Summer 06 the daily amplitude for gridpoints < 800 m is only slightly exaggerated with a bias which is mostly slightly positive (up to 1K). For the gridpoints in the height range > 1500 m the bias is always negative (1-2K). As compared to Summer 05 we have higher observed values (about 1K), a greater positive bias < 800 m and a greater negative bias > 1500 m.
- In Autumn 06 the daily amplitude is slightly exaggerated for gridpoints < 800 m: positive during the day (bias up to +1K) and slightly negative during the night. For the gridpoints in the height range > 1500 m the bias is always negative (2K).
- In all seasons the maxima for 2m-temperature is reached 1.5 hours too early and 70% of all forecasts corrected with Kalman filter are within ± 2K at each forecast hour.

2m-dewpoint

- Due to the introduction of the prognostic TKE scheme on 1 December 2005, the diurnal amplitude is less exaggerated (but for gridpoints < 800 m it is still about 3K instead of 1-1.5 K). The strong negative bias on the mountain gridpoints (> 800 m) disappeared.

10m-wind

- For gridpoints < 800 m the bias of the 10m-wind speed is always positive by 0.6 - 0.9 m s^{-1} (maximal at 06 UTC, minimal at 18 UTC). The diurnal amplitude is almost correct. For gridpoints > 1500 m the speed has a great negative bias, due to the same PBL-parametrization over mountains than over flat terrain.

Cloudiness

- The diurnal cycle of total cloudiness is not well reproduced. For gridpoints > 800 m there is a positive bias of up to 1.5 octa during nighttime. The 12 UTC forecasts (but not the 00 UTC forecasts !) start with a negative bias.
- By comparing the results for gridpoints < 800 m and > 1500 m for Winter 05/06 it is clear that the model is not able to forecast correctly the low level clouds (wintertime stratus, see Figure 3). But at analysis time at 00 UTC there is almost no bias for gridpoints < 800 m, i.e. the assimilation of low level clouds (stratus) in the nudging scheme during nighttime seems satisfactory.

Convection and Cloudiness

- A feature that should be investigated (by WG3) concerns the cloud cover in case of convection (already mentioned in the last report [Arpagaus, et.al., 2006]): results for summer over the Alps suggest that the cloud amount in convective situations is too low (see Figure 4). While the observed cloud coverage shows a clear diurnal cycle (lower panel) in accordance with the observed precipitation (upper panel), the diurnal variation is almost absent in the model cloud coverage. Figure 4 shows also results of the test chain with the new Kain-Fritsch-Bechtold convection scheme (for details see in this Newsletter the report in WG3 "Evaluation of the Kain-Fritsch/Bechtold convection scheme").

1.3 Verification of the vertical profiles at TEMP stations [*André Walser*]

Winter 2005/2006 (December, January, February)

The bias for temperature shows a clear cold bias up to 1.1 K (compared to 0.6 K in winter 2004/2005) between 1000 hPa and 300 hPa, with the maximum at 1000 hPa. The increase with forecast time is largest between analysis and +24h. While the bias is quite small at the tropopause height, we note another cold bias up to 1.2 K (at 50 hPa), also increasing with forecast time. This cold bias is clearly smaller than in winter 2004/2005 (2.0 K). Concerning the standard deviation, temperature shows largest spread close to the surface, around the tropopause level as well as in the stratosphere where it is clearly smaller than in winter 2004/2005. The scores for humidity and wind speed/direction do not show significant changes compared to winter 2004/2005.

Spring 2006 (March, April, May)

Good news: the cold bias in temperature between 600 and 300 hPa after analysis time noted for spring in the last years almost vanished and the cold bias above the tropopause is reduced as well (see Figure 5). On the other hand, the standard deviation is very similar compared to spring 2005. Also for this season, the scores for humidity and wind speed/direction do not show significant changes compared to spring 2005.

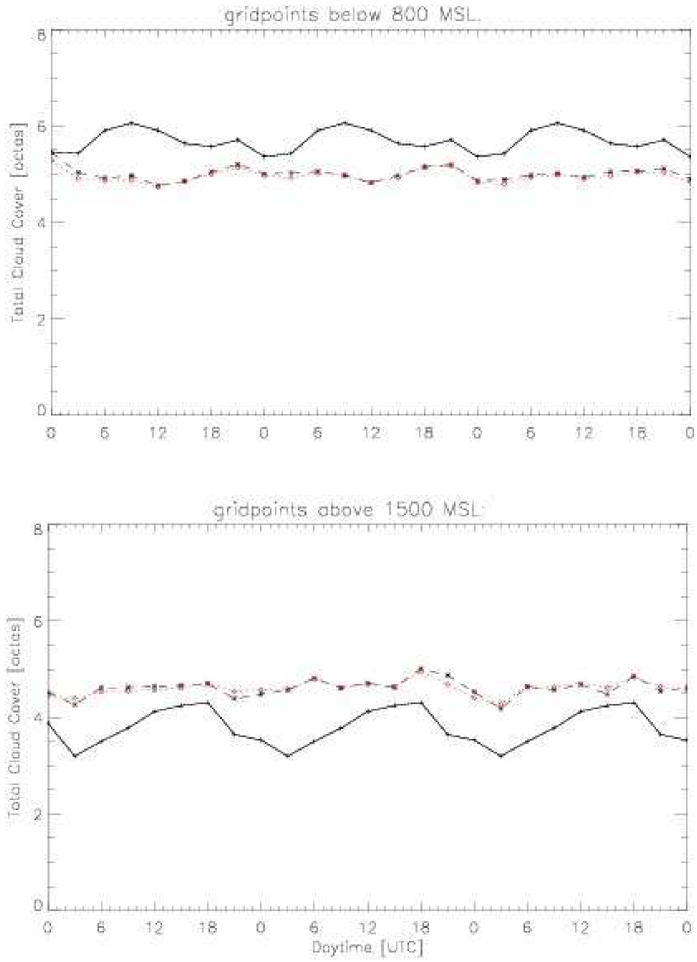

Figure 3: Verification of the diurnal cycle of total cloudiness of Winter 05/06 for gridpoints over Switzerland $<$ 800 m (upper part) and $>$ 1500 m (lower part). Observations (ANETZ): full line black; COSMO: dashed (in black verified with 1 gridpoint and in red verified with all gridpoints within 30 km around the observation location).

Summer 2006 (June, July, September)

We note no significant changes in the scores compared to summer 2005, except that for analysis time (i.e. +00h) the bias for temperature in the troposphere has almost vanished. However, it is the consequence of a new warm bias at 12 UTC compensating the known cold bias at 00 UTC.

Autumn 2006 (October, November, December)

As for spring, the known cold bias in temperature between 600 hPa and 300 hPa is substantially reduced and it is now in the order of only -0.2 K (2005 up to -0.6K). However, we note again a cold bias below 700 hPa (up to -0.6 K), that was almost vanished in autumn 2005. The bias of relative humidity is fairly small for analysis time (slightly positive) below 300 hPa. For forecast times, we note a moist bias up to 10% (2005: 8%) between 650 and 100 hPa. The known dry bias between 950 hPa and 700 hPa is almost vanished this autumn which is, however, related to the larger cold bias mentioned above. The mean error for wind direction is very small, especially in the free atmosphere. However, we note a new positive

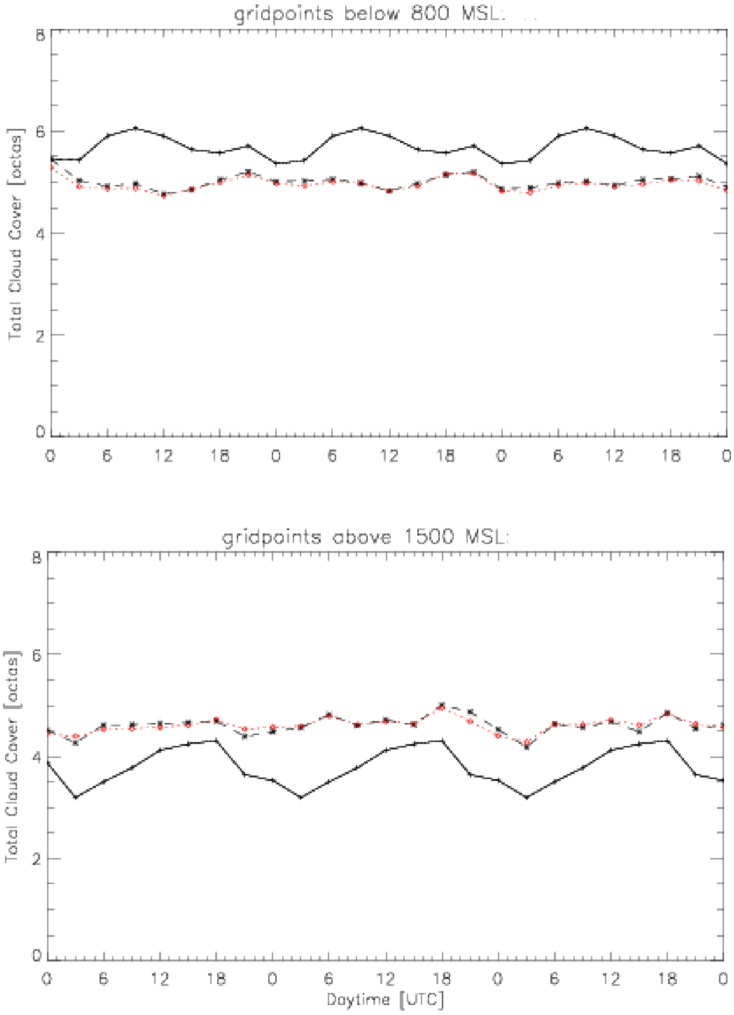

Figure 4: Verification of the diurnal cycle of precipitation (upper part) and cloud cover (lower part) from 20 May to 31 July 2006 for gripoints > 1500 m over Switzerland. Observations (ANETZ): full line black; operational COSMO: black dashed; COSMO with the Kain/Fritsch-Bechtold convection scheme: red long dashed

bias up to 5 degrees between 950 hPa and 750 hPa for all lead-times. On the other hand, the standard deviation is reduced by about 5 degrees for all three forecast times compared to autumn 2005. The scores for wind speed do not show significant changes.

2 Verification studies

2.1 Weather situation-dependent verification of upper-air data [*André Walser*]

A weather situation-dependent verification of the vertical structure of the COSMO Model based on the Schüepp classification (Schüepp 1979) is performed over the full data-set for the climatic year 2005 (1.12.2004 - 30.11.2005). The most interesting results are:

- Significant differences between classes high, flat, and low for temperature. The forecasts error (standard deviation) for the class low is almost twice as large as for the class high in the upper troposphere (but smaller in the boundary layer!), which is noted also for

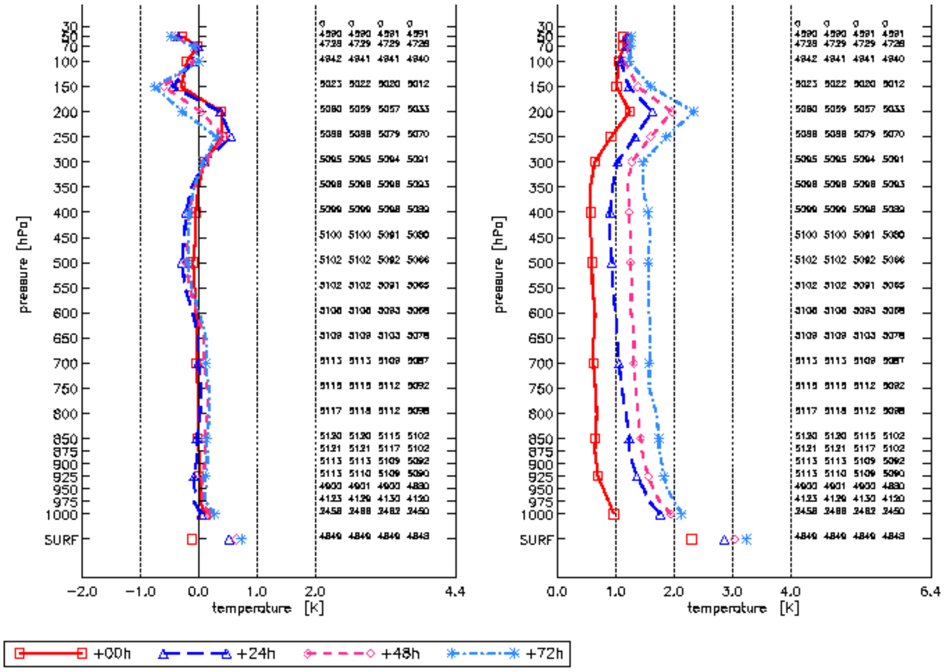

Figure 5: Vertical profile of temperature bias (left) and standard deviation (right) for Spring 06

the individual regions. The bias is also worse for this class.

- The forecasts error for wind speed is clearly larger in class low compared to class high, in particular between 700 hPa and tropopause. This is valid for every region, with the largest differences for stations ”south of Alps” and the smallest for stations ”north of Alps”.

- Differences between the classes for the 4 flow directions are smaller than expected. Overall, class east seems to reveal the largest forecast errors and biases, in particular for wind direction (but not for humidity).

2.2 Verification of COSMO precipitation forecast using radar composite network

[*Emanuele Zala*]

A weather situation-dependent verification of COSMO precipitation based on Swiss radar composite data was performed over the climatic year 2005. Two weather classification were used: the Schüepp classification (Schüepp 1979), which is used daily by MeteoSwiss forecast office, and a simple experimental classification based mainly on 500 hPa winds and surface pressure distribution over the alpine region.

Main results:

- better results in 2005 as compared to 2004, especially for the advective cases due to the introduction of the prognostic precipitation scheme. The pattern dry/wet/dry/wet in the cross-section from North to South is less pronounced

- significant differences of COSMO QPF for different weather classes

- confirmation of the COSMO QPF overestimation over the relief

- significant underestimation of precipitations over Swiss plateau, specifically in SW regimes
- generally good performance in situations with weak advection.

2.3 Verification of different test suites [*Francis Schubiger*]

In 2006 the following COSMO test suites have been verified with SYNOPs, hourly data from ANETZ and TEMPs (the verification results are documented on MeteoSwiss intranet webpages that can be made available on request):

- COSMO version 3.16 for the period 16-31.08.05
- prognostic TKE scheme and COSMO 3.16 for the period 1-15.09.05
- different versions of the multilayer soil model (namely a version with a merge strategy, instead of "free soil-model") for the period 18-30.06.05 starting from its own assimilation
- IFS boundary conditions from the IFS T799 (the new high-resolution global forecasting system of ECMWF) for the period 23.02-06.03.06
- COSMO version 3.19 for the period 15.05-01.06.06
- Kain-Fritsch-Bechtold convection scheme for the period 20.05-31.10.06: see Figure 4.
- Snow analysis and multilayer soil model with a merge strategy for the months of December 05, March 06 and July 06
- Higher frequency of the radiation call (15 minutes instead of 1 hour) for the period 14-30.06.06

References

Arpagaus, M., P. Kaufmann, G. de Morsier, D. Ruffieux, F. Schubiger, A. Walser, E. Zala 2006: WG5-report from Switzerland: Verification of aLMo in the year 2005. *COSMO Newsletter*, No. 6, pp. 165-171.

Comparison of aLMo2 with WINDBANK Measurements

Oliver Marchand and Pirmin Kaufmann

MeteoSwiss, Zürich, Switzerland

1 Introduction

The local dispersion modelling for the Swiss emergency response system for airborne pollutants is currently based on a set of pre-determined wind fields, from which the most appropriate is selected based on current measurements or COSMO (Consortium for Small Scale Modelling) model forecasts. The statistical method of selecting the appropriate predefined wind pattern is called the WINDBANK diagnostic system. The project *Centrale Nucléaire et Météorologie* (CN-MET) has the purpose to replace the current system with a system based directly on a fine-grid (2 km) weather prediction model. The set-up of the COSMO model used for this purpose is named aLMo2.

A comparison between aLMo2 simulations with the near-surface wind measurements used to establish the WINDBANK system is the first step to establish the validity of this concept. The comparison serves to discuss changes in model setup and the model evaluation process before the start of a one-year evaluation period.

Because the WINDBANK wind measurements are near-surface measurements, the main advantage of aLMo2 over the WINDBANK diagnostic system, namely to deliver fully three-dimensional wind information over the whole volume of interest, does not come into play in this comparison. The WINDBANK diagnostic system on the other hand has a clear advantage in this comparison, because it is optimised for these measurement sites. Unfortunately, independent measurements are not available.

2 The weather prediction model

The current operational short-range forecasting system of MeteoSwiss is the Swiss set-up of the COSMO model centered over the Alps, the "Alpine Model". It uses the *Integrated Forecast System* (IFS) as lateral boundary conditions provided by the *European Centre for Medium-Range Forecasts* (ECMWF). At MeteoSwiss, the COSMO model is calculated with $1/16°$ grid spacing, corresponding to about 7 km, hence the here used abbreviation aLMo7. The aLMo7 is used for providing lateral boundary conditions for aLMo2.

The aLMo2 has a grid spacing of about $1/50°$ (2.2 km). Its current domain of 520×350 grid points is centered over the Alps (Figure 1). It uses the same assimilation scheme as aLMo, namely nudging. The wind measurements above 100 m *mean sea level* (MSL) are however currently not assimilated.

Experimental setup, dates and scheduling

Our aLMo2 simulations are carried out in two modes:

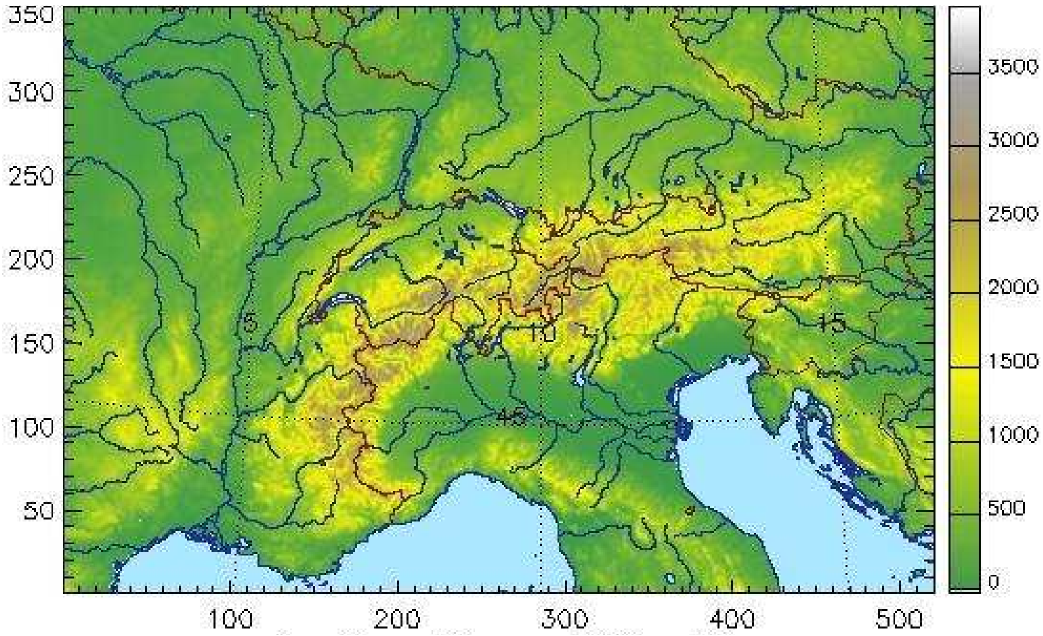

Figure 1: Domain of aLMo2

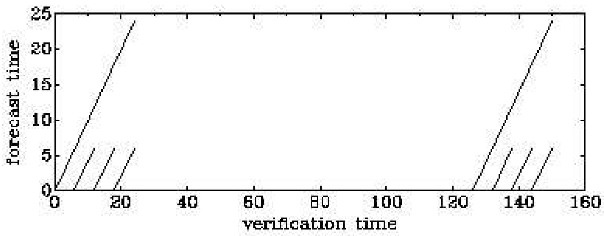

Figure 2: Schematic scheduling of the forecast modes of the aLMo2 simulations

Analysis mode Continuing assimilation with 24 hour spin-up with

- assimilation of observations,
- aLMo7 analysis as lateral boundary conditions.

Forecast mode 24h and 6h

- initialization with aLMo2 analysis,
- free forcast without assimilation of observations,
- with aLMo7 analysis as lateral boundary conditions.

The frequency of forecasts in the future aLMo2 system is planned to be every 3 hours, with a lead time up to 18 hours.

For a reduction of the needed computer capacity only 24 days from each measurement periode are chosen for the simulation. These days are spaced with a gap of 4 days, plus 6 hours to eliminate any systematic error introduced by a fixed initial time of day. Due to the fact that operationally the 3–6 h forecast will be of most interest, three forecasts are computed up to 6h lead time and one forecast is computed up to 24 h lead time for each selected day. Figure 2 shows schematically two blocks of 24 hour and 6 hour forecasts.

Nuclear Power Plant	Period	Permanent stations	Temporary stations
Beznau, Leibstadt	1 Jul. – 31 Oct. 1995	17	25
Mühleberg	1 Jul. – 31 Oct. 1997	20	22
Gösgen	1 Jul. – 31 Oct. 1999	21	22

Table 1: WINDBANK measurement campaigns

Verification of the COSMO model

The routine verification of the operational version of the COSMO model is done by several means. The vertical profiles are verified with the European radio soundings (Arpagaus 2005). The near-surface model predictions are verified on the European scale using SYNOP messages (Kaufmann 2005). A more detailed verification restricted to the Swiss area (Schubiger 2005) uses the Swiss network of automated measurements.

A similar suite of verifications has been applied to the aLMo7 version of this study to ensure the overall quality of the driving model for aLMo2. The description of these results however goes beyond the scope of this paper.

3 WINDBANK

A temporary network of wind measurements was installed in an area of approximately 20 km around each of the three sites with nuclear power plants in Switzerland to capture the near surface wind patterns. The three sites were under examination during four months from July to October, each site separately in a different year. The existing permanent stations in a larger area (out to approx. 60 km distance from the site) were also included in the studies. The four month period of all wind measurements conducted for a site form the data basis, to which the method of Kaufmann and Weber (1996; detailed description in Kaufmann, 1996) was applied to determine wind classes for the WINDBANK diagnostic system (Gassmann *et al.* 2005). The wind classes describe flow patterns with normalized wind speeds and are scaled to the actual wind speed before being provided to the dispersion model.

The observations of the three measurement campaigns (Gassmann *et al.* 2005) are present as hourly values of the wind, stored as components of the wind vector (Table). There are no common temporary sites among the three periods. The permanent stations are mostly part of the automated measurement network of MeteoSwiss, representing a larger area, and are partially used for more than one period.

4 Method

In this study we use traditional scores in meteorology, namely mean error and standard deviation of the error. DD and FF are used as superscripts for wind direction or wind speed, respectively. N^{DD} and N^{FF} indicate the number of matching pairs of values. The units are degree for wind direction and m/s for wind speed.

Points on a scatter-plot are located at the x–axis corresponding to the observation and at the y–axis correspoding to a model value (which might also be the WINDBANK diagnostic system). Due to the cyclic nature of the wind direction, the area of strong correlation is not only along the diagonal but also includes the upper left hand and lower right hand corners of the graph.

Model	ME^{DD}	σ^{DD}	N^{DD}	ME^{FF}	σ^{FF}	N^{FF}
aLMo2 analysis	3.230	47.22	23032	0.1722	1.749	64280
aLMo2 19-24h forecast	3.533	57.31	5424	0.0891	1.789	16347
aLMo7 analysis	8.257	53.49	15326	0.3606	1.743	44155
WINDBANK	0.151	30.62	23569	0.3116	1.281	66055

Table 2: Total scores for all stations (all WINDBANK campaigns)

Model	ME^{DD}	σ^{DD}	N^{DD}	ME^{FF}	σ^{FF}	N^{FF}
aLMo2 analysis	4.859	45.17	12115	0.4316	1.295	37911
aLMo2 01-06h forecasts	4.208	47.99	9125	0.3941	1.286	29261
WINDBANK	-0.091	28.14	12397	0.2540	1.047	38909

Table 3: Total scores for temporary stations (all WINDBANK campaigns)

For all statistical values related to *wind speed*, we use all matching data pairs. For the *wind direction* we use only samples where the *observation* of the matching pairs reports a wind speed larger than 2 m/s.

When interpreting the results, one should however keep in mind that the Windbank measurements are direct point-observations, whereas the aLMo2 forecasts represent a spatial mean over a whole grid cell. A perfect match thus cannot be expected.

5 Total scores for all stations and for temporary stations

Table 2 presents scores including all stations (temporary and permanent) and Table 3 for temporary stations only.

Mean error It is interesting to see that the bias of an aLMo7 analysis is significantly larger (8.257) compared to all other values reported for the bias (all $\leq$4.9; Table 2). Note that in the case of temporary stations the bias for an aLMo2 analysis is actually larger (4.859) than in the 6h forecast (4.208), but the difference is rather small (Table 3). This counter–intuitive order is common. Reasons can be a slightly unbalanced wind field in the analysis, the difference in number of verification pairs and the uncertainty in the statistical values itself.

Standard deviation of wind speed and direction

WINDBANK vs. aLMo The standard deviations reported for the wind speed for WINDBANK (1.047) are surprisingly close to those for aLMo ($\approx$1.3), when looking at Table 3.

A larger difference in standard deviation can be observed for the wind direction (45° for aLMo2 vs. 28° for WINDBANK). This shows the difficulty of aLMo2 to represent local effects, which seems to be more pronounced for the wind direction.

aLMo7 vs. aLMo2 Table 2 shows that aLMo2 is systematically better than aLMo7 in regards to standard deviation for both wind speed and wind direction.

analysis vs. 6h forecast The quality of the 6 hour forecast is almost equivalent to that of the analysis (Table 3). The loss of quality is obviously small for the first 6 hours (maybe even a quality gain !), which renders a recomputation of forecasts at a very high frequency (e.g. every hour) less relevant.

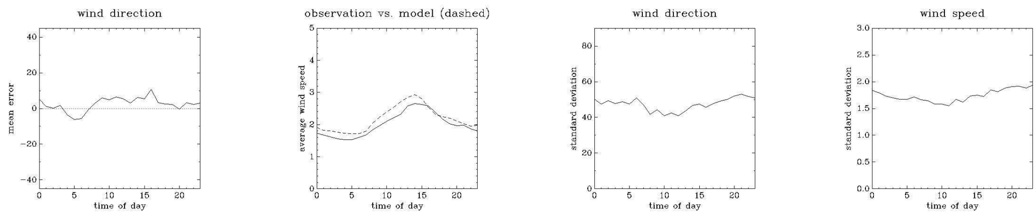

Figure 3: Mean error and standard deviation of the error for each time of the day for aLMo2 compared against WINDBANK data.

permanent vs. temporary stations Overall the results are essentially equivalent for “all stations” and “temporary stations”.

6 Verification of the aLMo2 analysis

For the overall verification of the aLMo2 analysis, the simulated winds are compared for all stations (permanent and temporary) and all three WINDBANK campaigns. Figure 3 summarizes the mean error and standard deviation for each hour of the day. The wind direction bias is well below 10° and the wind speed bias is far below 1 m/s.

Figure 4 shows the results for each of the different measurement campaigns separately. The similarity of the plots shows that there is no substantial difference in representativity of the three campaigns. We see that both aLMo2 and WINDBANK show an intensification of the scatterpoints near the main diagonal (and the opposite corners for the wind direction due to its circular nature). Both methods also reveal considerable spread and cluttering of the whole plotting domain. Both methods show dense regions for the wind directions which can be derived from the histogram of wind directions over the Swiss plateau.

The scatterplots displaying wind speed for aLMo2 show that the dynamic range of the weather model seems too narrow. Low wind speeds are overestimated, while high winds are underestimated. The model tends to favor moderate wind speeds and in average overestimates the 10 m winds slightly. This effect can partly be due to the fact that COSMO model winds are representative winds for a grid cell. Obviously point measurements of winds will show a greater range in values than an average over a cell. With decreasing cell size, of course, one hopes to bring the two quantities in accordance.

One important feature is the quantization effect for the wind directions stemming from the wind classes in the WINDBANK diagnostic system, resulting in horizontal stripes in the plot.

The statistical values for the overall standard deviations of the wind directions already indicate that there is a considerable spread in both WINDBANK and aLMo2 wind directions. This is confirmed in the scatterplots.

7 Single station comparison of the aLMo2 analysis

General observations We observe in the wind direction histograms for the WINDBANK that the accentuation of the channeled flow in the Swiss plateau is overemphasized by WINDBANK. This is due to the absence of certain wind directions due to the grouping into wind classes. The aLMo2 on the other hand underestimates the channeling effect at many stations.

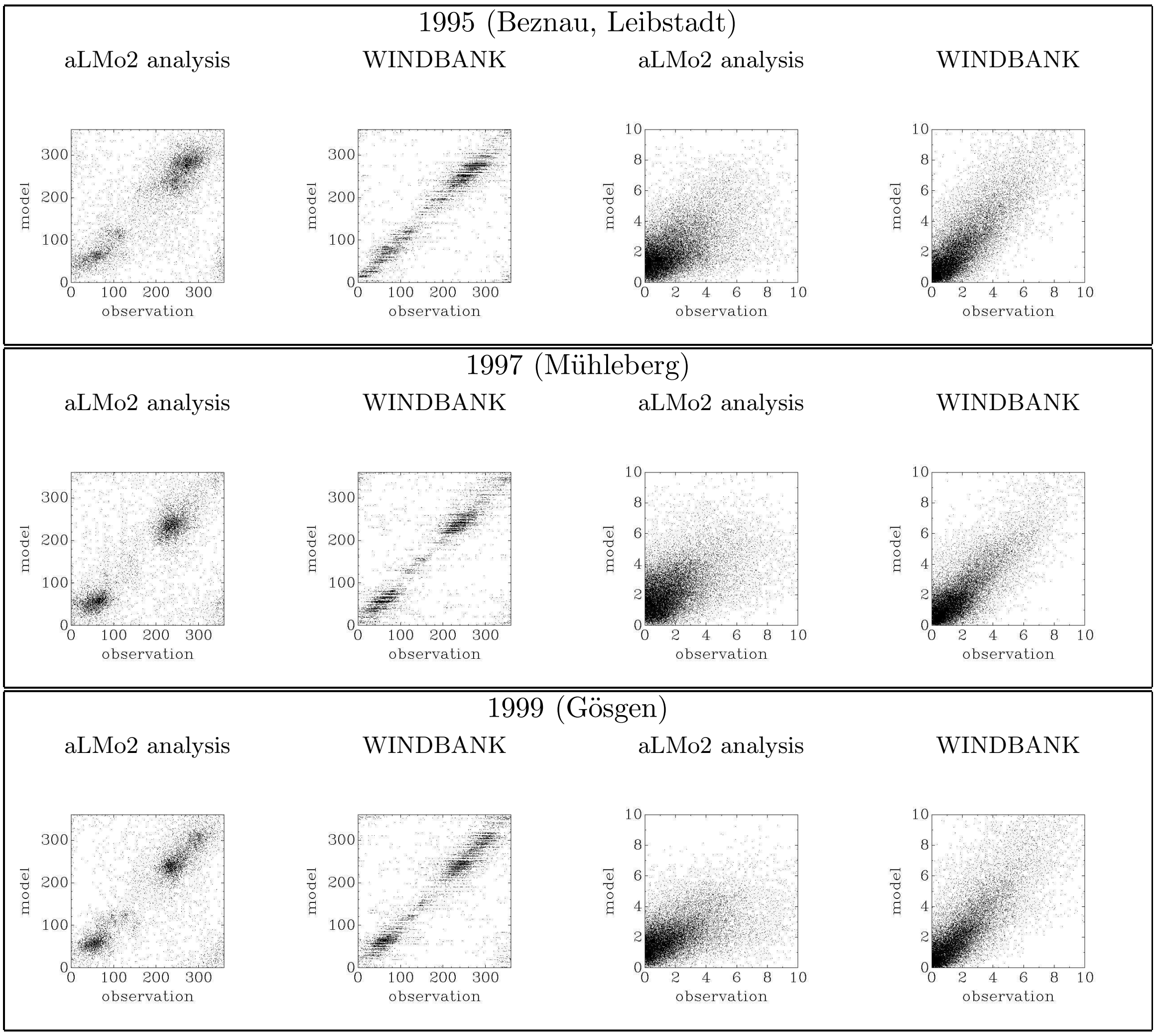

Figure 4: Scatterplots of wind direction and wind speed using all stations (permanent and temporary) for each of the three measurement campaigns.

Wind direction

- In some cases, aLMo2 and the WINDBANK reconstructed wind directions are of similar quality.
- The WINDBANK reconstructed directions are better at a number of stations. The exact number depends on the criteria, it lies however between 20 to 30 of the about 40 stations each year. This is expected due to the mesh size of aLMo2 that cannot resolve local orography, the possible influence of trees, buildings and the like on the stations, and WINDBANK being optimized for the station locations.
- aLMo2 wind directions are better at a few Stations.
- Some stations are badly reproduced by both aLMo2 and WINDBANK. High vertical bands appear in the direction scatterplot for aLMo2 and wide horizontal bands in the scatterplot for the WINDBANK system. These bands are partially the result of the under- and overestimation of the channeling effect by aLMo2 and the WINDBANK diagnosis system, respectively. For aLMo2, a phase shift might be adding to the broadness of the scatter plot.

Wind speed

- In general, the wind speed is too strong in both aLMo2 and the WINDBANK reconstructed winds.
- At locally influenced, sheltered, low wind speed stations, aLMo2 tends to overpredict the wind speed.
- In very few cases, the distribution of aLMo2 wind speeds is better than the WINDBANK reconstructed speeds.
- Some stations are grossly underestimated by the aLMo2 10 m wind, because the measurements are located much higher above ground than 10 m.
- Some mountain-top wind speeds are underestimated by aLMo2 due to inadequate representation of the boundary layer at the mountain top. The parameterization of the boundary layer in aLMo2 is representative for the whole grid cell (2 km by 2 km) and does not reflect the local effect of a mountain top.

8 Interpretation of the results

This study was proposed as a first "screening" of the quality of aLMo2 ground winds. We are satisfied by the statistical results, because

- aLMo2 compares quite well to WINDBANK, despite the fact that the WINDBANK diagnostic system is made solely for the purpose of 10 m wind analysis, and aLMo2 was not run with all available improvements available today. Particularly, the wind direction and speed of the Swiss (and many other) stations have not been assimilated.
- aLMo2 was proven to be systematically better than aLMo7, especially with respect to wind directions.

The overall results show that the dynamic range of the wind speed of aLMo2 seems to be too narrow. Individual station plots show that aLMo2 is very well suited for simulating local effects. For some stations aLMo2 has even been shown to provide a better model climatology for the wind directions than the existing WINDBANK system.

Concluding, aLMo2 has the potential to replace a statistical tool such as WINDBANK for simulating local winds.

References

Arpagaus, M., 2005: Verification of vertical profiles: Operational verification at MeteoSwiss. COSMO Newsletter, No. 5, pp. 102–105.

Gassmann, F., H. Isaak, and M. Tinguely, 2005: Projekt "Windbank", Schlussbericht. PSI Bericht 05-08, Paul Scherrer Institut, Villigen, Switzerland.

Kaufmann, P., 2005: Verification of aLMo with SYNOP and GPS data over Europe. COSMO Newsletter, No. 5, pp. 113–117.

Schubiger, F., 2005: High resolution verification of daily cycle over Switzerland. *COSMO Newsletter*, No. 5, pp. 88–93.

Comparing COSMO Models 3.19 vs. 3.5 on the 30h Precipitation Forecast by Parallel Run during July - September 2006 over Europe.

JAN WACŁAW PARFINIEWICZ

IMGW Poland

1 Introduction

During July-September 2006 two versions of COSMO-Model: 3.5 and 3.19 (both in terrain following coordinates) have been tested in parallel. Altogether 90 precipitation forecasts from parallel runs starting at 00 UTC for 30h have been completed and compared against daily totals GTS SYNOP data over Europe (the runs 20060701 and 20060729 have been dropped out). The models were run with diagnostic precipitation scheme version as it has been set into the operational IMGW model LM_3.5 14 km grid version (taken as reference), which is stably running there since about 2 years.

2 Standard statistics

The averaged results of the statistical indices used for quantification of precipitation forecasts LM_3.5 vs. LM_3.19 are the following (PC - proportion correct, HIT - probability of correct rain signal, FAL - false alarm, BIAS - systematic error, HSS - Heidke skill score, PSS - Peirce skill score, ETS - Equitable threat score, CHI - the measure of cross relationship with χ^2 distribution, DEV - standard deviation error, and, CC - cross correlation coefficient):

LM:	PC	HIT	FAL	BIA	HSS	PSS	ETS	CHI	CC	DEV
3.5	0.81	0.75	0.20	1.26	0.52	0.55	0.37	0.30	0.50	5.16
3.19	0.81	0.74	0.20	1.21	0.52	0.54	0.36	0.30	0.50	5.28

Table 1: Standard statistics: averaged values

An example of ETS diagram is presented in Fig. 1. The vertical lines indicate dates when significant errors occurred (in red for LM_3.5, in green for LM_3.19).

As standard statistics are not sensitive enough to assess model behavior in extreme cases, it is necessary to work with all spectrum of errors.

3 Comparing overall 30h forecast errors distributions: LM_3.5 vs. LM_3.19

Distribution of errors in both models was based on more than 50000 sample points alltogether. In Fig. 2 two diagrams of precipitation errors are presented; left: monotonically arranged (ranked) by self - order from smallest (negative) to largest (positive); right: by classes of errors' magnitude. As the errors of order $< -2, 2 >$ (the thick band for numbers between $\sim$ 5000 - 44000 on right panel) are negligible (however it may comprise cases of forecasts with severe precipitation), the further analysis will concentrate on separating extreme cases from dominating "dust" by zooming right and left parts of the diagram.

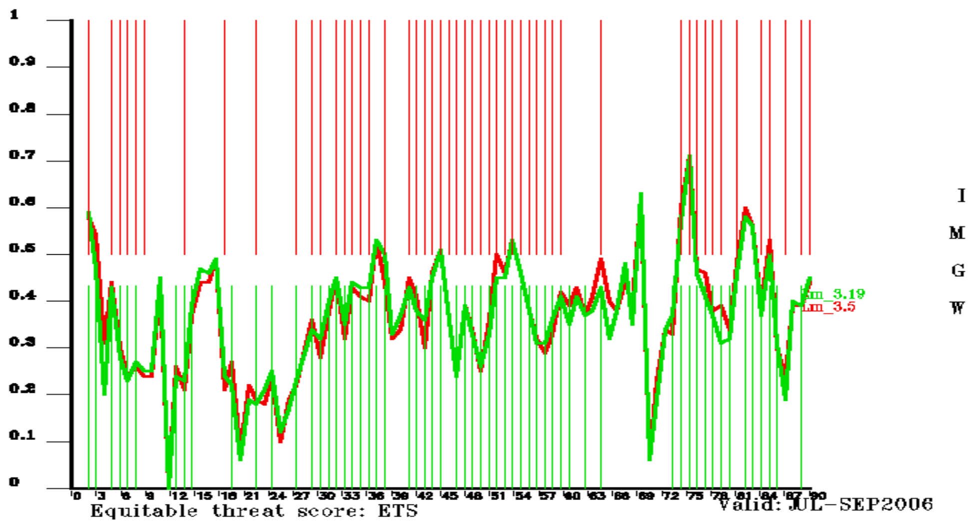

Figure 1: ETS diagram

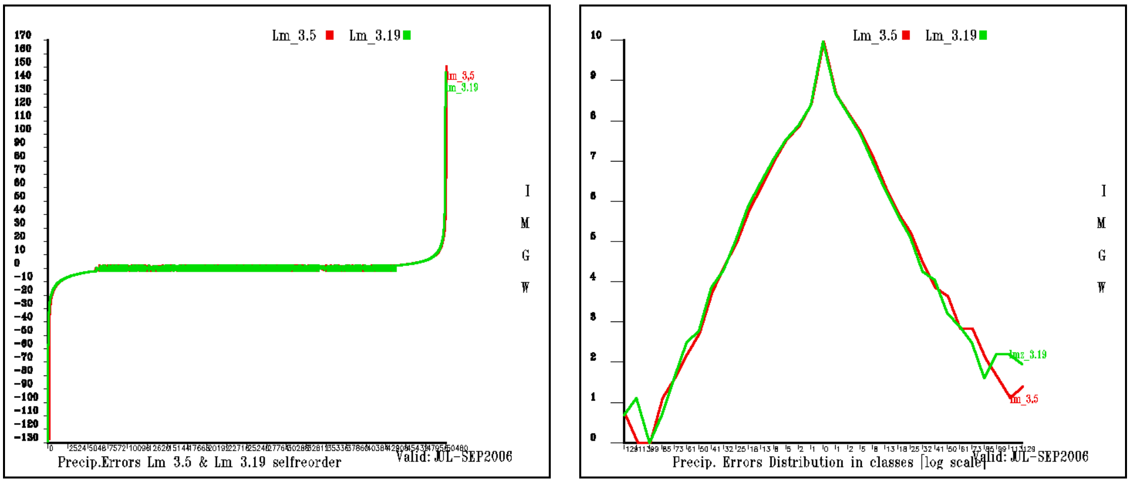

(a) Errors by selforder

(b) Errors by classes

Figure 2: Overall 30h forecast precipitation errors distributions

In Fig. 3 investigation of the two border distributions is presented in the following way: left for values under predicted ones (dry branch) and right for overshoots (wet branch).

The further way to proceed is clear: select doubtful, significant cases and attempt to develop new model version that would clarify situation (or enlarge range of clarity). A control list of 162 point-cases errors > 40 [mm/day] was selected, which gives altogether 56 dates to monitor model quality progression (the administration of such a list is a separate challenge). Each of such cases has its own metric and graphical illustration. An example of the extremely imperfect LM_3.19 forecast is the 8th of July, when daily total error for Chemnitz, Germany (10577) was 121 [mm/day], while for LM_3.5 "only" 53 [mm/day] (Fig. 4). The illustration shows influence of singular error signal onto water accumulation over a given station. When taking accumulated water amount for an enough long period of aggregation as an ultimate indicator of forecast quality, one may see how huge forecast collapses are then smoothly compensated by a number of less significant events.

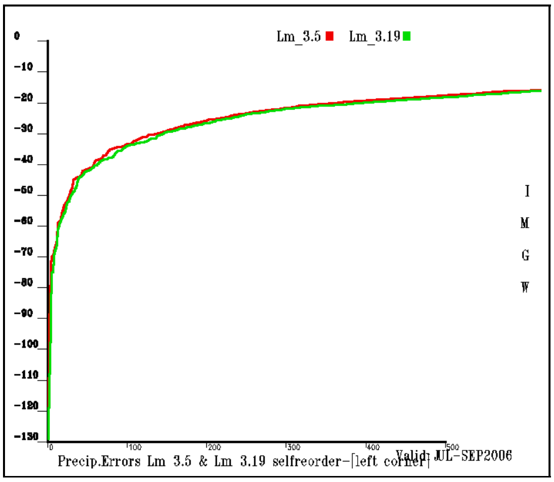

(a) Errors by selforder: left side

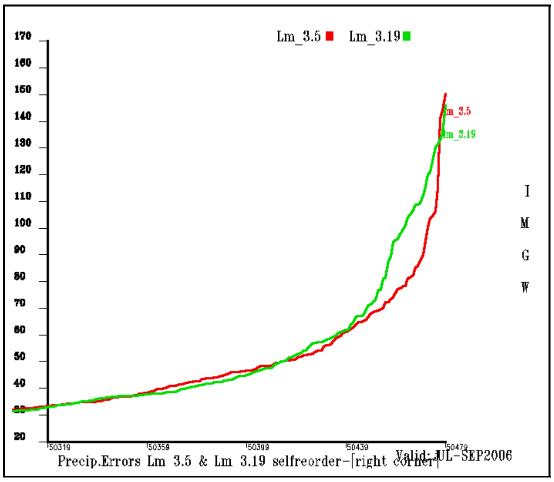

(b) Errors by selforder: right side

Figure 3: Investigation of the two border distributions

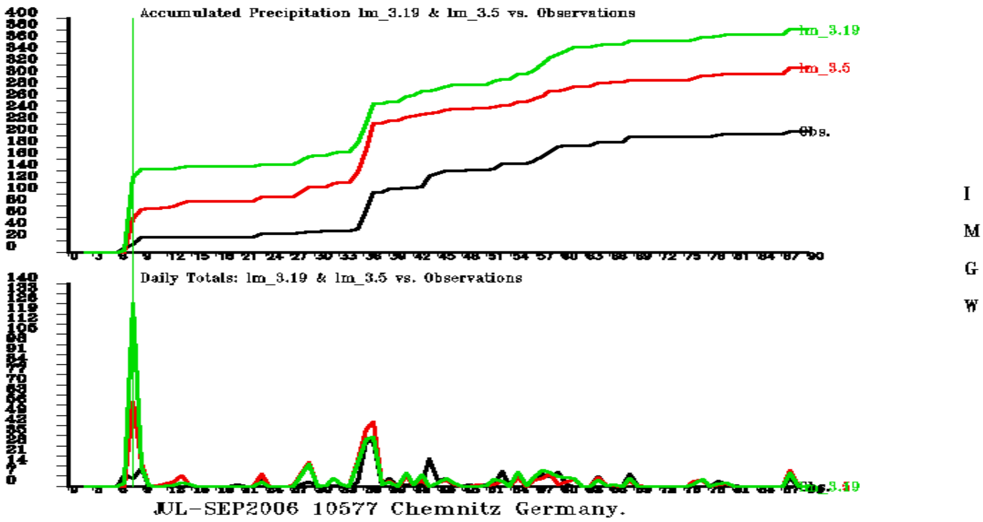

Figure 4: Accumulated precipitation and daily totals: Chemnitz Germany (10577)

4 Comparing accumulated precipitation water errors over Europe

a) Distribution of errors over Europe : LM_3.5 vs. LM_3.19. (Fig. 5)

b) Relative Predominance LM_3.19 over LM_3.5 regarding accumulated water (Fig. 6). To asses each particular relationship between errors over given geographical point, the simple predominance factor RP is proposed:

$$RP = (\text{Relative Predominance } (|\text{DelLM\_3.5}|)/(|\text{DelLM\_3.5}| + |\text{DelLM\_3.19}|)$$

where DelLM_(given version) means difference between 30 h forecast of daily total (i.e. 30h -06h model forecasts of total precipitation) and its realization over given station. If the number of errors in LM_3.5 is large, the RP of LM_3.19 approaches the value 1. Calculated RP of LM_3.19 of accumulated water allows for ultimate geographical review of errors over Europe (Fig. 6).

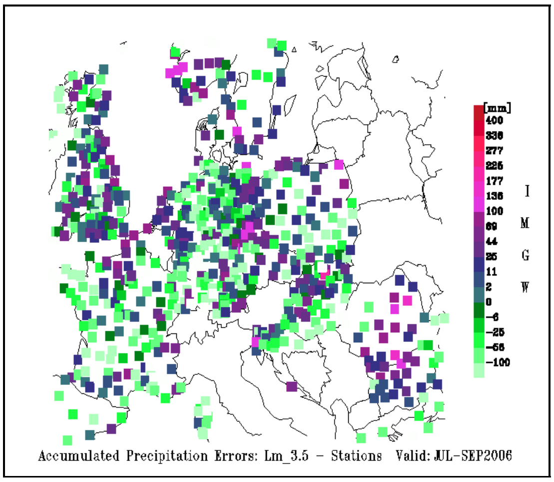

(a) Lm_3.5 errors

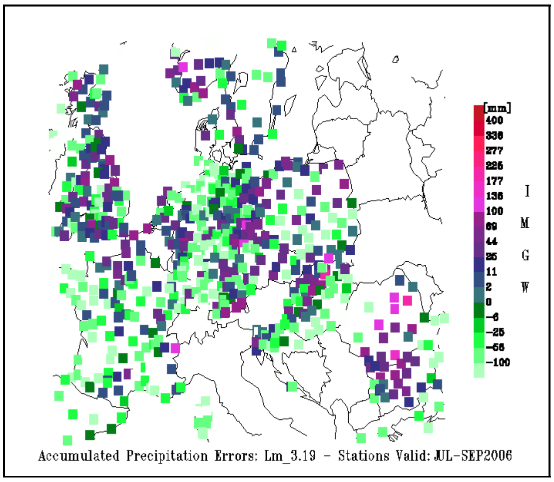

(b) Lm_3.19 errors

Figure 5: Comparing Accumulated Precipitation Water Errors over Europe

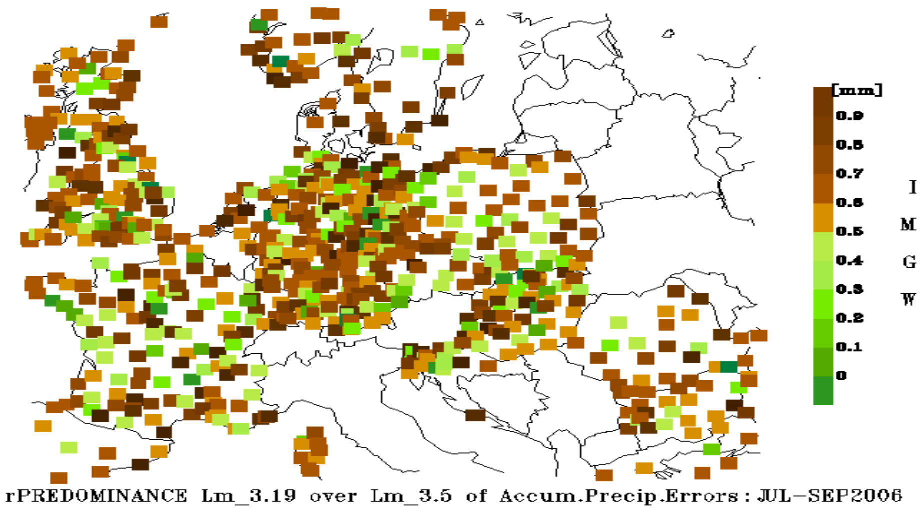

Figure 6: Relative Predominance LM_3.19 over LM_3.5 regarding accumulated water

5 Summary

Despite there is no evidence that Total_Precipitation LM_3.19 30h forecast errors are significantly smaller than in the LM_3.5 version, the accumulated water errors during the analyzed season indicate clear predominance of the newer version. This result, obtained for summer season, indicates that configuration applied at IMGW till now, should be changed to account for new developments - relevant to finer mesh size (2.8 km), the CLM developments and changes in the new multi-layer soil model. Similarly, the diagnostic precipitation parametrisation should be re-tested against the prognostic one in the near future.

Acknowledgments
I appreciate the input to this work by my valued colleagues: Uli Schättler, Marek Lazanowicz, Jürgen Steppeler.

Research Run Script System with Elements of Postprocessing

(Short note)

Witold Interewicz

Institute of Meteorology and Water Management
Centre of Numerical Weather Forecasts
61 Podlesna str., PL-01673 Warsaw, Poland

1 Introduction

COSMO projects require a lot of well prepared technical work. This includes multiple COSMO model runs and postprocessing tasks, followed by analysis. In order to do all those tasks quickly and thoroughly and to perform an analysis in a comfortable way one needs a set of tools operating on large amounts of data. Below are briefly described simple tools developed at IMGW to make research easier.

2 RRSS

RRSS is an acronym for Research Run Script System. It was presented at COSMO GM 2006 in a small poster as SRSS (Scientific Run Script System). It consists of a few scripts that:

- download and decompress the data sets,
- control multiple runs (for each data set and each configuration),
- perform run (preprocessing, run and postprocessing - including postprocessing in background)
- pack and upload the run results.

Scripts are written in Korn Shell (ksh). All tasks are run using queuing system to allow 'run and forget' performance. Core part of RRSS, responsible for running preprocessing and model, covers functionality of standard operational scripts.

3 Postprocessing for RRSS - visualisation system

Visualisation in RRSS is performed using Grads package (version 1.8 or newer is required). Recently an effort has been undertaken to build flexible, possibly widely configurable system of standard postprocessing. The idea was to:

- supply a standard tool that will allow scientist to review the results before detailed analysis,
- build a flexible, standard interface between shell scripts and Grads scripts,
- supply a framework of the Grads script,

- supply a set of functions (like scale/legend building, advanced string writing, time handling operations)

so that scientist or technican could port, configure, enhance and use the system without any special effort in each new project.

Visualisation system is adjusted in RRSS through settings in a configuration file (Korn Shell script). Thus it can be easily adopted for any experiment.

Visualisaton in RRSS uses 2D plots. These are standard surface or screen level fields and also vertical and horizontal slices in pressure and geometrical coordinate. Unfortunately, to the authors' knowledge there is no way to generate proper slice from the data in hybrid coordinate. Slice in hybrid coordinate is going to be included in RRSS just to allow a look at the order of magnitude of non-interpolated data.

System also allows to plot vertical profiles in pressure, geometrical and hybrid (respectively converted to geometrical) coordinate. The last of the mentioned profiles, drawn in geometrical coordinate, based on non-interpolated data taken directly from the grid of the model, can be useful in developers work. Preparation of those profiles requires additional freely available tool: wgrib.

Grads functions included in RRSS allow to draw meteograms as well. Scripts for meteogram plots are in preparation.

Grads software allows to handle station data. There is an idea to prepare portable (in Fortran) converter and visualise results from COSMO model as station data. Sense of this conversion is to use freely available scripts for meteorological diagram plotting. This feature of RRSS has to be implemented in future.

4 Offline data archiving

A problem that appears in large simulations is the data amount. While having short investment budget one has to manage with simple resources like DVD recorder. RRSS includes a script for data partitioning and archiving on DVD. This script uses standard linux tool 'growisofs'. However this part of RRSS requires further development yet.

5 Results and further plans

At the moment a preliminary version of RRSS is being used in COSMO QPF priority project.

Further development of RRSS is planned and it is going to include:

- better modularisation of shell scripts,
- better handling of structures for single run definition,
- Vis5D graphics (it is expected to be used for isosurfaces plotting),
- html/JavaScript viewer for comfortable results viewing.

The last task is intended in order to make easier the analytic work. RRSS's viewer tool is expected to support kind of conditional review. This future is in project/components development phase.

List of COSMO Newsletters and Technical Reports

(available for download from the COSMO Website: `www.cosmo-model.org`)

COSMO Newsletters

No. 1: February 2001.

No. 2: February 2002.

No. 3: February 2003.

No. 4: February 2004.

No. 5: April 2005.

No. 6: July 2006; Proceedings from the COSMO General Meeting 2005.

No. 7: April 2008; Proceedings from the COSMO General Meeting 2006.

COSMO Technical Reports

No. 1: Dmitrii Mironov and Matthias Raschendorfer (2001):
Evaluation of Empirical Parameters of the New LM Surface-Layer Parameterization Scheme. Results from Numerical Experiments Including the Soil Moisture Analysis.

No. 2: Reinhold Schrodin and Erdmann Heise (2001):
The Multi-Layer Version of the DWD Soil Model TERRA_LM.

No. 3: Günther Doms (2001):
A Scheme for Monotonic Numerical Diffusion in the LM.

No. 4: Hans-Joachim Herzog, Ursula Schubert, Gerd Vogel, Adelheid Fiedler and Roswitha Kirchner (2002):
LLM – the High-Resolving Nonhydrostatic Simulation Model in the DWD-Project LIT-FASS.
Part I: Modelling Technique and Simulation Method.

No. 5: Jean-Marie Bettems (2002):
EUCOS Impact Study Using the Limited-Area Non-Hydrostatic NWP Model in Operational Use at MeteoSwiss.

No. 6: Heinz-Werner Bitzer and Jürgen Steppeler (2004):
Documentation of the Z-Coordinate Dynamical Core of LM.

No. 7: Hans-Joachim Herzog, Almut Gassmann (2005):
Lorenz- and Charney-Phillips vertical grid experimentation using a compressible non-hydrostatic toy-model relevant to the fast-mode part of the 'Lokal-Modell'

No. 8: Chiara Marsigli, Andrea Montani, Tiziana Paccagnella, Davide Sacchetti, André Walser, Marco Arpagaus, Thomas Schumann (2005):
Evaluation of the Performance of the COSMO-LEPS System

No. 9: Erdmann Heise, Bodo Ritter, Reinhold Schrodin (2006):
Operational Implementation of the Multilayer Soil Model

No. 10: M.D. Tsyrulnikov (2007):
Is the particle filtering approach appropriate for meso-scale data assimilation?